THE HYDRODYNAMICS OF SIEVE PLATE COLUMNS

A Thesis submitted for the

degree of Doctor of Philosophy

in the Faculty of Engineering

by

Robert Charles Schroter, B.Sc.(London), A.C.G.I.

Department of Chemical Engineering
and Chemical Technology,
City and Guilds College,
Imperial College,
London, S.W.7.

June 1967.

ABSTRACT

High speed cine and still photographic observations have been made of the two phase dispersion produced on sieve plates. In particular the effect of plate geometry on dispersion structure was studied. At low superficial vapour rates, a cellular foam structure was observed, while at high vapour rates the structure was far more complex. The processes of bubbling and foam breakdown were also investigated.

The dispersion structure was also studied using the established gamma ray absorption method. Extensive pressure drop measurements were made for the full range of liquid and vapour rates studied. It was found that the two regimes of dispersion observed visually were not apparent from the hydrodynamic studies. It is shown that it is reasonable to consider the total plate pressure drop as the sum of the true liquid hold up and the dry plate pressure drop. There is a small addition term, the residual head due to flow through the wet plate, which may be ignored as it is always less than 0.3cm water.

A mathematical model describing the hydrodynamics of the two phase gas liquid dispersion generated on a sieve plate has been developed in an effort to obtain more information about the variables controlling the quality of the dispersion.

To my parents and Veronica

for their patience and understanding.

ACKNOWLEDGEMENTS

The author wishes to express his most sincere thanks to Professor R. W. H. Sargent, his personal supervisor, for his invaluable stimulation and advice throughout the course of this work.

Assistance during the project has been received from almost all the technical staff in the department and this is gratefully acknowledged. The author would particularly like to thank Mr. J. S. Oakley, Mr. L. Tyley and their staffs for their frequent technical advice and assistance.

Finally, the author would like to thank the Institution of Chemical Engineers for the award of the Ure Bursary which financed the first two years of the work.

CONTENTS

INTRODUCTION

INTRODUCTION

It is perhaps not an overstatement to say that absorption and distillation columns are as old as the chemical industry. Even during the Middle Ages, simple types of fractionating columns were used for the distillation of alcohol and other mixtures. Continuous stills, such as the famous Coffey Still, were first introduced early in the last Century. However, it is only during the last thirty to forty years that the mass transfer processes involved have been studied. Today design procedures far more certain than the old 'trial and error' techniques are available, though precise prediction of the performance of a plate is still impossible as much of the essential information for an accurate design is lacking.

Whilst the performance of a perfect or theoretical plate can be predicted with reasonable satisfaction, the separation achieved with a real plate as a function of its hydrodynamic parameters is not well understood. Consequently it is difficult to design an operating column to tight specifications, and for a complex separation it may be impossible.

Understandably, in recent years, Industry, Government Institutions and Universities have spent a very considerable effort investigating many aspects of the field of distillation. One excellent example of such a project was the coordinated research programme sponsored by the American Institute of Chemical Engineers (1, 2, 3). The work reported in this thesis stems from a similar coordinated project.

The Association of British Chemical Manufacturers (A.B.C.M.) and the British Chemical Plant Manufacturers Association (B.C.P.M.A.), through their joint research committee in 1958, set up a Distillation Panel. The terms of reference of the Distillation Panel were to evaluate the results of the A.I.Ch.E. research projects (1, 2, 3) and to recommend any particular topics requiring investigation. It transpired that the findings of the A.I.Ch.E. projects were frequently at variance with the experiences and feelings of the members of the joint panel. In particular there was deep disagreement over the significance of the role of the 'foam' produced on a plate in the mass transfer that occurred. Professor J.A. Gerster controller of the Delaware Project (1) was emphatic that the foam had a most important role in the mass transfer process (4).

The need to resolve this important point led to the initiation of the project at Imperial College to study the mechanism of the production of the foam, its effect on the separation performance and the effect of design parameters on its structure. This work began in 1958 and the findings so far have been reported by Macmillan (5) and Bernard (6).

Projects have been conducted on a large 16in. diameter column and a smaller 4in. diameter column both of which were separating normal and iso-pentane. Macmillan worked on the small column obtaining preliminary empirical information about the effects of design parameters on the separation performance. Bernard reported and extended these empirical studies in the large column.

The present investigations have been of a somewhat more basic nature. Considerable attention has been given to the proper measurement and interpretation of plate pressure drops. Visual observations, facilitated by use of very high speed cine-photography and microsecond flash photography, of operating plates and simulation rigs have also been made in order to develop a clearer understanding of the processes involved in the production and breakdown of the foam. A simplified mathematical model to describe the hydrodynamical situation obtained on the plate has been developed for numerical solution.

PART 1

VISUAL STUDIES OF DISPERSIONS FORMED ON SIEVE PLATES

PART 1

VISUAL STUDIES OF DISPERSIONS FORMED ON SIEVE PLATES

Chapter 1.1. INTRODUCTION

The prediction of the mass transfer performance of any contacting system such as a sieve tray requires a knowledge of the characteristics of the dispersion actually produced on the tray. In fact the surface area available for mass transfer, the liquid and gas phase mass transfer coefficients and the residence time distribution functions of the phases are the controlling factors. The first of these, the true interfacial area, must vary considerably with the dispersion structure, which may itself be strongly dependent upon the plate geometry, vapour and liquid loadings and even with the physical properties of the fluids.

Crozier (8) using a light scattering technique attempted to measure the variation of gas hold-up with height above the plate floor. Subsequently, time average foam densities have been measured by various workers, particularly Calderbank (12), Macmillan (5) and Bernard (6), using the established method of gamma ray transmission reported elsewhere in this thesis. However, direct studies of the dispersion structure have not been widely made. Pozin (7) characterised froths as being of either 'cellular' type at low vapour rates or 'mobile' at higher vapour rates. More recently, Calderbank and Moo-Young (9) have attempted to measure gas-

liquid interfacial areas with light reflectivity and transmission probes presuming that measurements in the vicinity of the walls were indicative of the actual interfacial areas in the bulk of the foam. However, discrepancies in predictions of the reflectivity and transmission probes led them to rely more upon transmission probes for the determination of bulk froth properties.

Zuiderweg and Harmens (10) showed that the nature of the foam is dependent upon liquid physical properties, such as surface tension and viscosity, and upon the liquid composition on the plate. They further found that the quality of the dispersion obtained depended quite strongly upon the surface tension gradients existing in the column. Planck (11) has presented evidence that liquid hold-up shows marked variations between systems as well as with composition in a given system.

Considerations of the phenomena of entrainment and weeping have also been of a somewhat empirical nature despite the fact that studies of the effects of entrainment are widespread in the literature. Hunt, Hanson and Wilke (14) produced a generalised entrainment correlation for sieve plates showing that the entrainment rate was a function of the superficial gas velocity rather than hole velocity or plate free area. The 'effective' plate spacing, or space between the foam surface and the plate above, also had a very marked effect - the correlation gave an inverse relationship to the power 3.2. Many workers (15, 16, 17, 18, 19, 20) have obtained entrainment data for bubble-cap trays; the values are some

three to five times greater than for sieve trays. Jones and Pyle (23), who compared sieve trays and bubble-cap trays operating under similar conditions, found that the entrainment from a bubble-cap plate was five to ten times as large as from a sieve tray.

That the entrainment rate is so vastly different for sieve and bubble-cap plates under the same operating conditions would suggest that the amount and probably droplet size distribution of the entrained liquid is dependent on the foam structure rather than simply upon the superficial velocity as suggested by Hunt et al.

Several workers have made attempts to describe the entrainment phenomenon using mechanics and probability functions and have justified their approaches experimentally under limited conditions. Cheng and Teller (29) developed a correlation for the quantity of entrainment between trays as a function of superficial velocity, projection velocity and particle size distribution. Using these ideas, Bostian (24) developed a model employing droplet mechanics and statistics to try and predict entrainment values for sieve trays. However the simplifications forced into the model restrict its predictions of the effects of design parameters to a qualitative level. Realising that approaches of this type are always extremely difficult if not impossible, Teller and Rood (30) visually studied entrainment from sieve trays. To simplify photography of the bubbling and bubble bursting processes, they studied a plate with only three holes. It is evident from their description of the bubbling mechanism that three holes

function in a different way from operating plates with uniform bubbling conditions.

Prince (21) and Prince and Chan (13) have made a study of the lower limiting condition of weeping - "dumping", when liquid can no longer be supported on the plate to the level of the outlet weir. However, they provide no information on the effect of weeping on the separation performance or on the actual mechanism of the process.

Lockhart and Leggett (25) have produced a purely empirical correlation for weeping based upon the observations of Leibson et al. (26) and Mayfield et al. (27). The graphical correlation relates the dry tray pressure drop to the calculated head of liquid on the plate at the outlet weir.

Very recently Kastanek and Standart (31) have produced general material balance relationships for plate columns with carry-over of each phase in both directions. They show that these relations can be reduced to standard forms by suitably defining flow rates and compositions. Thus efficiencies can be determined if the relevant flow rates and compositions are known. Equally, entrainment and weep rates can be deduced if the efficiencies and compositions of a plate operating under these conditions are known.

The Michigan report of the A. I. Ch. E. research program (2) in the short section of 'Froth Stratification' mentions that a very brief photographic investigation of the mechanism of froth production from a bubble-cap was carried out. It was found that, at all gas velocities in

the normal operating range, the vapour issued from the slots as a continuous jet which was subsequently broken down into bubbles. Unfortunately, the application of the observations made to correlations of mass transfer rates and prediction of efficiencies was not considered possible. Recently, Rennie and Smith (22) published certain observations of the production of froths by bubbling from submerged orifices. Attention was restricted to single orifice deep pool bubbling and the true condition obtained on an operating sieve plate was not studied. The authors were apparently unaware of the work carried out by Helsby in 1958 (28). Helsby showed that the horizontal coalescence of the bubbles from multiple orifices markedly affected both the bubbling pattern and the froth produced.

Reported in this thesis are visual studies of the froth, its general structure and mechanisms of formation and breakdown, obtained on a small sieve plate. The effect upon foam structure of the absolute surface tension and viscosity of the liquid phase was also studied.

Chapter 1.2. EQUIPMENT AND PHOTOGRAPHIC TECHNIQUES

Since the processes involved in the generation and degradation of the froth occur so rapidly, it is not possible to follow events with the unaided eye, nor adequately by normal cine-photography. In order to improve definition, two techniques of high speed photography were employed.

The processes of bubbling, weeping and entrainment, being very short time varying phenomena, necessitated the use of very high speed cine-photography. For this purpose, a Fairchild camera and synchronized stroboscopic light source were purchased with a generous grant from D.S.I.R. The camera was capable of speeds up to 10,000 f.p.s. full frame or 20,000 f.p.s. half frame and the strobe, manufactured by Impulsphysik, was capable of flash rates of $10^5 sec^{-1}$ with a minimum flash time of 0.5 microsec. and 4 joules power.

The general foam structure was studied with the aid of single shot photography. Again, the very fast movement of the bubbles in the froth required very short exposures of approximately micro second duration. The camera used was a standard Kodak Specialist $\frac{1}{2}$ plate camera (adapted for $\frac{1}{4}$ plate format). The light source used was an Ernest-Turner 2 microsec. 5 joule flash gun.

Film for both cameras was chosen to possess very fine grain size and fast emulsion speeds. Eastman Kodak 'Tri-X' was used in the Fairchild camera; this has a strong polyester base capable of with-

standing the tensions set up during the initial acceleration when operating at nominal framing rates of 5000-6000 f.p.s. Development was by commercial processing. Ilford '$\frac{1}{4}$ plate N5.31 fine grain ordinary' negative film was used for the flash photographs; the negatives were developed in Ilford 'PQ Universal' developer under normal conditions.

The main programme of observations was carried out on an air/water simulator rather than on a distilling column. Such a set-up was far more suitable for preliminary studies and any conditions could be set up at will. The column used had flat walls and was made completely out of perspex to reduce viewing problems. It is described in detail in appendix A.1.1.

In all the photographic work, three major problems were continually encountered:

(1) Liquid flowing down the inner surface of the wall produced lens effects which blurred vision. Stray bubbles dragged down to the plate surface caused similar troubles when the bubbling mechanism was being photographed.

(2) Associated with the lens effects of the bubbles and liquid films was the impossibility of obtaining a depth of focus of more than one or two bubble diameters in the turbulent froth.

(3) When using rear lighting, there was always a considerable loss of the input light power by scattering at the myriad of bubble surfaces. The last problem presented a considerable dilemma, for frontal

lighting produced strong highlights on the nearest bubble surfaces, so obliterating all definition of the froth structure. Rear illumination provided the best quality of lighting at the image plane; but to obtain an adequate intensity very high energy light sources had to be used.

Since rear lighting from the back wall is so inefficient, an improvement could be obtained by effectively placing the light source in the foam just behind the image plane. In fact this was tried using a flexible random quartz fibre probe. The probe, 12in. long and $\frac{1}{2}$in. diameter, consisted of a large number of parallel, fine (5μ) quartz fibres. Each of these fibres is surface coated with a material of somewhat lower refractive index. A high proportion of the light introduced at one end is therefore transmitted to the other end by total internal reflection at the side walls, and the light emerging from a bundle of fibres is nearly parallel (in fact the probe used had a transmissivity of about 80%). Light from the power source was condensed on to one end face of the probe and its other end was placed in the middle of the foam projecting the light towards the camera. Unfortunately, such a large object in the foam created serious distortions in the structure and improvement in the illumination was offset by these distortions. It was not feasible to reduce the probe diameter significantly for two reasons. Firstly, condensing such a large power source to a point of about $\frac{1}{8}$ in. diameter would produce an enormous local concentration of heat. More important is the fact that the field of illumination produced by a point source of light just behind the image plane would be

insufficient for the required field of view.

The lighting technique finally adopted was that of simple rear view lighting, the light source being placed directly behind the rear window of the column. No diffuser plate was used as the foam itself balanced the illumination level.

Note: All photographs of the dispersion reproduced in this thesis are actual size and the plane of focus is $\frac{1}{2}$ in. beyond the inner face of the window.

Chapter 1.3. THE EFFECT OF PLATE GEOMETRY AND VAPOUR RATE ON DISPERSION STRUCTURE

It was expected that the mechanisms involved in the generation and breakdown of a froth would be similar for pentane and air/water; however, a few preliminary observations of bubbling and entrainment of the n-pentane/iso-pentane system under distillation conditions were made with the aid of the high speed cine camera.

1.3.1 Preliminary Visual Studies of the Bubbling Process

Runs were carried out on the 4" rectangular column described by Macmillan (5). However, instead of using all the available bubbling area, only five adjacent holes in a line were allowed to pass vapour. The holes were $\frac{1}{8}$" dia. on $\frac{1}{4}$" pitch.

It was found that although the holes appeared to bubble independently, the bubbles formed at adjacent holes possessed a considerable attraction for each other as well as the normal vertical attraction of successive bubbles from any particular hole. It further appeared that bubble trains were not longer than three to four bubbles long. Clear vision of this phenomenon was impossible however owing to the blurring effect of old bubbles being dragged to the plate floor by the natural circulation of the process. These observations agreed well with Helsby (28) who studied similar plate geometries but used liquids of far higher viscosity, of the order of 1 poise.

TABLE 1.1

Characteristic dimensions of plates

PLATE NO.	1	2	3	4	5	6	7	8
HOLE DIA.	1/16"	1/16"	1/16"	1/8"	1/8"	1/8"	1/4"	1/4"
APPROX. FREE AREA	5%	10%	15%	5%	10%	15%	10%	15%
P/D RATIO	4	3	2	4	3	2	3	2

TABLE 1.2

Table of vapour rates and plate geometries studied

Gas Rate M/Sec. / Plate No.	RUN NUMBER					
	0.23	0.61	0.99	1.37	1.75	2.15
1	1	2	3	4	5	6
2	7	8	9	10	11	12
3	13	14	15	16	17	18
4	19	20	21	22	23	24
5	25	26	27	28	29	30
6	31	32	33	34	35	36
7	37	38	39	40	41	42
8	43	44	45	46	47	48

FIG. 1.1.

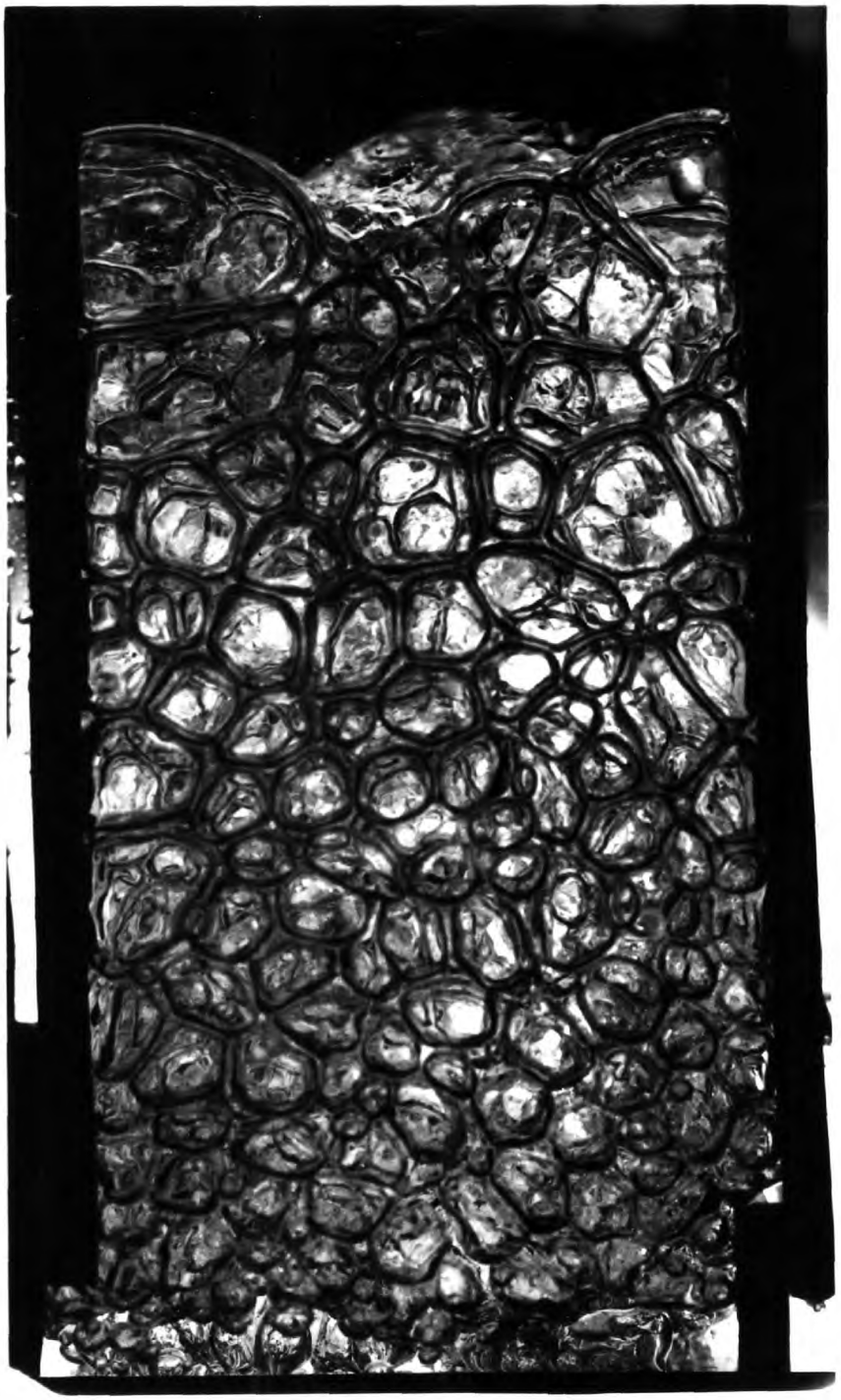

V_s = 0.23 M/sec.

(1/16 in. holes 10% f.a.)

FIG. 1.2.

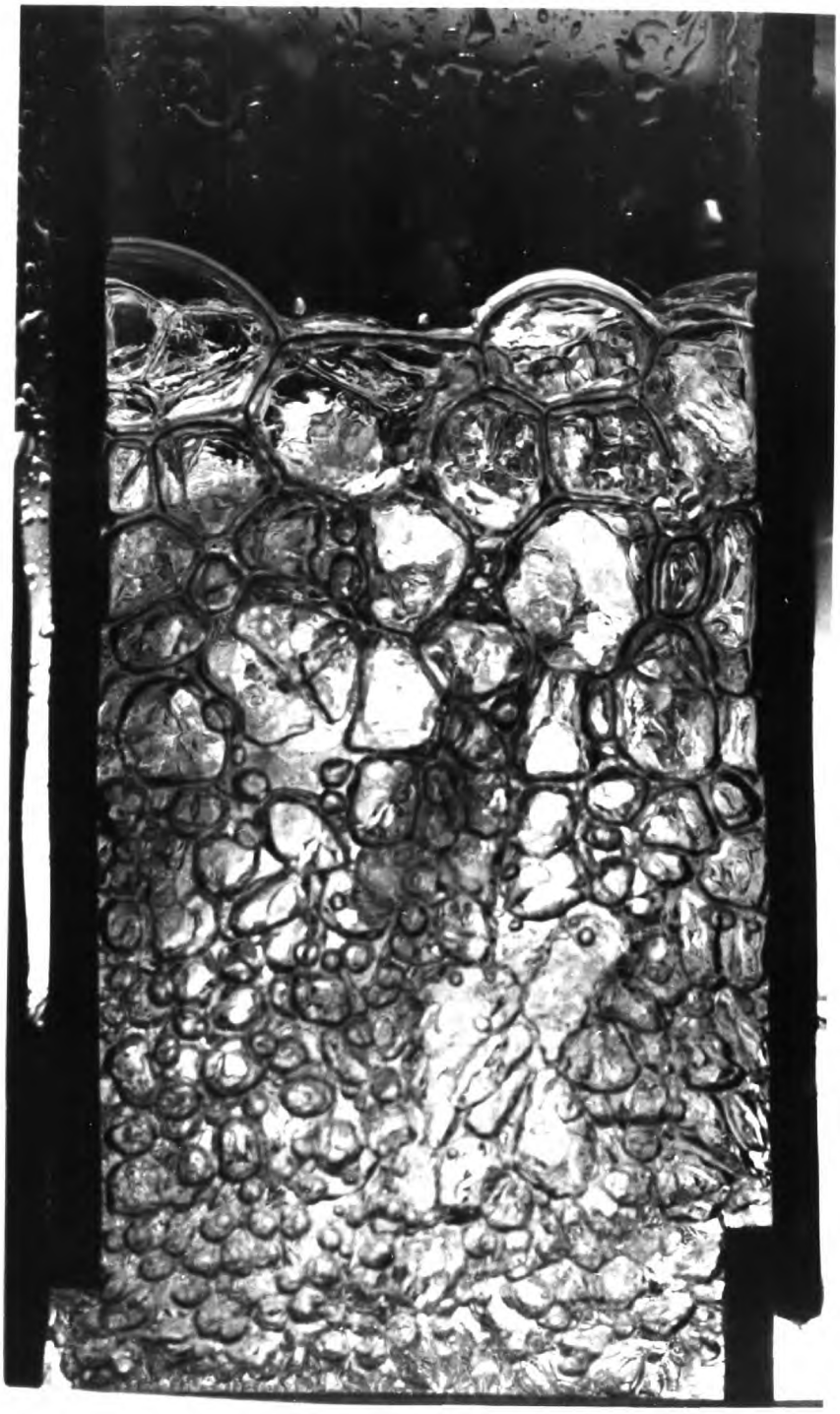

V_s = 0.61 M/sec.

(1/16 in. holes 10% f. a.)

FIG. 1.3.

V_s = 0.99 M/sec.

(1/16 in. holes 10% f.a.)

FIG. 1.4.

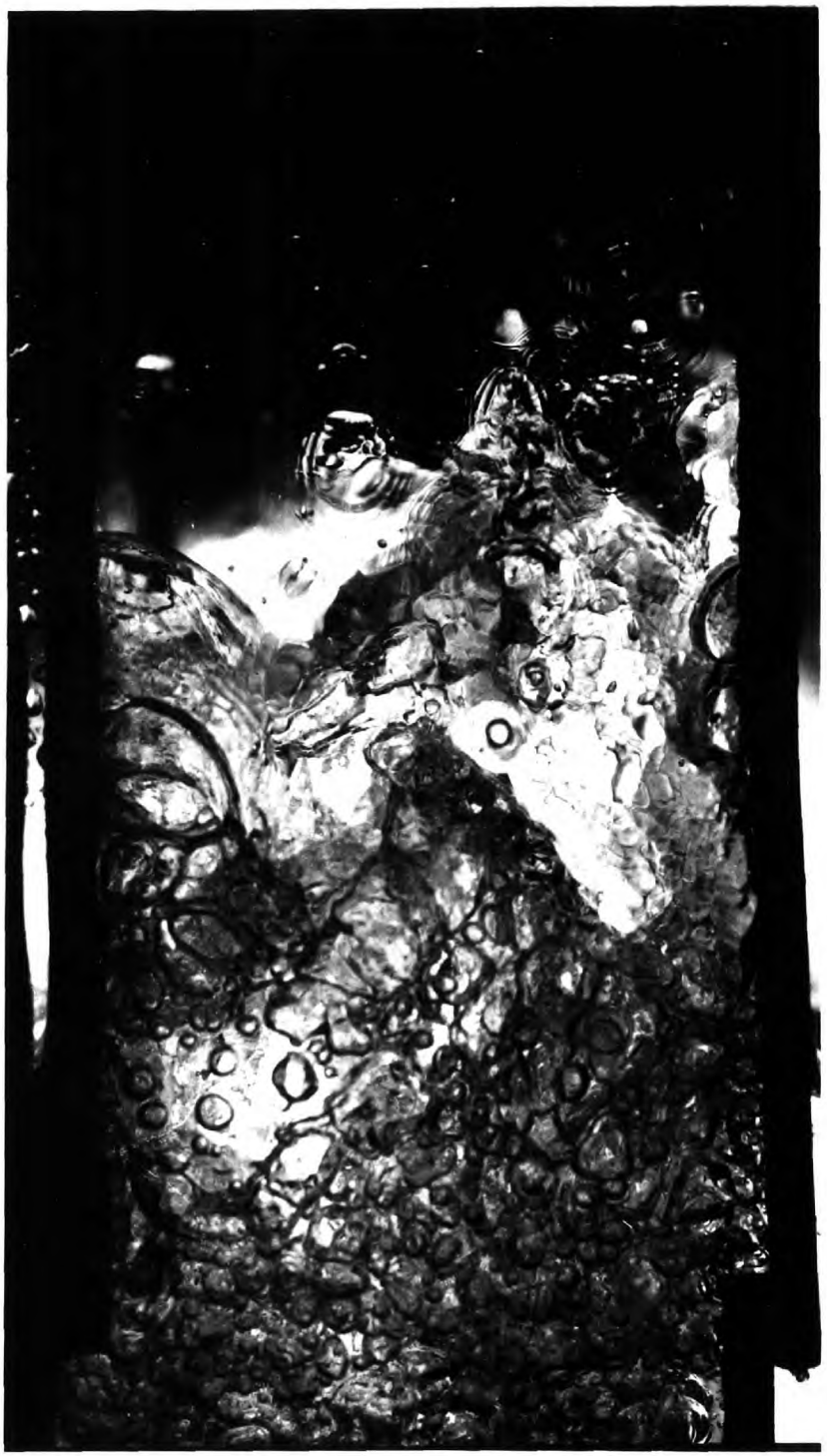

V_s = 1.37 M/sec.

(1/16 in. holes 10% f.a.)

FIG. 1.5.

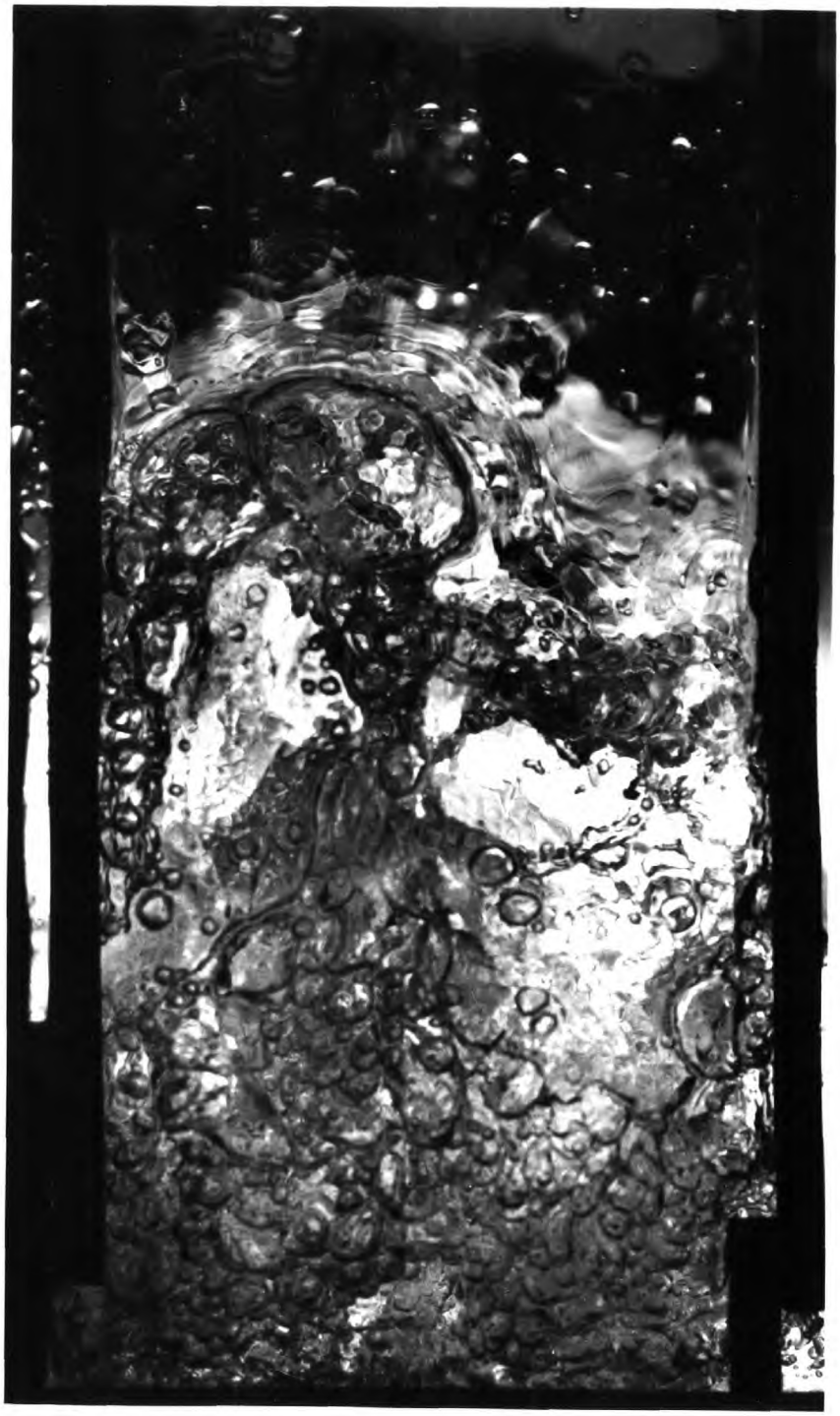

V_s = 1.75 M/sec.

(1/16 in. holes 10% f.a.)

FIG. 1.6.

V_s = 2.15 M/sec.

(1/16 in. holes 10% f.a.)

The actual shapes of the bubbles during formation were however very different. Helsby always obtained pear shaped bubbles, whereas with the pentane system the bubbles spread out across the plate. Sometimes the bubble diameter would be as great as about 3 orifice diameters and coalescence of adjacent bubbles would occur at plate level. This difference in behaviour was probably due to the very great difference in viscosity of the system.

1.3.2. Main Program of Observations of Dispersion Structure

The main program of observations was conducted on the rectangular perspex column. The studies of the effects of vapour rate and plate geometry were carried out with the air-water system. The system glycerol/water and air was used in the study of the effect of viscosity on froth structure.

The liquid rate in the air-water runs was 4 litres/min. A rate of 2 litres/min. was used for the viscosity studies. Superficial air rates (Vs) ranged from 0.23-2.15 M/sec. The geometries of the plates studied are given in Table 1.1. Details of the plate geometries and gas rates for the various runs are given in Table 1.2., all plates were $\frac{1}{8}$" thick.

1.3.2i The Effect of Vapour Rate on Dispension Structure (plate 2)

The sequence of figures (1.1. - 1.6.) for plate 2 typically shows the way in which the foam character changes as the vapour rate is increased from 0.23 to 2.15 M/sec.

At the lowest vapour rates the foam possesses a well defined cellular structure. This is maintained up to a vapour rate of about 0.9 to 1.2 M/sec. In this region the well defined cellular foam breaks down to a highly agitated froth of indeterminable structure. At the highest vapour rates (1.75 and 2.15 M/sec.) the surface of the froth was surmounted by a region of spray.

The cellular foam obtained at the lower vapour rates appears to consist of fairly thick lamellae around each bubble. This may be in part an optical illusion and in part the effect of the wall supporting the foam. It is interesting to note that in the plane of the wall, each bubble is surrounded by five or six nearest neighbours. This is the low energy state configuration that stable foams adopt (28). At the higher rates when the rigid foam structure breaks down, small thick walled bubbles can be seen streaming down the walls. These bubbles tend largely to obscure vision of the interior and eruptions at the surface cause large optical distortions on the upper part of the wall. At the highest vapour rates, there are considerable local variations in the density of the photographs. These variations suggest the presence of either large gas bubbles or gas jets - in either case this would mean that gross vapour by-passing was occurring.

The foam height decreases steadily as the vapour rate is raised from 0.23 to 1.37 M/sec. After this transitional region of velocity, the foam height rises again, though since the froth is so agitated, the time average froth height is not as easily determinable.

FIG. 1.7.

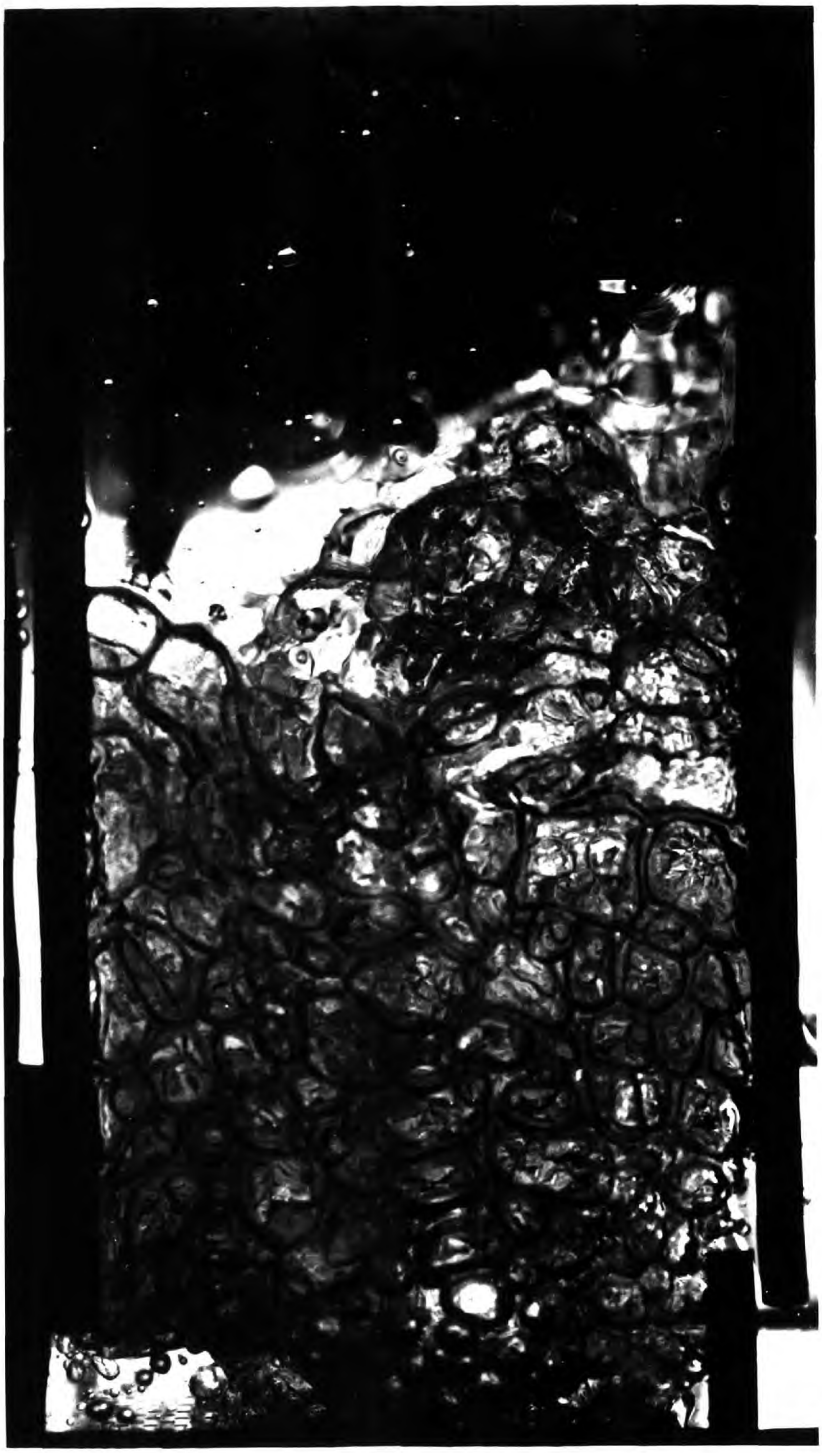

V_s = 0.61 M/sec.

(1/16 in. holes 15% f.a.)

FIG. 1.8.

V_s = 0.61 M/sec.

(1/8 in. holes 15% f.a.)

FIG. 1.9.

V_s = 0.61 M/sec.

(1/4 in. holes 15% f. a.)

FIG. 1.10.

V_s = 1.75 M/sec.

(1/16 in. holes 15% f. a.)

FIG. 1.11.

V_s = 1.75 M/sec.

(1/8 in. holes 15% f. a.)

FIG. 1.12.

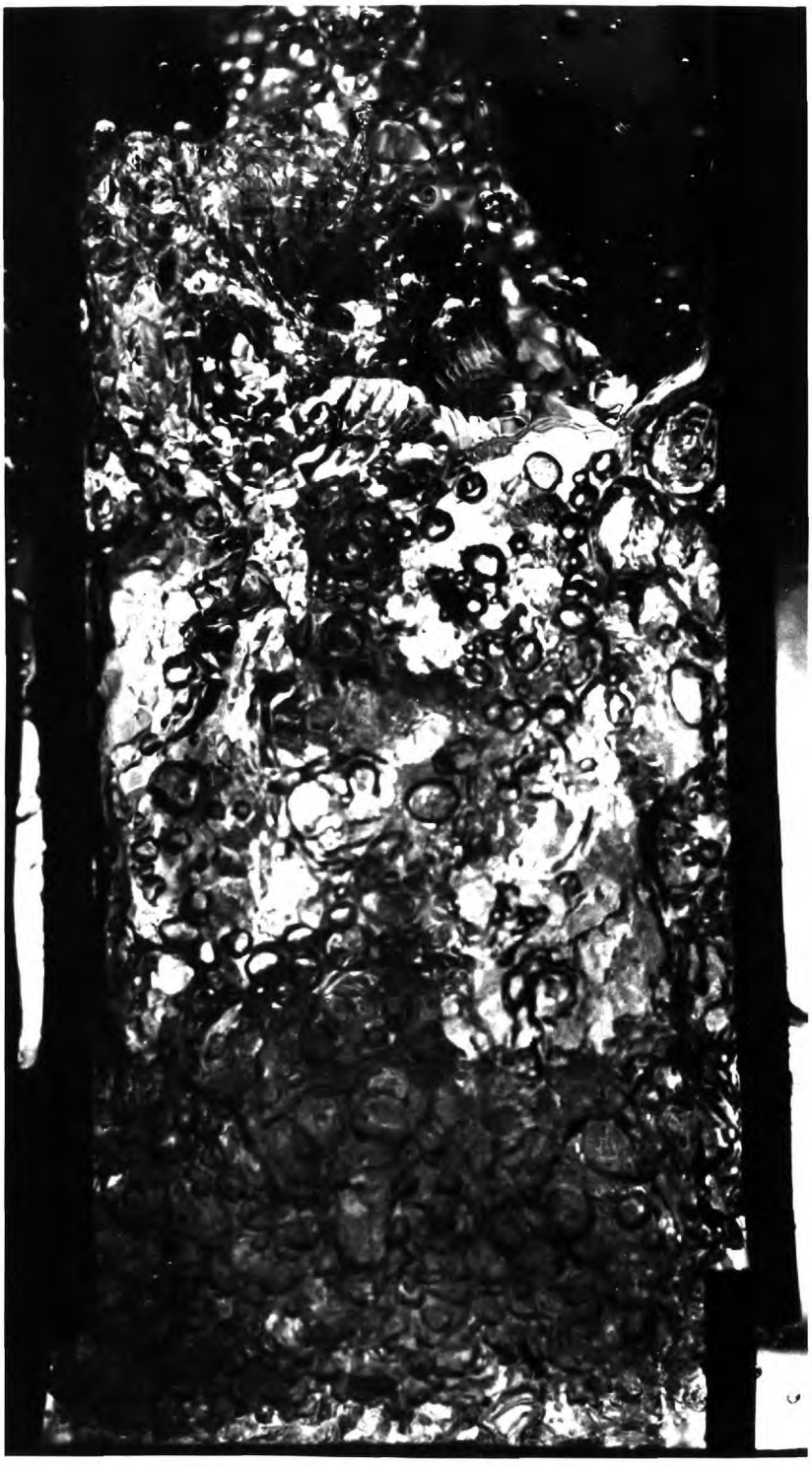

V_s = 1.75 M/sec.

(1/4 in. holes 15% f. a.)

1.3.2ii The Effect of Hole Size on Dispersion Structure (Plates 3, 6 & 8)

The effect of the hole size can be seen from the sequence of figures (1.7., 1.8., 1.9.) and (1.10., 1.11., 1.12).

At the lowest column velocity (0.23M/sec), the foam structure was different for the three hole sizes studied. The foam height for the smallest holes (1/16 in. dia. plate 3) was over 5 in. high, whereas the larger holes produced foams only $3\frac{1}{2}$ to 4 in. high. The 1/16 in. holes also generated a foam that looked to be quite regular in cell shape and size. Although vision through the nearest layer of bubbles was limited, it appeared for this plate that the internal structure was the same as at the walls. The cell size of the foam increased from approximately $\frac{3}{8}$ in. to $\frac{5}{8}$ in. with height above the plate floor. For plates 6 and 8, the foam produced was less clearly defined and less rigid in structure. The cell size increased from about $\frac{3}{4}$ in. to 1 in. with height above the plate floor.

Increasing the vapour rate to 0.61M/sec. caused the foam on plate 6 to increase considerably in height to 6 in. The foam on the plate appeared to exist right down to the plate floor - the bubbles, after formation and breakaway, joining the foam as discreet cells (figure 1.8). The foams on plates 3 and 6 were then much more similar. The foam produced by the largest holes on plate 8 was changed in the same way as for plate 6 but to a much lesser extent.

At the vapour rate of around 1.0M/sec. the foam on all three plates began to change as explained in chapter 1.3.2i. and observation of the froth

FIG. 1.13.

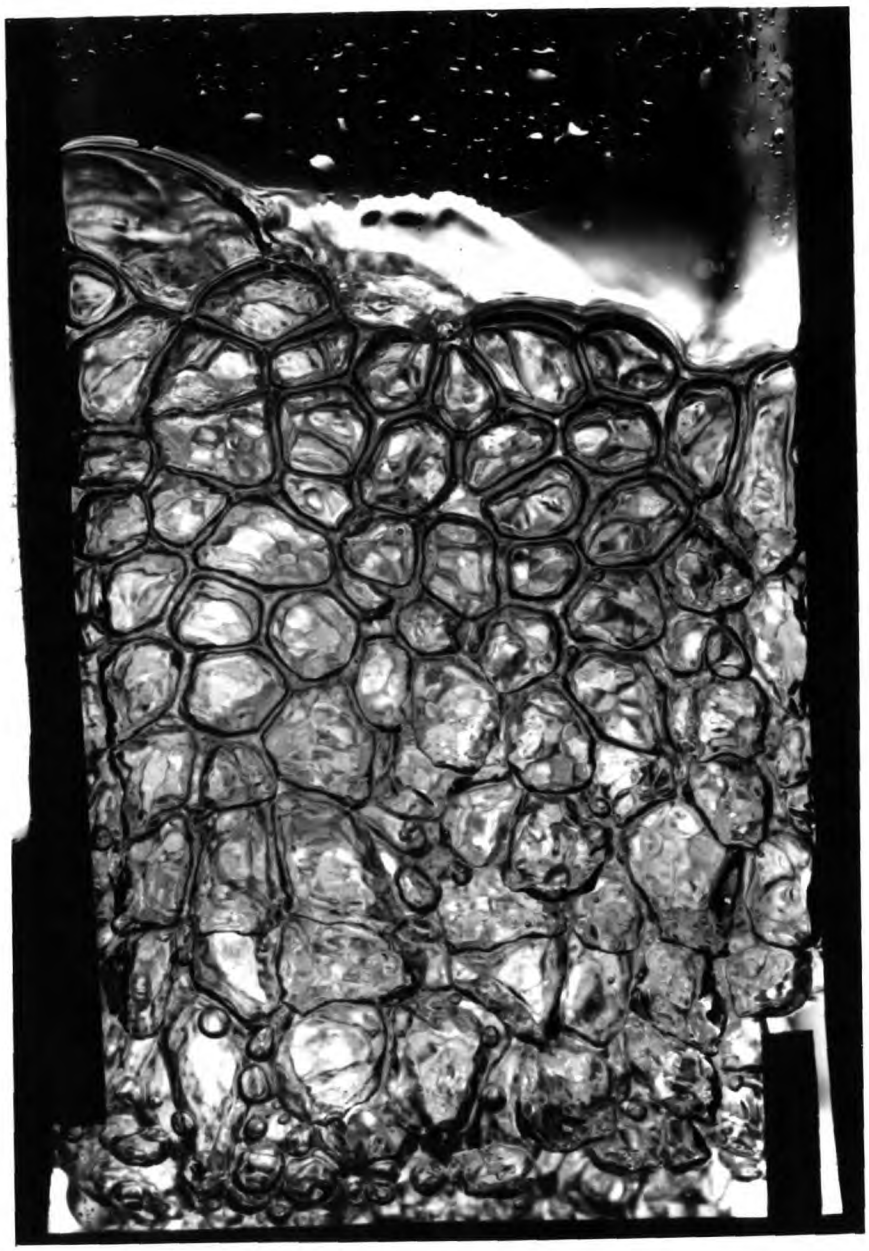

V_s = 0.23 M/sec.

(1/16 in. holes 5% f.a.)

FIG. 1.14.

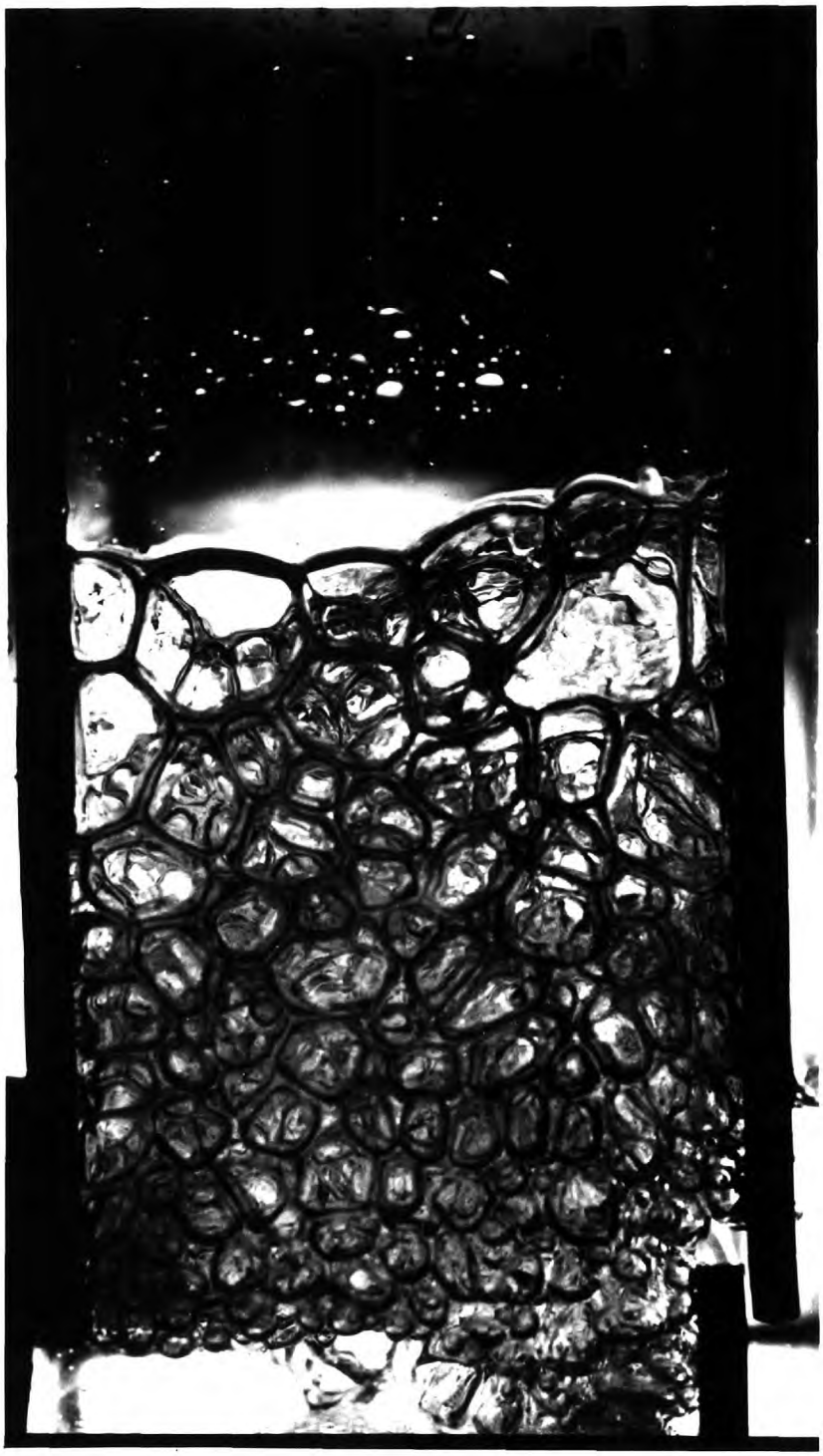

V_s = 0.23 M/sec.

(1/16 in. holes 15% f. a.)

FIG. 1.15.

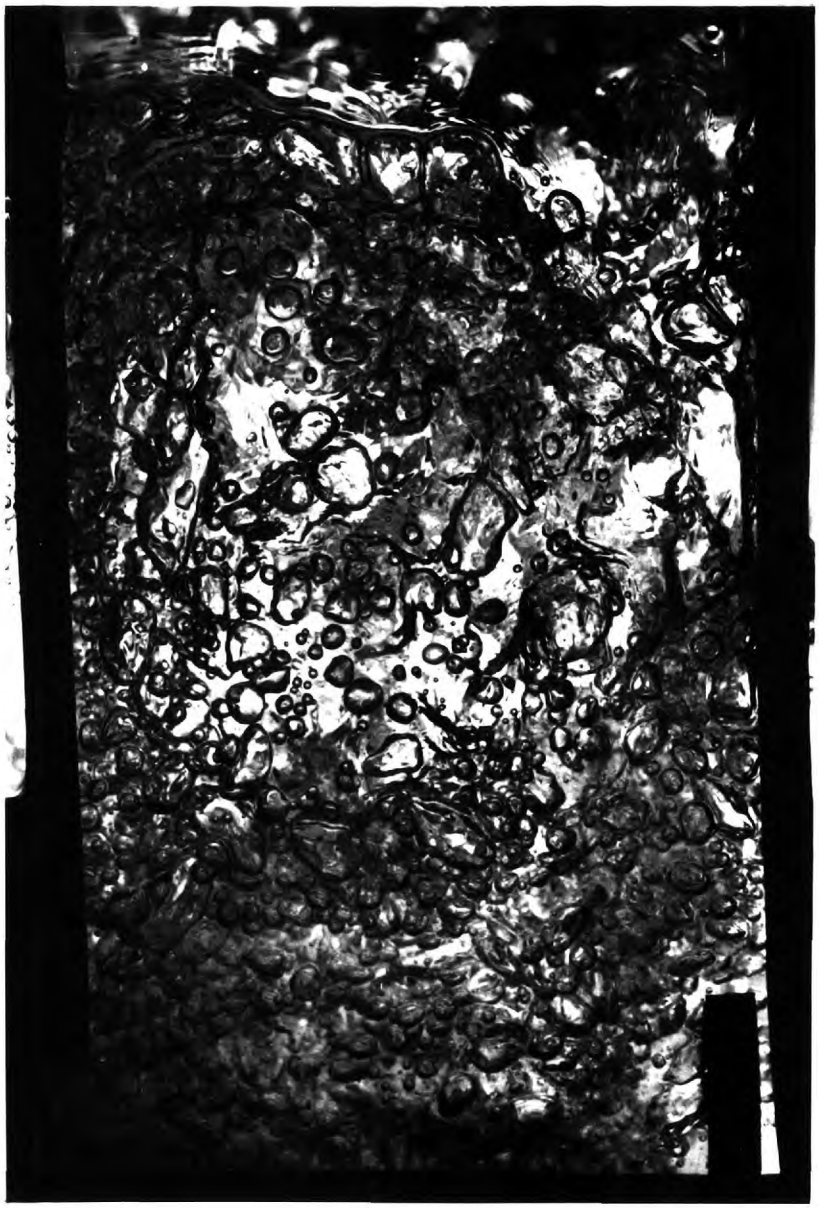

V_s = 1.75 M/sec.

(1/16 in. holes 5% f. a.)

became much more difficult. However it appeared, in this changed regime of froth dispersion, that hole size did not affect the quality of the froth to any marked degree.

1.3.2iii The Effect of Plate Free-Area on Dispersion Structure

(Plates 1, 2, 3, 4, 6)

The effect of free area can be observed from figures (1.13., 1.1., 1.14.) and (1.15., 1.5., 1.10.).

At low vapour rates, the foams generated on plates 1 and 2 are very similar in both height and texture. However, the whole of the plate floor is not active for plate 3 at the lowest vapour rate of 0.23M/sec. This condition could be observed with plates 6 and 8 at the same air rate and is not the result of the plate floor being grossly non-horizontal.

At medium air rates no marked effect of free area could be discerned for plates 1, 2 and 3. However, at the high air velocities, the froth formed on plate 1 was somewhat higher than that on plates 2 and 3.

Comparison of plates 1, 3, 4 and 6 (i.e. low and high free areas for 1/16 in. and $\frac{1}{8}$ in. holes) showed similar effects. At low vapour rates, the structures of the foams on the low free area plates for both hole sizes appeared more rigid than the froth on the high free area plates. At high velocities, the froth heights were consistently about 2 in. higher for the low free area plates. Although vision of the interior is limited it can be seen that the cellular structure breaks down at around 1.0M/sec for all plate geometries.

1.3.3. Conclusions

It can be deduced from the observations reported above that for any given liquid flow rate, it is the superficial velocity of the gas that is the most important parameter determining the structure of the dispersion. Variations of hole size and plate free area were only of rather secondary importance.

In agreement with de Goederen (32), Pozin (7, 33) and many others, more than one regime of dispersion was observed as the vapour loading was increased from the lowest to the highest levels used in commercial equipment. The various regimes usually have been defined in terms of the dispersion height and structure as shown below. Pozin (7) considered

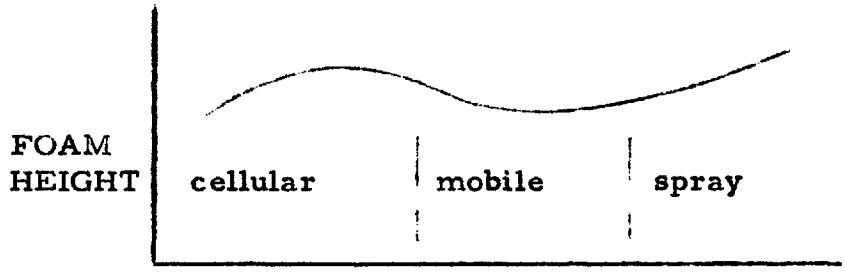

The Effect of Vapour Rate on Dispersion Structure

that the cellular structure gave way to an indescribable mobile froth at medium vapour rates and that this in turn degenerated to a spray régime at the highest vapour rates. De Goederen, on the other hand, considered that the cellular régime on breakdown formed a spray régime. Both these authors restricted their studies to use of the unaided eye. Hence the

alternative definitions resulted not from studying systems of grossly differing behaviour, but probably from the difficulty of observing just what is happening on the plate.

The observations for the air-water system reported in this thesis suggest that, for the normal region of commercial operation, only two regimes of dispersion exist. At low vapour rates an "almost rigid" structure could always be observed. At somewhat higher superficial vapour rates, the rigid structure broke down and the dispersion was clearly highly agitated. To describe this regime accurately would be most difficult. However, most of the photographs (e.g. figure 1.15) presented do suggest that some sort of cellular bubble structure does still exist.

Calderbank et al.(9, 12) refer to this agitated dispersion as a "bubble cloud" of small thick-walled bubbles floating in the dispersion with occasional by-passing of gas. However, as described earlier, it is considered that the small thick-walled bubbles exist mainly in the region of the walls and that the interior of the dispersion still possesses a weak cellular structure. There is apparently distinct slopping of the dispersion with ligaments of liquid being thrown up on alternate sides of the column. The result of this turbulent state is that frequently very large gas bubbles, or even gas jets, are produced in the regions of the plate where the hydrostatic head is relatively low. This must inevitably lead to gross by-passing of the gas. Under no conditions was a true spray formed on the plate; it was, however, possible to produce this condition at the highest gas rates

with very low liquid rates of the order of 0.5 litres/min. Since liquid gas molar ratios in distillation columns are of the order of unity, it is likely that true sprays are only obtained under freak dynamic conditions or in badly designed columns.

To see if the foam produced at low velocities was supported on top of liquid flowing virtually undisturbed along the plate floor, a simple experiment was conducted. A pulse of permanganate dye was injected into the top layer of the foam at different positions and the rate at which it mixed into the mass of froth observed. This was repeated for various points on the floor of the plate from inlet to outlet weirs. Although the mixing was only observed by eye, no difference at all in mixing rate could be detected. The experiment was admittedly fairly crude, but it showed that mixing was very rapid and fairly uniform and that there was no stagnant foam layer present.

The effect of hole size was only noticeable in the cellular foam regime where small holes produced a slightly more well defined foam than larger holes. At high velocities, hole size had no discernable effect on the dispersion character. At low velocities, there was little effect of free area on the foam. However at high column velocities, the lower free area plates gave consistently greater dispersion heights. These observations are to be expected, for the quality of the dispersion would naturally depend upon the initial projection or hole velocity as well as the column velocity.

It is most interesting to observe for the air-water system that the

column velocity at which the cellular foam regime breaks down is quite independent of plate geometry. In all cases this transition velocity was around 1 M/sec. Zuiderweg and Harmens (10) also found that, for any system, there was a characteristic velocity above which a cellular foam could not exist. Analysis of de Goederen's results (32) shows the same effect, though the transition velocity was a function of liquid hold-up.

That the transition velocity is independent of the plate geometry raises the question of whether viscous, surface or inertial forces are dominent in determining the form of the dispersion generated. It was therefore decided to investigate the effects of bulk viscosity and surface tension upon the nature of the dispersion.

Chapter 1.4. EFFECT OF PHYSICAL PROPERTIES ON DISPERSION STRUCTURE

1.4.1. The Effect of Bulk Viscosity on Dispersion Structure

The effect of absolute viscosity of the liquid on the dispersion character was studied in the same perspex simulator used in the main program. Air was passed through glycerol/water mixtures of viscosities ranging from 2.5 cp. (34% glycerol) to 12.5 cp. (62.5% glycerol). The liquid rate was maintained at 2 litres/min. Glycerol and water were used for a number of reasons, the most important, obviously, being the wide range of viscosity obtainable. At the same time, the surface tensions of water (72 dynes/cm) and glycerol (64 dynes/cm) are not greatly different, and particularly, the densities of the mixtures were all approximately 1 gm/cc. It was essential that the density of the mixture should not be varied much for otherwise the inertial effects of the fluids might be changed.

Flash photographs of the dispersion were taken for various gas rates, viscosities and plate geometries as shown in Table 1.3.

1.4.1i. The Effect of Vapour Rate for different Liquid Viscosities

For all viscosities, increasing vapour rate had the same general effect on the dispersion structure as discussed in chapter 1.3.2i. As can be seen from figures (1.22 - 1.25), the absolute viscosity had little effect on the quality of the froth, and in particular the transition from cellular to non-cellular dispersion took place consistently at around 0.9 M/sec.

FIG. 1.16.

μ = 10.0 cp. V_s = 0.70 M/sec.
(1/8 in. holes 10% f.a.)

FIG. 1.17.

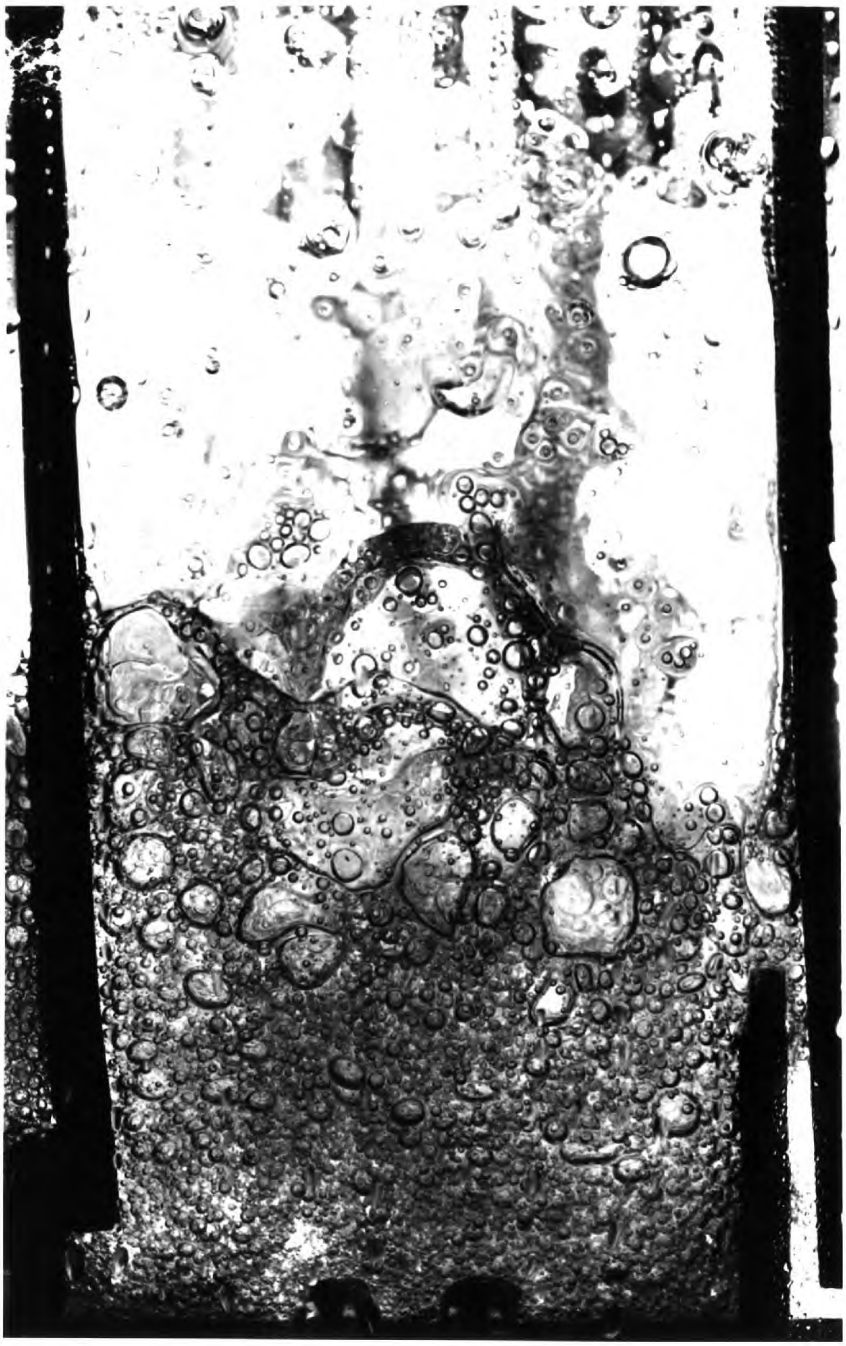

μ = 10.0 cp. V_s = 1.0 M/sec.
(1/8 in. holes 10% f. a.)

FIG. 1.18.

μ = 7.5 cp. V_s = 0.70 M/sec.

(1/8 in. holes 10% f. a.)

FIG. 1.19.

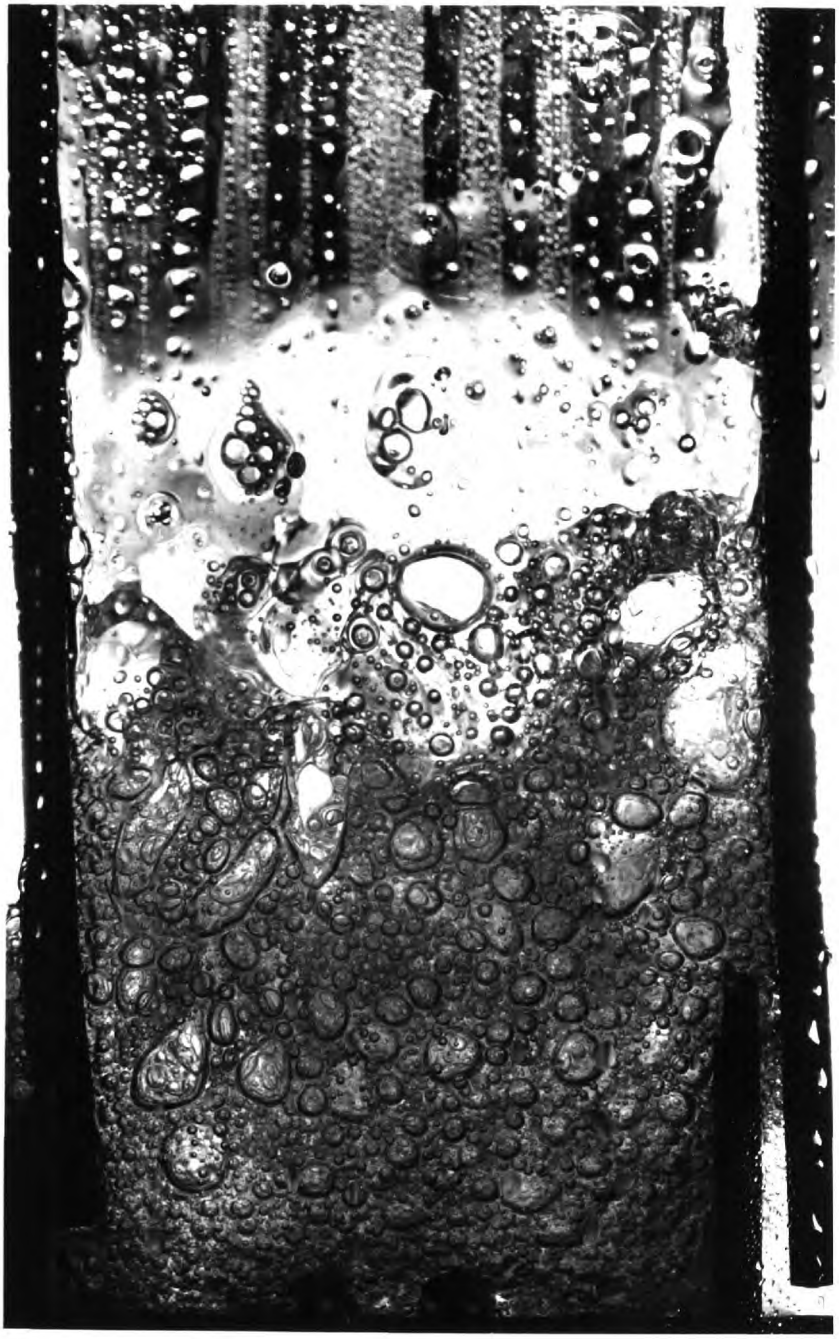

μ = 7.5 cp. V_s = 1.0 M/sec.
(1/8 in. holes 10% f. a.)

FIG. 1.20.

μ = 5.0 cp. V_s = 0.70 M/sec.
(1/8 in. holes 10% f. a.)

FIG. 1.21.

μ = 5.0 cp. V_s = 1.0 M/sec.

(1/8 in. holes 10% f. a.)

FIG. 1.22.

μ = 12.5 cp. V_s = 0.23 M/sec.

(1/8 in. holes 15% f.a.)

FIG. 1.23.

μ = 12.5 cp. V_s = 0.70 M/sec.
(1/8 in. holes 15% f. a.)

FIG. 1.24.

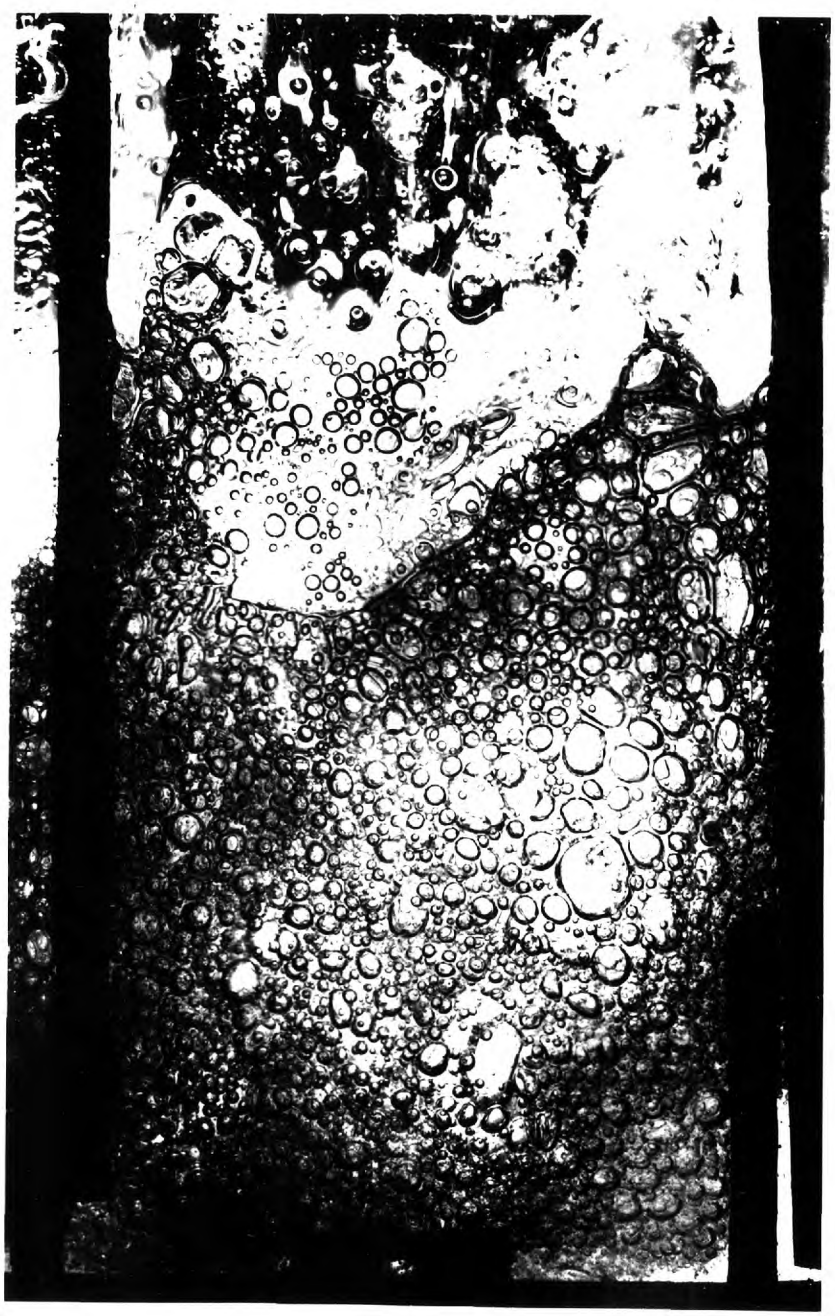

μ = 12.5 cp. V_s = 1.0 M/sec.
(1/8 in. holes 15% f. a.)

FIG. 1.25.

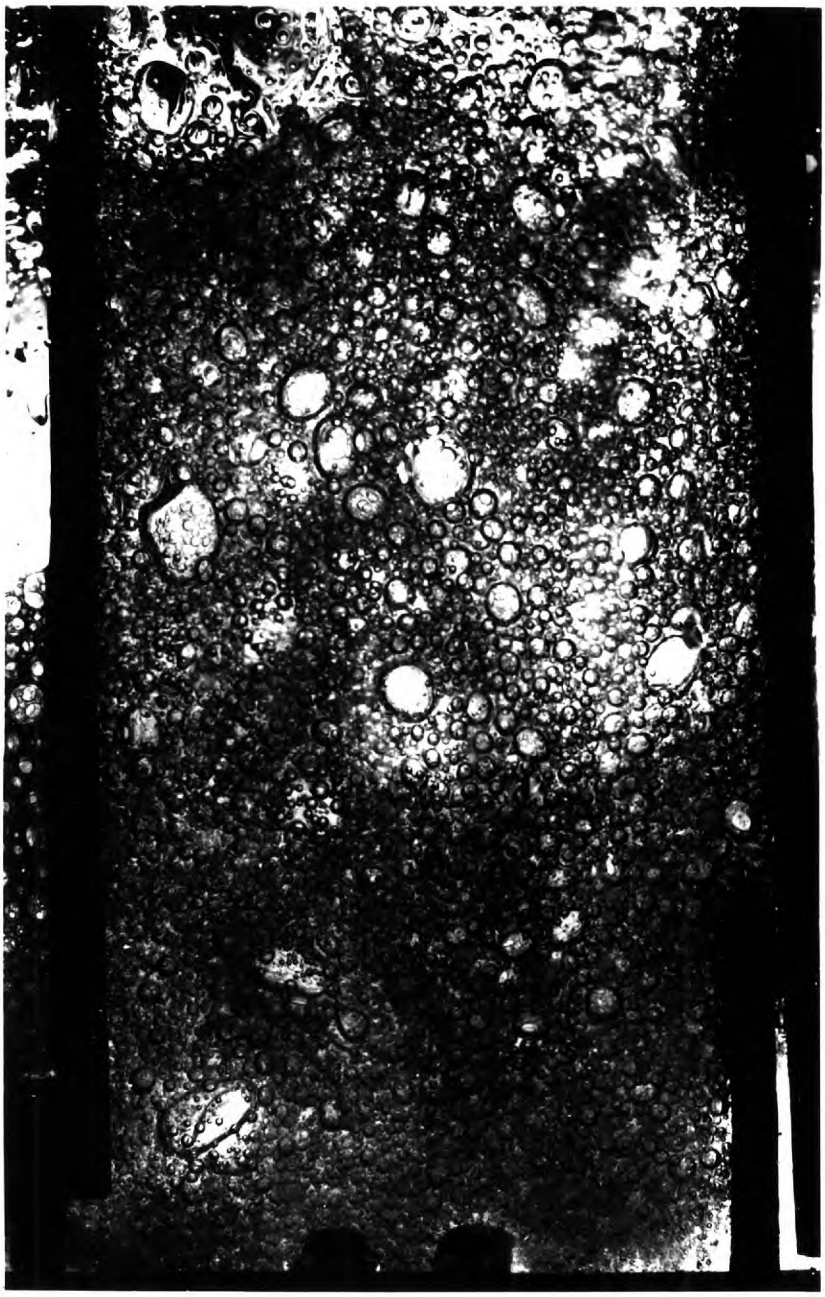

μ = 12.5 cp. V_s = 1.40 M/sec.
(1/8 in. holes 15% f.a.)

TABLE 1.3.

Table of Plate Geometries and Viscosities Studied

Run No.	Plate[x] No.	Superficial Vel. M/S.	Viscosity cp.	Run No.	Plate[x] No.	Superficial Vel. M/S.	Viscosity cp.
1	5	0.23	10.0	17	2	0.23	12.5
2	"	0.70	"	18	"	0.70	"
3	"	1.00	"	19	"	1.00	"
4	"	1.40	"	20	"	1.40	"
5	5	0.23	7.5	21	7	0.23	12.5
6	"	0.70	"	22	"	0.70	"
7	"	1.00	"	23	"	1.00	"
8	"	1.40	"	24	"	1.40	"
9	5	0.23	5.0	25	5	0.23	12.5
10	"	0.70	"	26	"	0.70	"
11	"	1.00	"	27	"	1.00	"
12	"	1.40	"	28	"	1.40	"
13	5	0.23	2.5	29	6	0.23	12.5
14	"	0.70	"	30	"	0.70	"
15	"	1.00	"	31	"	1.00	"
16	"	1.40	"	32	"	1.40	"
				33	4	0.23	12.5
				34	"	0.70	"
				35	"	1.00	"
				36	"	1.40	"

[x]Plate numbers refer to Table 1.1. chapter 1.3.2.

(figs. 1.16 - 1.21).

In the cellular foam régime, the foam height was quite insensitive to changes in viscosity and the rigidity of the foam was unaltered. However, in the non-cellular froth régime the froth height tended to decrease as the viscosity decreased.

1.4.1ii. Effect of Plate Geometry on Dispersion Structure at High Viscosity

For a liquid viscosity of 12.5 cp., the separate effects of hole size and free area were studied. It was found that the dispersion character was affected in exactly the same way as for the low viscosity runs as discussed in chapters 1.3.2ii. and 1.3.2iii.

1.4.2. The Effect of Surface Tension on Dispersion Structure

De Goederen (32) who studied the effects of physical properties on mass transfer in the gas phase for the systems air/water, air/ethanol and air/toluene, concluded that surface tension only had a very slight effect on dispersion height. Particularly, it can be deduced from his results that surface tension had no effect on the transition from cellular to non-cellular régimes. However, a definite correlation did exist between liquid hold-up and the transition velocity. For a hold-up of 1 to 3 cm of liquid, the transition velocity was around 1 M/sec.

An interesting, but simple, experiment was performed that gave further weight to the belief that surface tension was not important in determining the transition velocity. A very small amount of 'Teepol' was added to the water entering the plate. This had the effect of drastically lowering the surface tension of the liquid without altering its density or viscosity.

The effect of the surface active agent on the froth was considerable. At low vapour rates, such a vast amount of thin walled, rigid foam was produced that it flowed out of the top of the column. As the air rate was increased, the foam height slowly decreased, till at approximately 1 M/sec. the foam rapidly collapsed to the mobile structure usually obtained in the absence of the detergent. At vapour rates above the transitional velocity, the presence of the detergent, even in increased amounts, had no effect on the dispersion structure. It is appreciated that the surface forming process may have become so fast at 1 M/sec that the surface active

molecules were no longer able to cover the surface of the liquid and orient themselves correctly; it is interesting, however, that the transition velocity was the same as in all other cases.

From approximate data on the oxygen/nitrogen system operating at atmospheric pressure and 80°K, Gardner (54) has found that below superficial vapour velocities of the order of 0.7 metres/sec. a distinct cellular foam is obtained on a sieve plate. Above approximately 0.72 metres/sec. the liquid appears to exist predominantly in the form of a spray. The surface tensions encountered in the oxygen/nitrogen system are far lower than those studied by de Goederen (32), yet the transition from cellular to non-cellular regime still occurs at a superficial vapour velocity not far below 1 metre/sec.

1.4.3. Conclusions

Naturally, it is important that great care be exercised in drawing conclusions from the observations described above of the effects of bulk viscosity and surface tension on the dispersion structure. However, the observations do agree with the briefly reported findings of other workers.

The viscosity had no great effect on the structure of the dispersion. At low vapour rates, for all viscosities, the foam looked very similar to an air/water foam. The most marked difference could be seen at high gas rates where the high viscosity liquid produced a froth of somewhat greater height than the air water froth under similar conditions. That the transition velocity was unaltered by the viscosity was most clear and important. Reported briefly in the A.I.Ch.E. research report (2) is the observation that viscosity was not a factor affecting foam height or liquid hold-up; however, a detailed study of the effect of viscosity had not been carried out.

The work by de Goederen showed quite clearly that the absolute surface tension of the liquid mixture did not affect the transition velocity for the different systems he studied. However, when surface tension gradients exist in the dispersion its structure may well be affected in the way observed by Zuiderweg and Harmens (10) and Bainbridge (44).

In view of the insensitivity of the dispersion structure to the viscosity and surface tension of the liquid, these properties are likely to be of minor importance in determining the behaviour of an operating sieve tray. It is also probable that the inertial forces between the gas and liquid phases are the most important in producing the dispersion.

Chapter 1.5. MECHANISM OF BUBBLING & DISPERSION GENERATION

1.5i. Photographic Observations

Various suggestions have been proposed in the literature about the bubbling mechanism on sieve plates. It has generally been supposed that at all but the lowest hole velocities, jetting must occur. These views however have not been based upon photographic observation.

To investigate exactly how the two phase mixture is generated, a detailed study was made of the bubbling behaviour of a typical hole in an operating sieve plate. Both still photographic and high speed cine techniques were used on perspex plates in the 4in. perspex simulation column. The behaviour of the hole could only be studied at superficial vapour rates below around 1.5 M/sec., or maximum hole velocities of 30 M/sec., because of the effects of circulation currents at higher vapour rates.

Contrary to the suggestion that one would observe jetting from a sharp-edged orifice, bubbling was observed at even the highest hole velocities studied. Furthermore, the hole frequently contained a collar of liquid; this collar can be seen fairly clearly in figures 1.9. and 1.30. It appeared in fact that the liquid produced a smooth edged orifice whose shape and size varied with the gas flow through it. This in fact is a perfectly conceivable situation for the pressure drop across a smooth orifice of slightly smaller dimensions than a sharp edged orifice is likely to be considerably less. Davidson and Walters (55) in their work on bubbling from single orifices also found intermittent bubbling rather than jetting occurred

even at very high vapour rates.

On formation, the bubbles were far from spherical; in fact bubbles tended to spread across the plate floor to as much as 3 orifice diameters and coalescence with bubbles from adjacent holes even occurred. The extent of this spreading can be observed in figure 1.8. Under the influence of strong local circulation currents, the bubbles issuing from the holes could be bent and elongated to a considerable extent as can be seen from figure 1.9.

At the lower velocities, the bubbles formed as discreet units; but at the higher velocities trains of connected bubbles were formed. The depth of the bubbling zone was never more than one bubble unit and it was impossible to observe the exact way in which the bubbles broke down into the dispersion. It appears possible, however, that the dispersion consists initially of cells produced by the individual bubbles.

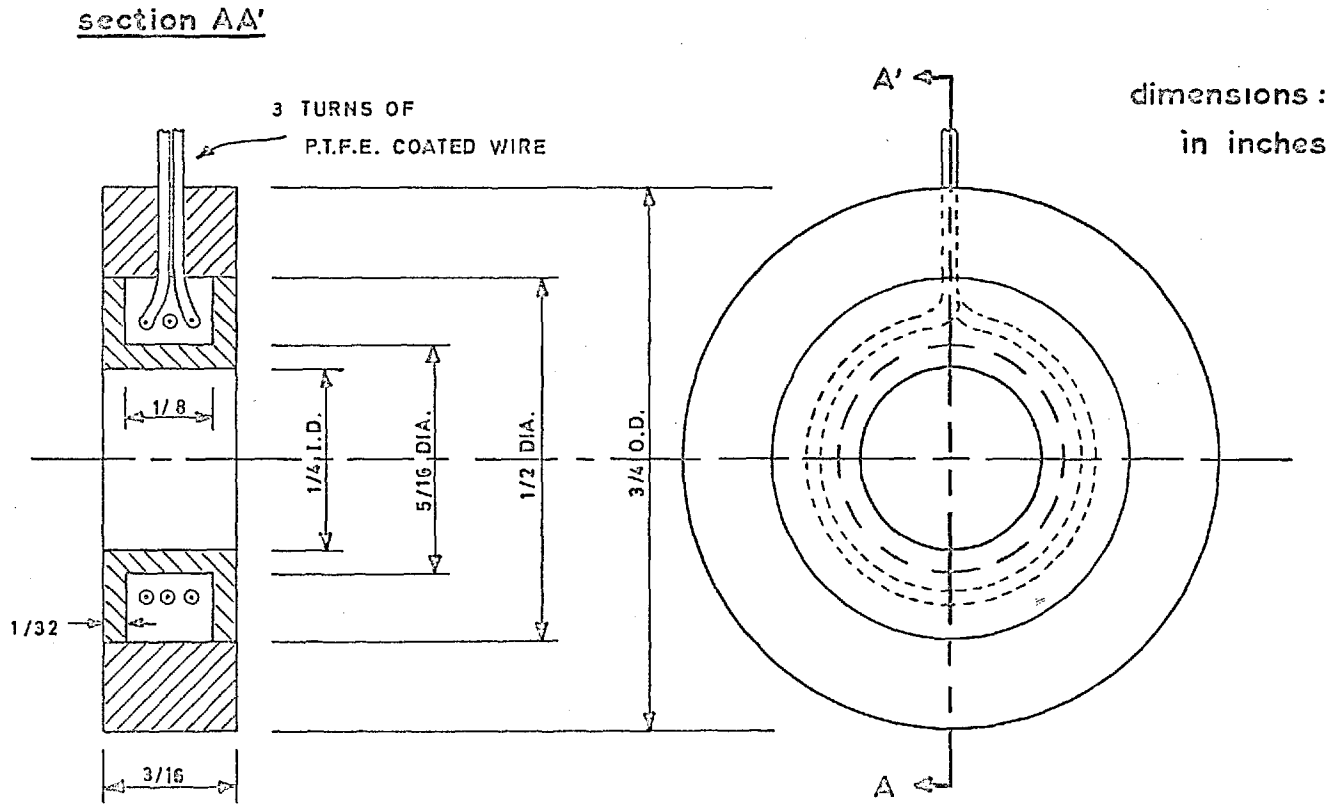

DETAILS OF INDUCTANCE COIL

FIG. 1.29

CIRCUIT DIAGRAM FOR INDUCTANCE MEASUREMENT

FIG. 1.27.

1.5ii. Electrical Studies of Bubbling Frequency

The observation in chapter 1.5i. that a hole usually contained a collar of liquid and that when bubbling ceased, the liquid tended to bridge right across and fill the hole, gave rise to the idea of determining the bubble frequency by measuring the electrical capacitance of the hole.

A number of attempts were made to continuously monitor the capacitance; however, all met with differing degrees of failure. The technique finally adopted was to build a coil into the plate around a hole and observe the variation in inductance as the amount of liquid within the sphere of influence of the coil varied. Details of the coil can be seen in figure 1.26 and the circuit diagram is shown in figure 1.27.

The permeability of the medium surrounding the hole and covering the wire in the coil is extremely important and the only material available with satisfactory dielectric properties was P.T.F.E. Thus a coil of very fine P.T.F.E. coated wire was wrapped on a core of P.T.F.E. tube. This was then housed in P.T.F.E. and the whole assembly fitted into an ordinary perspex plate. The two leads from the coil were taken through the plane of the plate to the column wall.

It can be shown that as the inductance of the coil varies with the amount of fluid present, so the voltage output across it varies. Oscilloscope traces of the voltage variation were recorded on polaroid film.

In practice, two problems prevented the development of the device to a very useful level. The most severe problem arose from the enforced

↑air water↓

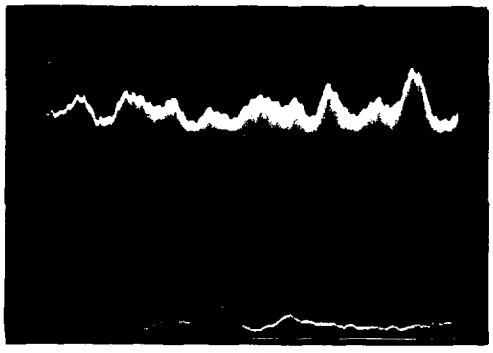

A V_h = 7.5 m/sec.

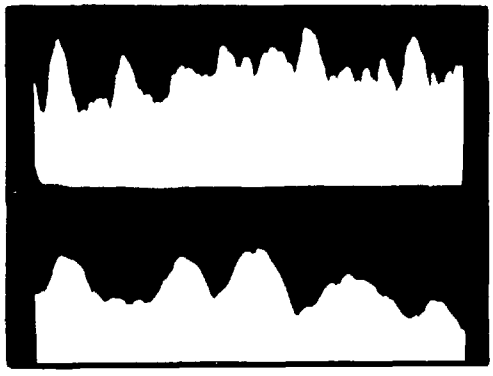

B V_h = 15.8 m/sec.

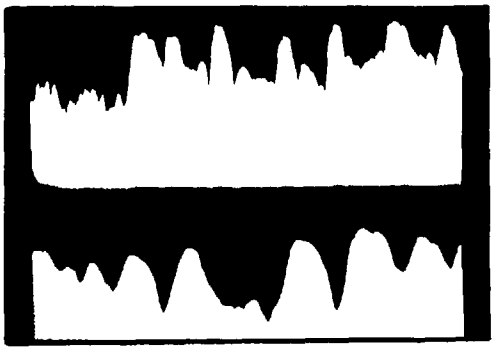

1/2 sec.

1/5 sec.

C V_h = 27.7 m/sec.

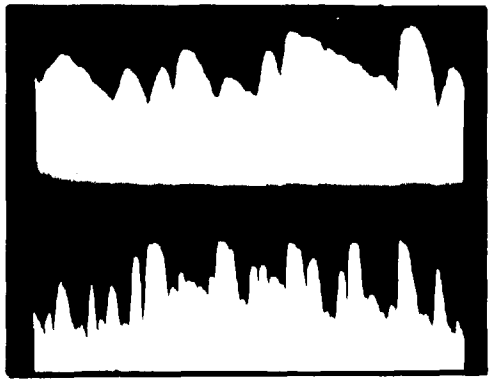

D V_h = 44.2 m/sec.

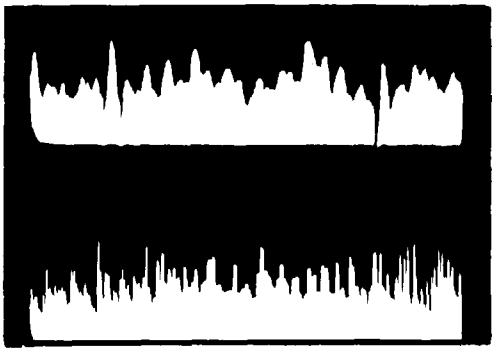

E V_h = 4.3 m/sec.

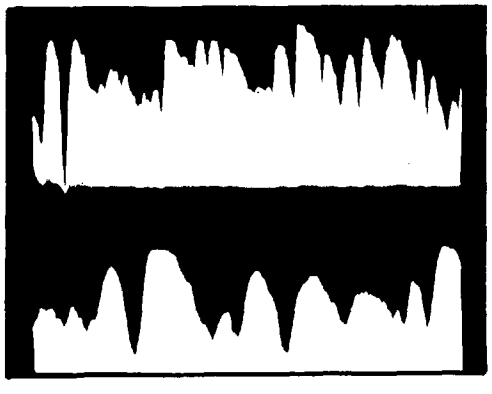

F V_h = 27.7 m/sec.

OSCILLOGRAPHS OF BUBBLING FREQUENCY

use of P. T. F. E. This material is not wetted by water, nor in fact by most other liquids, thus the bubbling mechanism may be different. Secondly, since the inductance of the coil is affected by any material present in its sphere of influence, bubbles at the surface of the plate and stray bubbles brought to the plate floor by circulation currents all affect the periodicity measurements.

Oscilloscope traces obtained using a 5% free area plate and $\frac{1}{4}$in. holes are shown in figure 1.28. Trace A, at low vapour and liquid loadings, shows regular bubbling at approximately 15 per second. However, at higher gas rates, as in traces B, C and D, it is not really possible to assess the true bubbling rate. This is probably because of the effects of stray bubbles at the plate surface. Traces E and F, taken for greater liquid hold-ups, both clearly indicate that weeping from a hole can be detected by the occasional deep trough obtained.

Design of coils suitable for the smaller holes would enable these electrical studies to be extended considerably. From such observations at a pattern of holes in the middle of a plate, more information could be obtained not only on weeping and bubbling characteristics of single holes, but also on the interactions between holes.

Chapter 1.6. MECHANISM OF WEEPING

1.6i. Photographic Observations

When the pressure drop associated with the vapour flow through the holes is less than the hydrostatic head of the liquid above, the liquid "dumps" through the holes. However, even when the plate pressure drop is greater than the hydrostatic head, periodic "weeping" of the liquid through the holes still occurs. Weeping is greatest at lower vapour hole velocities, but it does persist, at a reduced rate, at quite high vapour rates. The reason for this is not clear, but it must be connected with the local variations in hold-up that occur as the result of pulsation and slopping on the plate. The pressure fluctuations occurring when the bubble leaves the plate, as studied by Jameson and Kupferberg (49), must also be contributory.

It was found for the air/water system that weeping did not occur to any extent with 1/16in. holes, even for large free area plates. A more detailed photographic study of weeping from $\frac{1}{8}$in. and $\frac{1}{4}$in. holes was made with the aid of high speed cine photography. The photographic evidence shows very clearly that simultaneous flow of liquid and vapour through small holes does not occur. It may be possible of course for two-phase flow to take place when very large holes ($\frac{1}{2}$in. to 1in.) are used, but then the mechanisms involved are likely to be different. The observation that simultaneous gas and liquid flow does not occur is in agreement with the visual observations of Prince and Chan (13). On the other hand, Jameson and Kupferberg (49) in their photographic studies of two dimensional bubbles

FORMATION OF A WEEPING DROPLET

FIG. 1.29

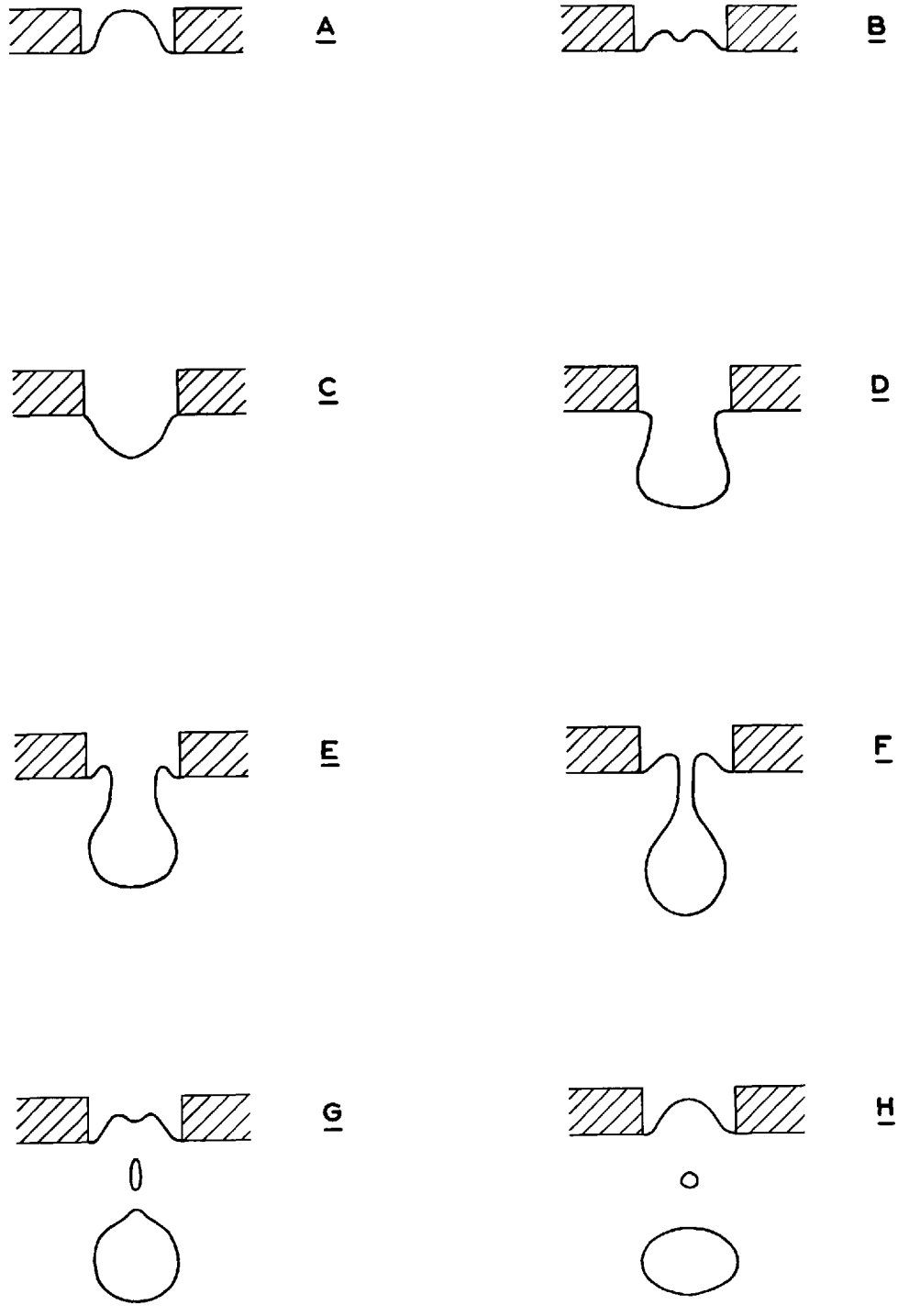

formed at single orifices suggest that simultaneous flow of both phases can occur. This would suggest that the weeping and bubbling processes in single orifice two dimensional holes are somewhat different from those existing on operating sieve plates.

The detailed mechanism of the process is extremely complex and it would appear that a number of slight variations of the basic pattern of behaviour do occur. The development of a weeping droplet can be seen diagrammatically in figure 1.29 and was deduced from studies of cine films

The condition that may be termed "stable bridging" can be seen in (A); a collar of liquid surrounds the hole. From this condition, bubbling from the orifice may recommence as discussed in Chapter 1.5i. or the "unstable bridging" condition (B) may develop. The spur of liquid that has begun to form may continue to condition (C) or the stable condition (A) may be re-established. In fact the whole process of weeping seems to be reversible till after the stage represented in (E). The pendant droplet (C) continues to increase in size to (D) when the first signs of necking can be observed. After this stage, the drop volume appears to remain constant and the process of detachment begins. Thinning around the base of the hole continues as shown in (E) till ultimately the irreversible stage (F) is reached. The thin neck then breaks as shown in (G) and the droplets fall away from the hole. The hole itself is rebridged in the stable way depicted in (H) or (A).

Usually after one cycle of weeping, the hole either remains stably

bridged for a period, or bubbling restarts. It is only when operating in the dumping region that a hole persistently passes liquid. Under these conditions, the stages from (E) to (G) often do not appear and "dripping" from condition (D) occurs.

Chapter 1.7 MECHANISM OF DISPERSION BREAKDOWN AND ENTRAINMENT

1.7i. Photographic Observations

A brief study, using high speed cine and still photographic methods, was made of the air-water dispersion produced in the perspex column.

Even to the unaided eye, it is very clear that there are two types of entrained droplet formed on breakup of the surface of the froth. A very fine mist can always be seen rising out of the column even at low vapour rates. The droplets comprising this mist are so small that their terminal falling velocity is far exceeded by the superficial vapour velocity. However, the mass flow of these particles is less than a fraction of a percent of either vapour or liquid bulk flows and consequently can have very little effect on the performance of an operating stage. At the same time a much coarser spray is generated, the amount of which increases with gas rate. At low gas velocities, in the region of the true cellular foam, there is very little spray apparent. However, as the gas rate is increased a very coarse spray becomes discernible. The droplets in this spray are only projected a short distance, of the order of two to three inches, above the surface of the dispersion. The amount of liquid supported in this spray can however be considerable and if another plate were placed only a couple of inches above the dispersion surface, the amount of liquid carry-over would be very high as observed, for example, by Bernard (6).

The fact that two types of spray are discernible accounts for the

FIG. 1.30.

V_s = 0.23 M/sec.

(1/4 in. holes 10% f. a.)

FIG. 1.31.

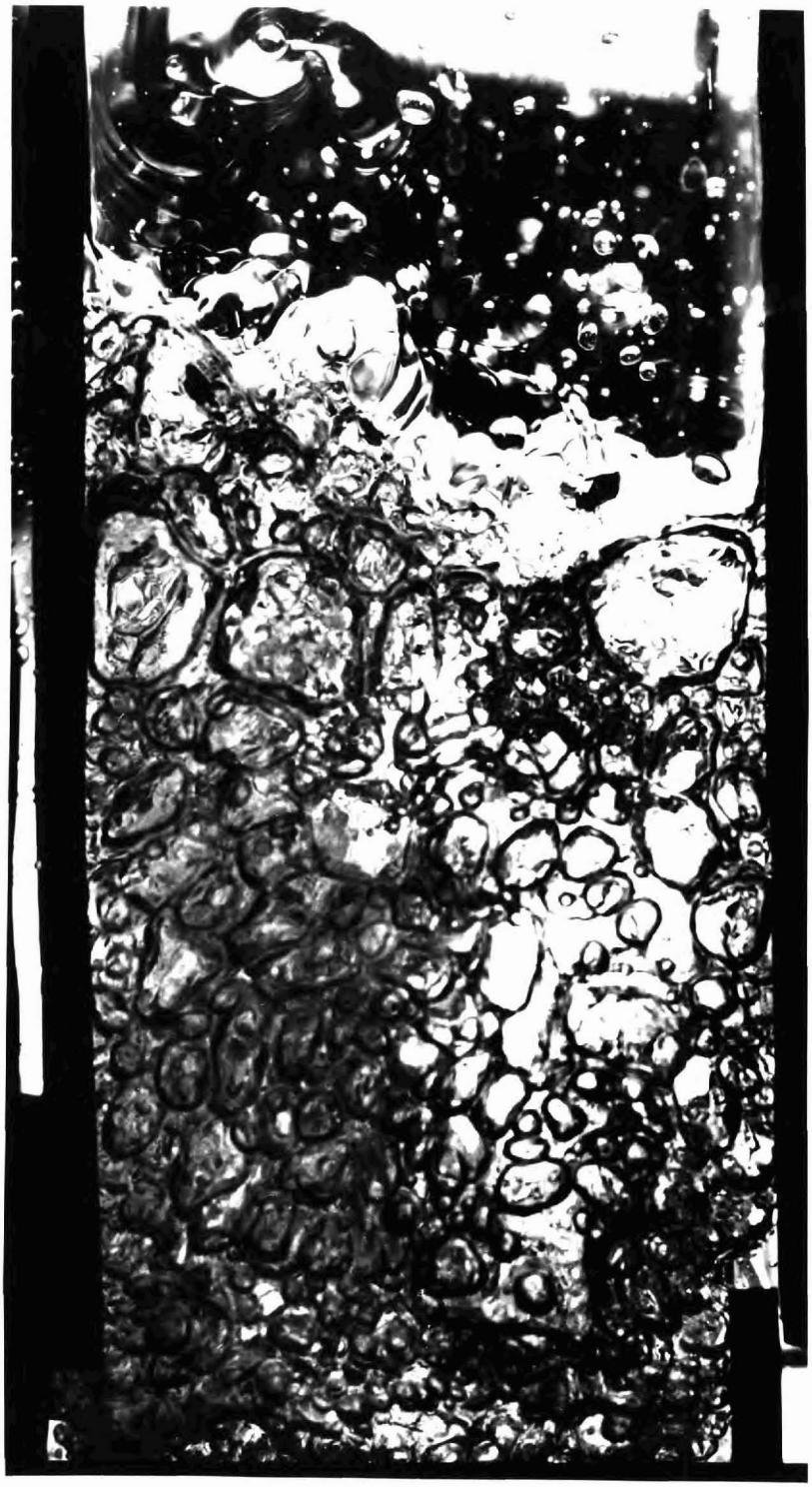

V_s = 1.37 M/sec.

(1/16 in. holes 15% f.a.)

FIG. 1.32.

V_s = 0.66 M/sec.

(1/8 in. holes 10% f.a.)

FIG. 1.33.

V_s = 1.75 M/sec.

(1/4 in. holes 10% f. a.)

very strong dependence of carry-over on effective plate spacing as shown by Hunt et al.(14) in their generalised entrainment correlation.

The coarse spray generated can be seen on most of the air-water dispersion photographs reproduced in the thesis, but is most obvious in figures (1.6., 1.12., 1.31.). The way in which the spray forms can be deduced for all but the highest velocities from figures (1.3., 1.4., 1.9., 1.30., 1.32., 1.33.). A bubble at the surface of the dispersion thins generally, then at one point a subsidiary bubble forms on the surface (figure 1.32.). This smaller bubble, being weaker, bursts first, the surface tension forces on the skin of the bubble then tear it open as can be clearly seen in figures (1.3., 1.4.). As the liquid film folds back, it forms into ligaments (figures 1.9., 1.30.) which become very elongated and finally break up into a string of droplets. It is these droplets that form both the fine and coarse sprays (figure 1.33.).

The high speed cine runs support this explanation, and in fact it is clearly the same mechanism as Teller and Rood (30) observed in their studies of entrainment from a few adjacent orifices.

Even at high velocities, figure (1.33.) suggests that a similar mechanism with liquid ligaments and daughter droplets is still in evidence.

Chapter 1.8. GENERAL CONCLUSIONS

Too often in the past experimental studies in distillation have been interpreted on the basis of considerable conjecture as to the true nature of the processes occurring on the plate. The visual studies reported in this thesis help to clarify many of these issues.

The observation that bubbling rather than jetting still occurs at high hole velocities helps to explain the phenomenon of the "residual head" as discussed fully in chapter 2.3.

Further, unless liquid loadings on a plate are very low, it is unlikely that a true spray regime will exist. That two different regimes may occur depending upon the superficial vapour velocity raises the possibility that one may be more efficient and suitable from the stand-point of mass transfer. This can only be determined by careful hydrodynamic and mass transfer studies on actual plates.

Because of the strong interaction between interfacial surface formation and local mixing there seems little point in attempting separate quantitive correlation of interfacial areas and mass transfer coefficients, using either direct measurements (Calderbank and Rennie (9)) or indirect methods such as the approach adopted by Porter et al.(50). However, such studies may shed further light on the nature of the dispersion and perhaps reinforce the admittedly subjective interpretations of visual evidence of the kind presented here.

PART 2

HYDRAULIC STUDIES ON A SMALL SIEVE PLATE

PART 2

HYDRAULIC STUDIES ON A SMALL SIEVE PLATE

Chapter 2.1. INTRODUCTION

Of all aspects of distillation, the one that has received the most attention is the hydraulic characteristics of operating plates. A vast amount of data is available from studies on columns of both laboratory and industrial size operating with commonplace and exotic mixtures. However, despite this, there is little agreement amongst the various workers about which parameters have a great or small effect on the hydrodynamic behaviour of a column. The reasons are many, but two are of supreme importance, namely measurement techniques have often been crude and varied between workers and, secondly, there often appears to be confusion as to just what is being measured.

Extensive critical reviews of work carried out in this field have been given by many authors, particularly Macmillan (5), the Michigan A.I.Ch.E report (2) and Bernard et al. (40). It is therefore not necessary to do so here. These authors also discuss the suitability of various techniques of measurement.

The studies reported in this thesis were made in an attempt to obtain a clear idea of the effects of liquid and vapour rates, and plate geometry on the various pressure drops on a plate and on the foam structure. Macmillan (5) and Bernard (6), both using the n-pentane/iso-pentane

system, though in small and large columns respectively, found very different hydrodynamic behaviour. In particular, the foam density profiles obtained under similar operating conditions were very different in the two columns. Furthermore, Bernard and Sargent (41) report very curious pressure drop phenomena at high vapour and liquid loadings.

Using improved measuring devices on a small air/water test plate, it was hoped to obtain more information about these two points and also on the separate effects of liquid and vapour rates.

The photographic results reported in Part 1. of this thesis clearly indicate two types of structural regime and it is of definite importance to determine whether this change is connected with any variation in the hydrodynamic performance. Thus hydrodynamic studies have also been made on the dispersion structure and the total liquid hold-up under various conditions of plate geometry and vapour and liquid rates.

Chapter 2.2. EQUIPMENT AND EXPERIMENTAL DETAILS

2.2.1. Equipment

2.2.1i. Column Design

The constructional details of the column are fully described in Appendix A.1.1. In fact it is the same column as was used for the photographic studies reported in Part 1.

2.2.1ii. Pressure Measurement

The overall pressure drop across the plate was measured on a water-filled U-tube manometer, one limb being positioned in the middle of the column 1.5in. below the plate. The other limb was left open to the atmosphere.

Many workers (1, 27, 46) have used manometers installed in the floor of the plate to obtain a measure of the total liquid hold-up. Such manometers have one leg flush with the floor of the plate and the other projecting into the vapour space above the plate. Their reading is commonly supposed to be the liquid hold-up per unit bubbling area, or the height to which the dispersion would collapse in the absence of vapour flow. The reading is often referred to as the "equivalent clear liquid height"; however, a preferable name and the one used hereafter in this thesis is the "dynamic head". It should be noted that the actual reading must be corrected for capillary rise, since the manometer has only one leg.

Initially a grid of dynamic head probes was installed in the experi-

mental column. Instead of using the conventional "internal" manometer, the plate floor tappings led to manometers placed outside the column. This arrangement was much more convenient as it caused no disturbances to the froth. It was found that probes placed near the walls and weirs tended to give unstable and non-reproducible readings; in fact, only in the central region of the plate was it possible to obtain reproducible readings. For this reason the grid of probes was discarded and the plate dynamic head was characterised by the reading at a single manometer placed in the middle of the plate.

Earlier studies (40) had shown that in fact the dynamic head is not a direct measure of the true liquid hold-up and a survey was made of the suitability of other pressure measuring devices. The possibility of using a very small solid state pressure transducer to measure pressure locally at any position in the foam was investigated but the cost of development of such a device was prohibitive. A differential pressure air probe of a type similar to that used by Brown (56) was then developed for investigation of the pressure profiles in the foam. Using this kind of device, it had been hoped to throw some light on the diffusion and absorption of vapour momentum. However, difficulties of non-reproducible readings were again experienced and eventually traced to the variable conditions at the probe top. It made an appreciable difference whether the probe tip was in air or water and, in addition, it was found that the fluctuating pressure caused liquid to enter the air probe thus tending to cause vapour locks. It was therefore

decided that this form of device was incapable of providing reliable results and its use was abandoned. Classical dynamic head measurements only were used.

2. 2. 1iii. Dispersion Density Measurement

Dispersion density traverses in the foam were made using the accepted technique of gamma-ray transmission. The detailed method used was very similar to that employed by Bernard (6); however, certain modifications were made to both the Caesium source and the scintillation counter.

Both Bernard (6) and Macmillan (5) measured long time-average dispersion densities over periods of the order of 100 secs. Further, the characteristics of the scintillation crystals and pulse amplifiers were such that in order to obtain a reasonable number of counts (5×10^4) a fairly wide band of radiation energies had to be monitored.

For the present studies a 9.9 millicurie Caesium 137 Source was used. This gave a far higher radiation emission rate than the previous sources. A 3in. x 3in. thallium/sodium iodide crystal was used in the scintillation counter and with these two modifications it was possible to measure 50,000 counts of very narrow energy spectrum in approximately 1 sec. It was then possible to maintain steady hydrodynamic conditions for the necessary time with far less difficulties.

2. 2. 2. Experimental Programme

All the experimental studies were carried out using liquid and vapour loadings similar to those employed industrially. Thus the superficial air rates ranged from 0. 2 to 2. 0 Metres/sec., and the total liquid loadings varied up to 4 litres/min. (or 5 galls/(min. ft of weir)). More particularly these loadings and the plate geometries were very similar to those used in the A. I. Ch. E. Research Programme (1, 2, 3).

The experimental programme may best be described under separate sections covering dispersion densities, total liquid hold-up and pressure drop studies.

2. 2. 2i. Dispersion Density Studies

To compare the photographic observations of the dispersion structure with the actual foam densities, vertical profiles were obtained for similar plate geometries and vapour and liquid loadings as used in Part 1. The results are presented in graphical form in figures 2. 1 to 2. 7.

2. 2. 2ii Liquid Hold-up Studies

Integration of the area under the curves of the dispersion density gives the total liquid hold-up in the dispersion. Thus for the runs carried out in chapter 2. 2. 1ii., the effects of plate geometry and vapour rate can be seen in figures 2. 8 to 2. 11.

2. 2. 2iii. Pressure Drop Studies

For a single plate (1/16in. holes, 10% free area), an extensive study was made of the effects of vapour and liquid rate on the various pressure drops associated with an operating sieve plate. The dry plate overall plate pressure drops, the dynamic head and total liquid hold-up were all measured directly.

The total liquid hold-up on the plate was taken to be the liquid head in the inlet downcomer to the test plate. This was reasonable as a check had earlier been made by comparison with the value derived by integration of the foam density profile. Furthermore, the resistance of the inlet downcomer was made very small.

The results of these studies are summarised in figures 2. 12 to 2. 20.

Chapter 2.3. DISCUSSION OF RESULTS

2.3.1. Dispersion Density and Liquid Hold-up Studies

All the dispersion density profiles shown in figures 2.1 - 2.7 very clearly show the non-uniformity of the structure of the two phase mixture. This non-uniformity has been observed by others (5, 6) but there is clearly very little similarity in the detailed patterns of behaviour. Bernard (6) has shown, however, that even the most bizarre profiles are reproducible.

As the vapour rate is raised, progressively more liquid is held up on the plate (figure 2.1.). At the lowest vapour rate of 0.39 M/sec., the density varies smoothly with height - at this velocity the foam is distinctly cellular. At the higher vapour rate of 0.93 M/sec., the profile has become much more wavy and the increased liquid hold-up has occurred in the "foam zone" above the plate floor region. At the highest vapour rate of 1.73 M/sec., the change in shape of the curve has become even more emphasised and a region on "constant density" of the type observed by Macmillan (5) can be seen. Very large bulges as observed by Bernard and Sargent (41) are not present. A further similarity with Macmillan's (5) observations is that at the highest vapour rates, the near constant density region occurs at a dispersion density of 0.15 to 0.20. However, at lower vapour rates, a constant density region definitely does not exist.

The dispersion density at plate level is never anywhere near the value expected on the basis of plate free area. However, observations in

FIG. 2.1

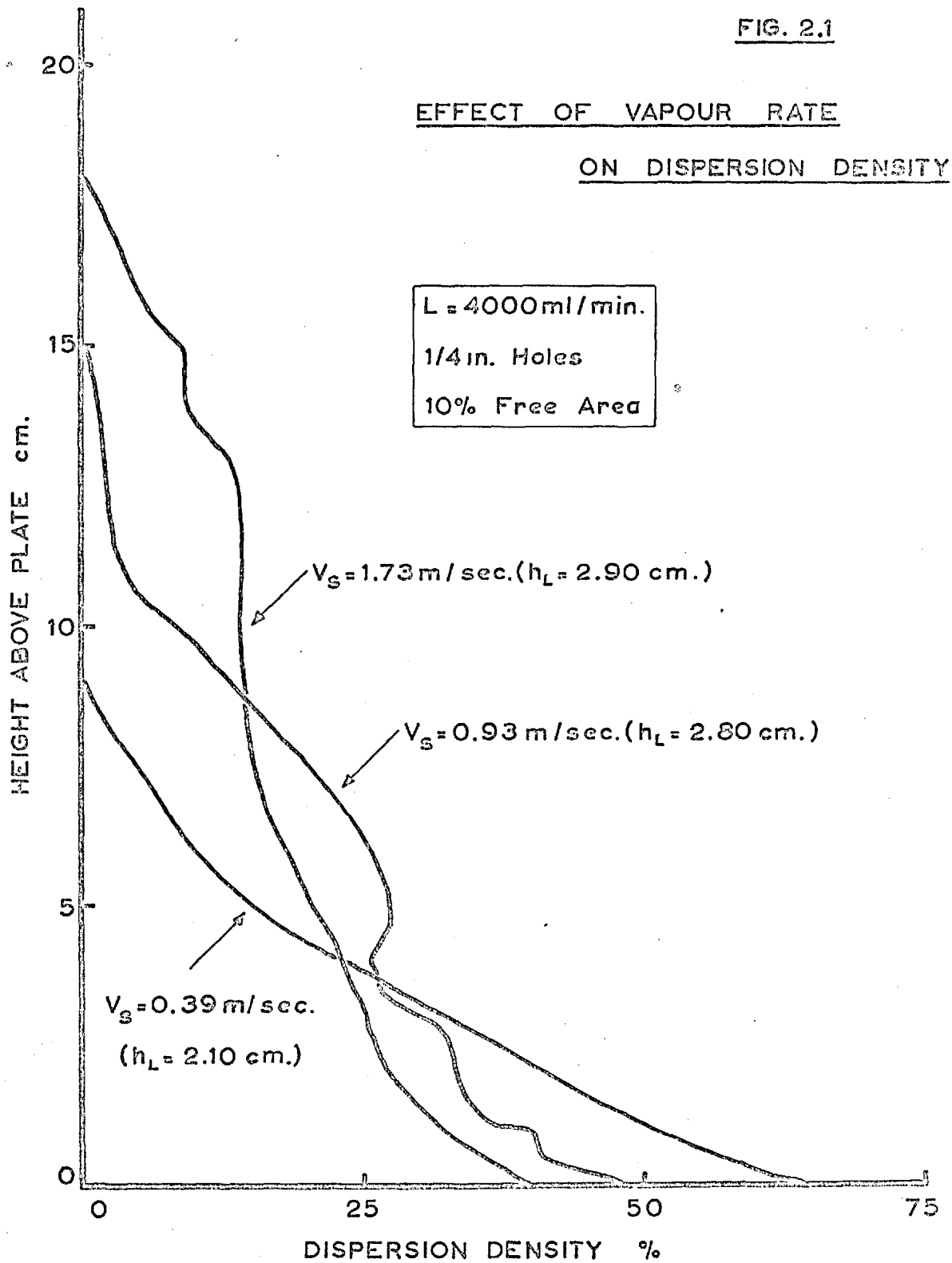
EFFECT OF VAPOUR RATE
ON DISPERSION DENSITY
L = 4000 ml/min.
1/4 in. Holes
10% Free Area
V_S = 1.73 m/sec. (h_L = 2.90 cm.)
V_S = 0.93 m/sec. (h_L = 2.80 cm.)
V_S = 0.39 m/sec.
(h_L = 2.10 cm.)
HEIGHT ABOVE PLATE cm.
DISPERSION DENSITY %
0
5
10
15
20
0
25
50
75

FIG. 2.2

EFFECT OF FREE AREA ON DISPERSION DENSITY

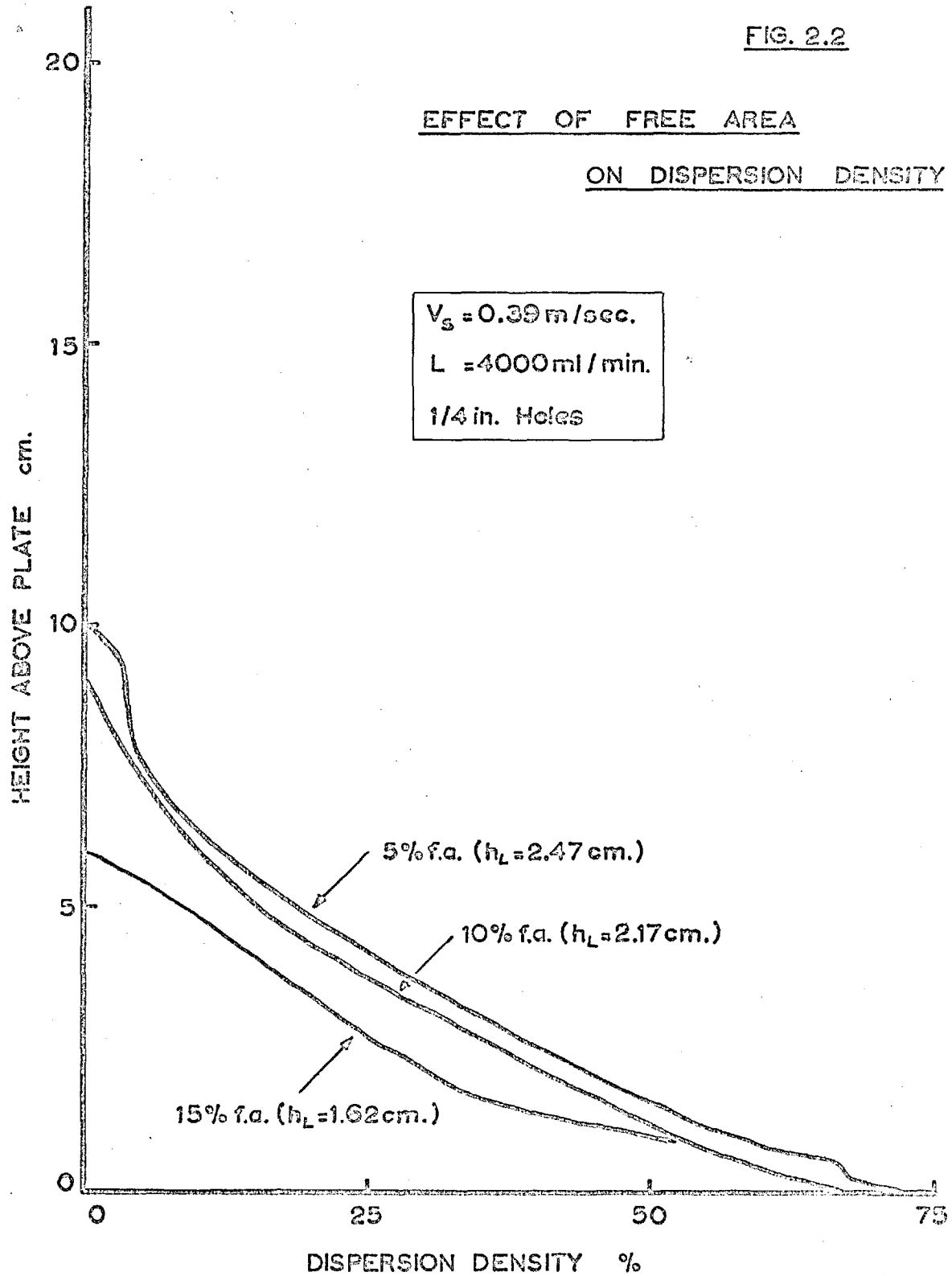

FIG. 2.3

EFFECT OF FREE AREA ON DISPERSION DENSITY

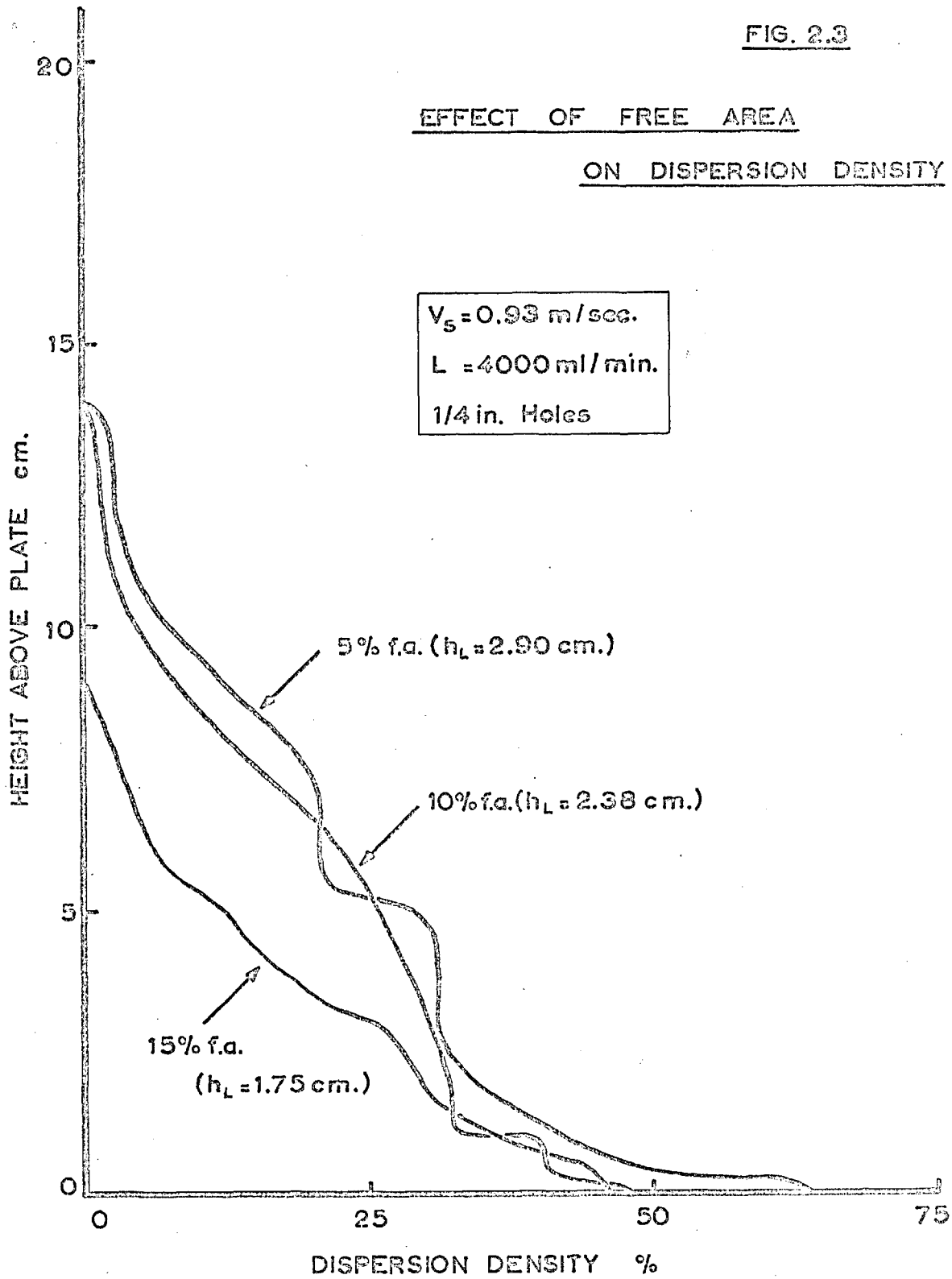

FIG. 2.4

EFFECT OF FREE AREA ON DISPERSION DENSITY

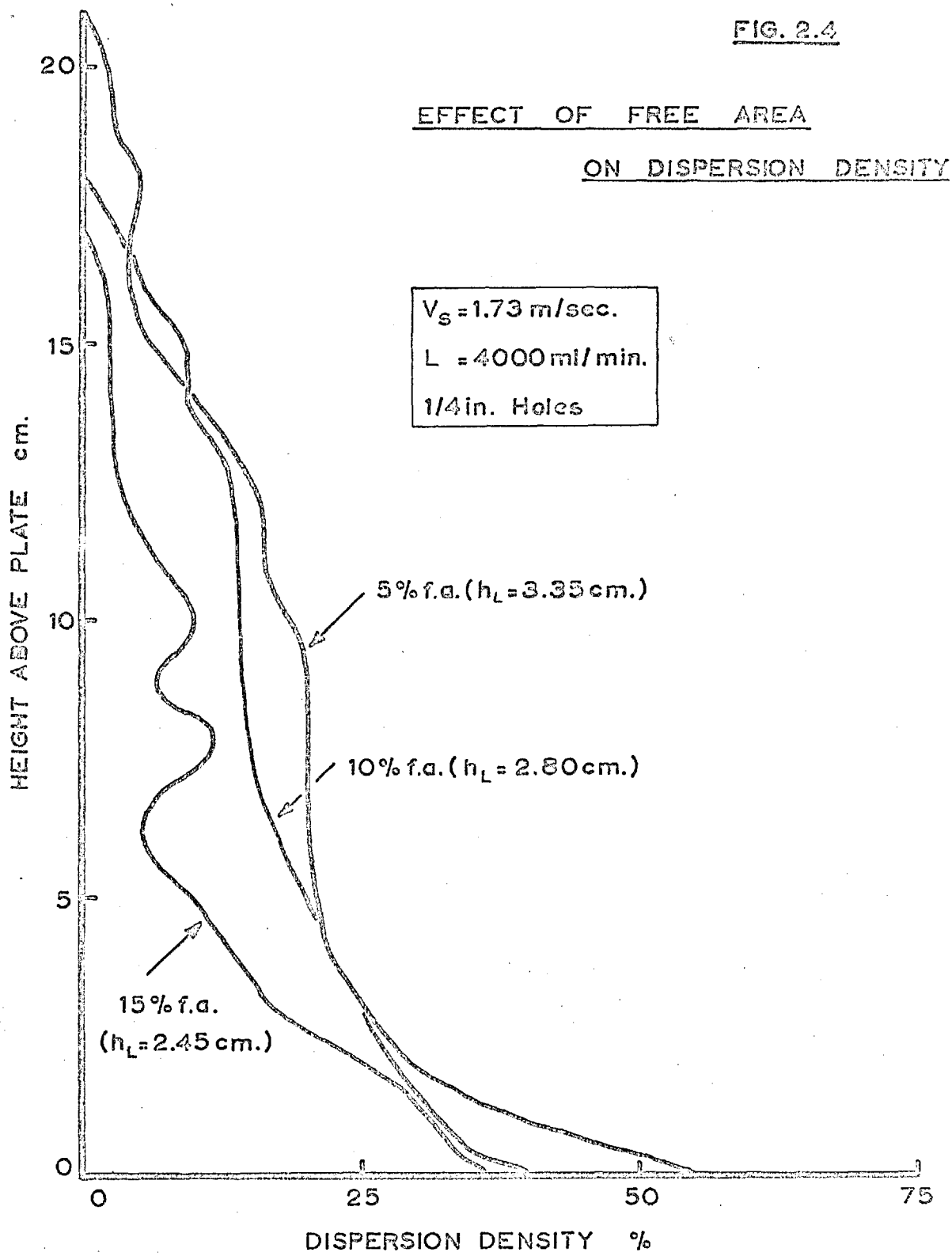

FIG. 2.5

EFFECT OF HOLE SIZE ON DISPERSION DENSITY

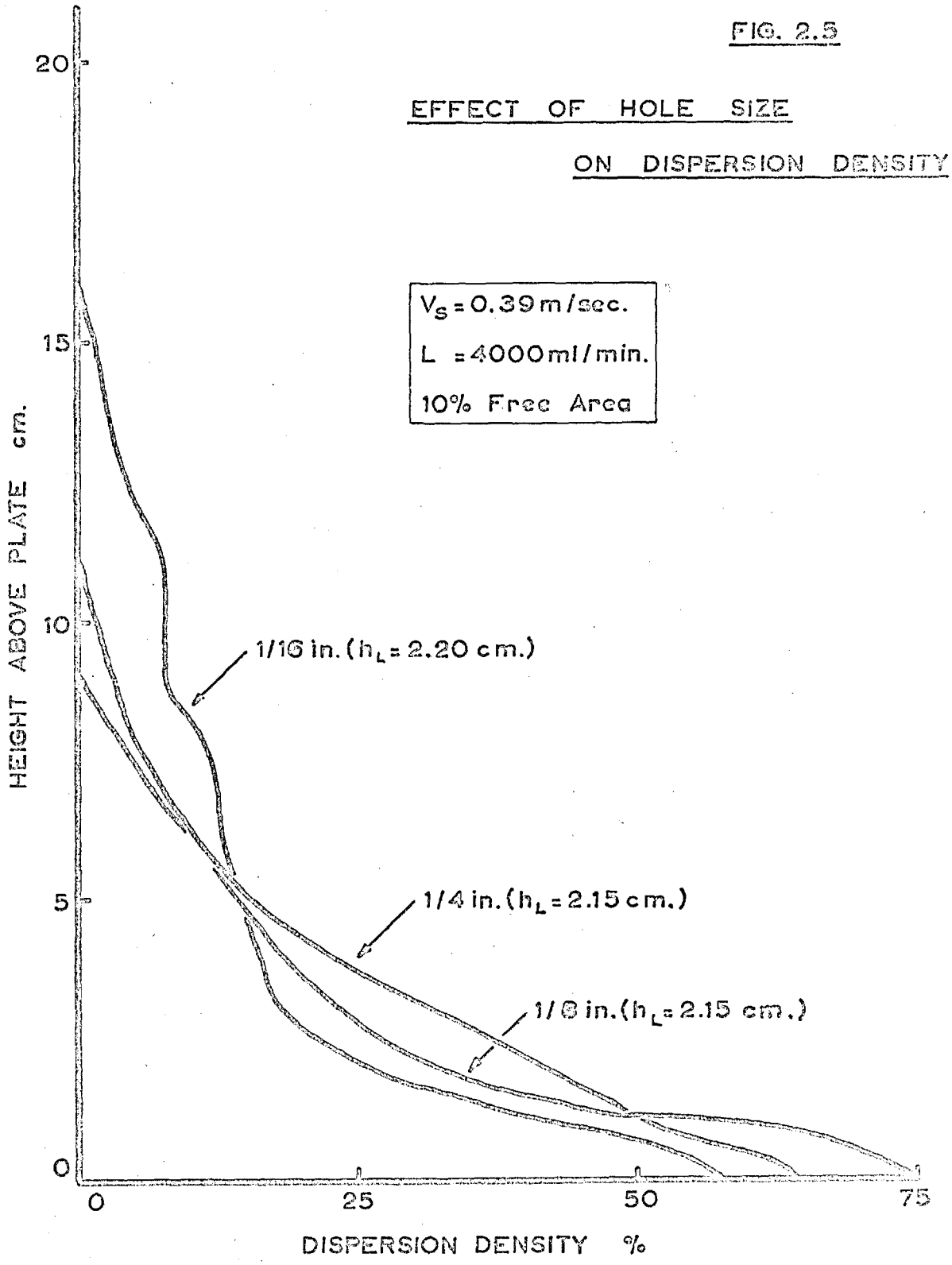

FIG. 2.9

EFFECT OF HOLE SIZE ON DISPERSION DENSITY

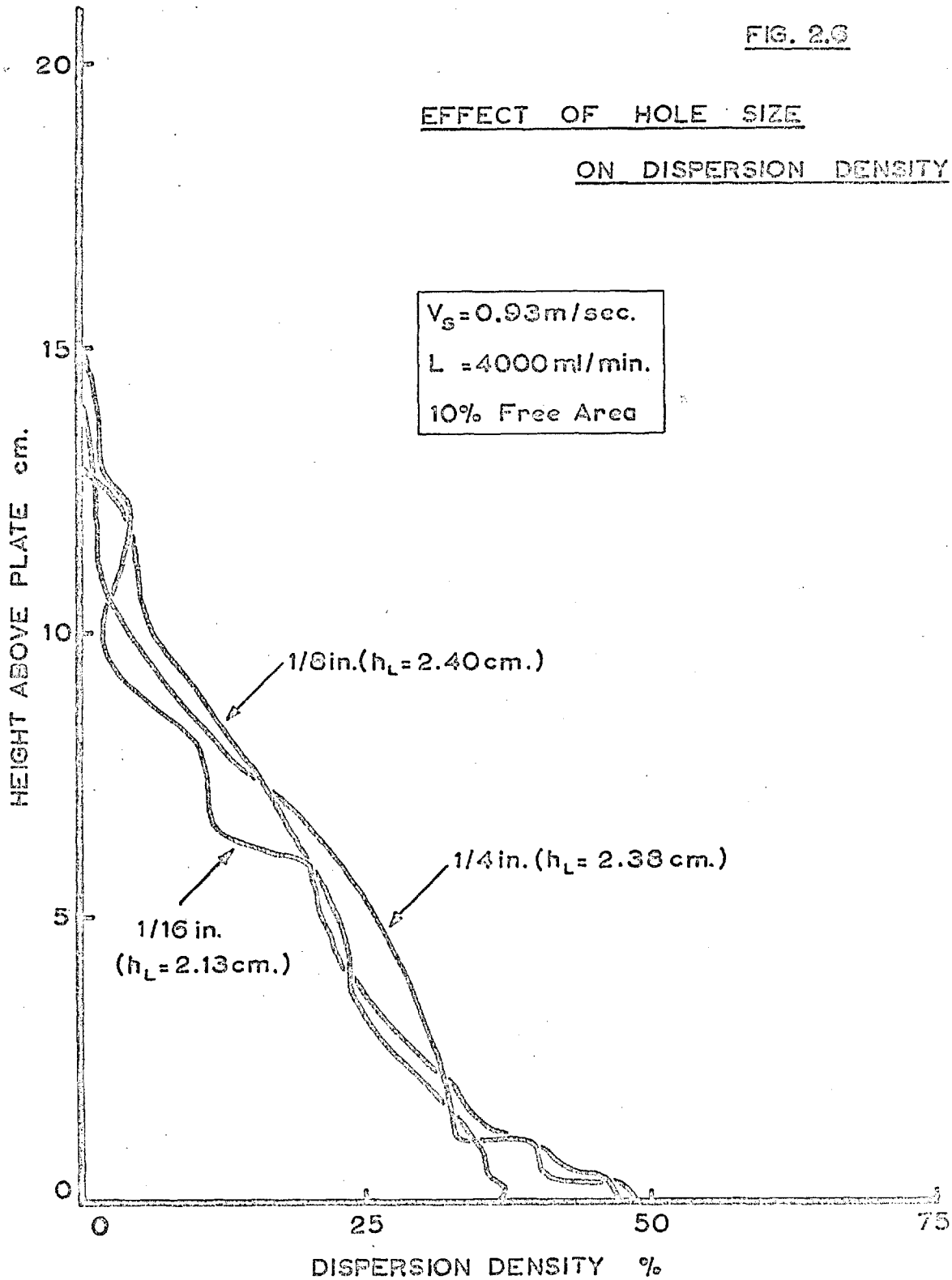

FIG. 2.7

EFFECT OF HOLE SIZE ON DISPERSION DENSITY

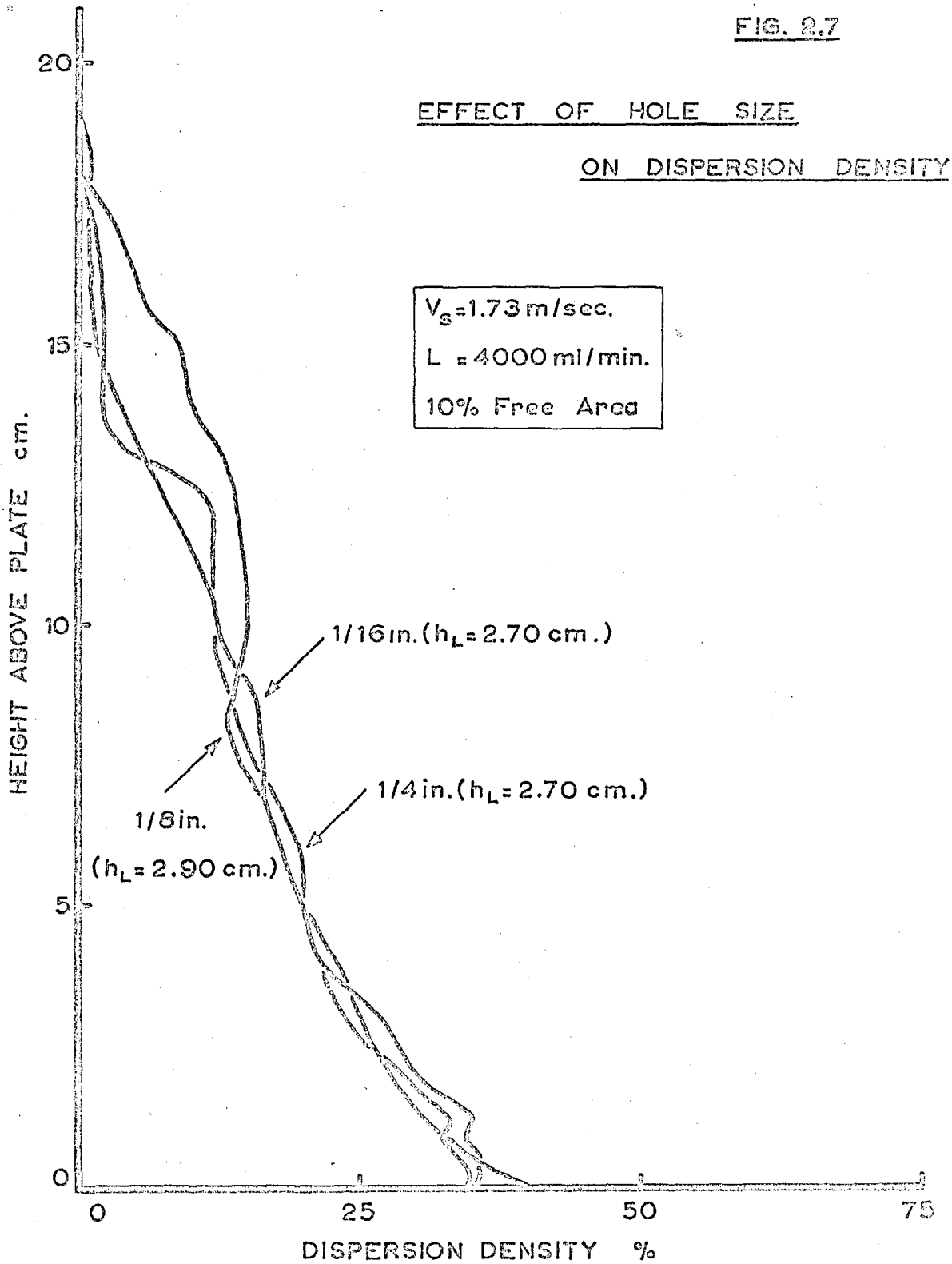

section 1.5i. of the considerable horizontal expansion of the vapour on passing through the holes and the obvious circulation of bubbles down to the plate floor fully explain this large discrepancy.

Comparison of the dispersion density profiles presented in figures 2.1 to 2.7 with the photographs of the dispersion reproduced in Part 1. of the thesis suggest that the breakdown of the "rigid" cellular structure is associated with the commencement of the wavy patterns in the dispersion density profiles.

Figures 2.2., 2.3. and 2.4. show the effect of plate free area on the dispersion density at progressively increasing vapour rates. The most apparent feature of the profiles is the similarity of the curves for 5% and 10% free areas at all velocities. The curves for the 15% free area plate are consistently lower. At all vapour rates, the liquid hold-up and foam height increase as the plate free area decreases. This pattern of behaviour is very similar to that reported in chapter 1.3.2iii. on the visual effect of free area for both 1/16in. and $\frac{1}{4}$in. holes. Macmillan (5) also found, using 1/16in. and $\frac{1}{8}$in. holes, that for a given superficial velocity the hold-up increased as plate free area decreased. The effect of free area is not so clear from Bernard's (6) measurements as considerable weeping occurred with high free area plates at all but the greatest vapour throughputs.

Macmillan (5) found that there was a distinct effect of hole size on the dispersion density and upon liquid hold-up. In contradiction, Bernard and Sargent (41) found that hole size had no significant effect in

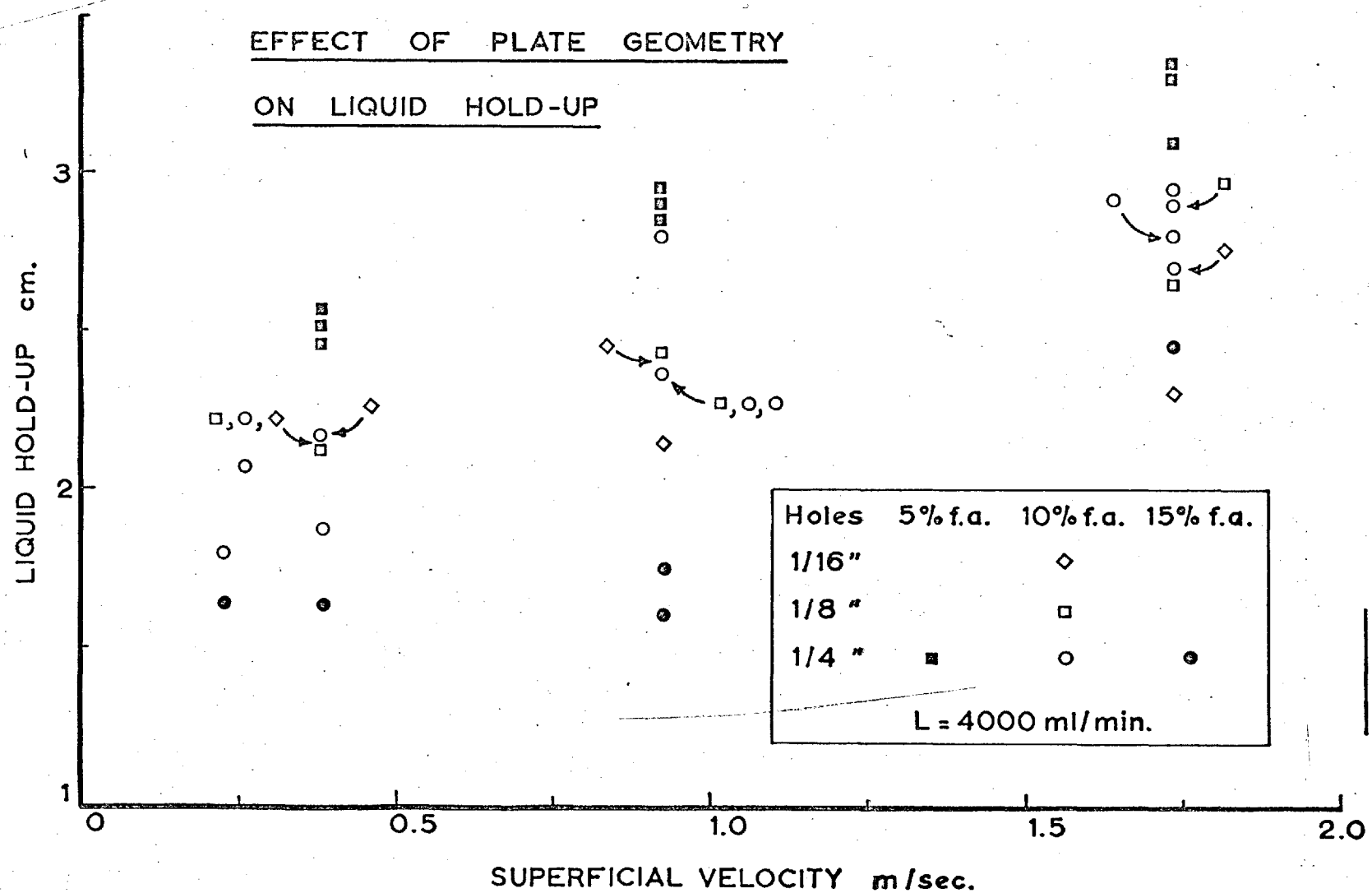
EFFECT OF PLATE GEOMETRY
ON LIQUID HOLD-UP
LIQUID HOLD-UP cm.
3
2
1
0
0.5
1.0
1.5
2.0
SUPERFICIAL VELOCITY m/sec.
Holes 5% f.a. 10% f.a. 15% f.a.
1/16"
1/8 "
1/4 "
L = 4000 ml/min.

FIG. 2.8

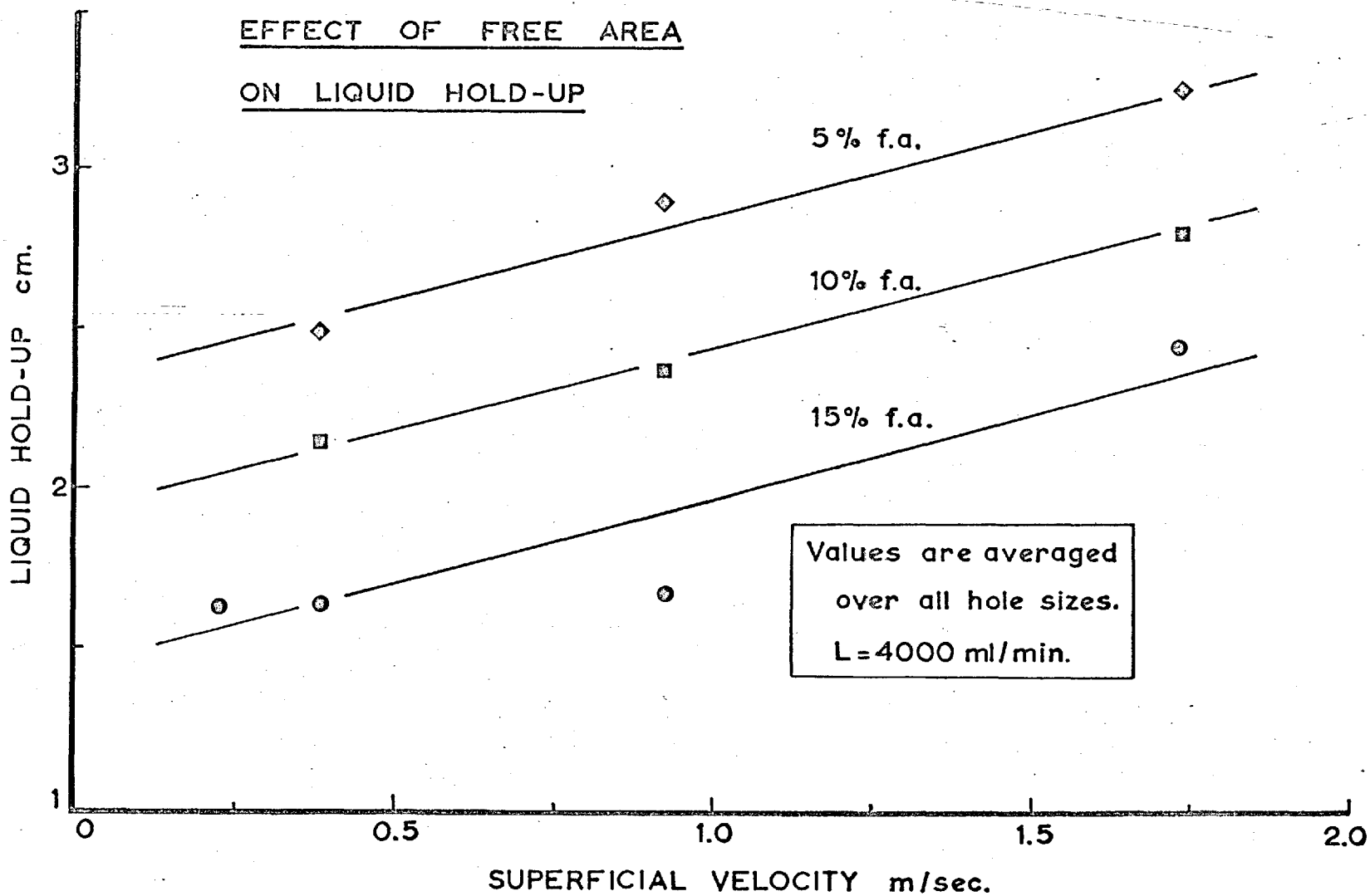
EFFECT OF FREE AREA
ON LIQUID HOLD-UP
5% f.a.
10% f.a.
15% f.a.
Values are averaged over all hole sizes.
L = 4000 ml/min.
LIQUID HOLD-UP cm.
SUPERFICIAL VELOCITY m/sec.
1
2
3
0
0.5
1.0
1.5
2.0

FIG. 2.9

EFFECT OF FREE AREA

ON LIQUID HOLD-UP

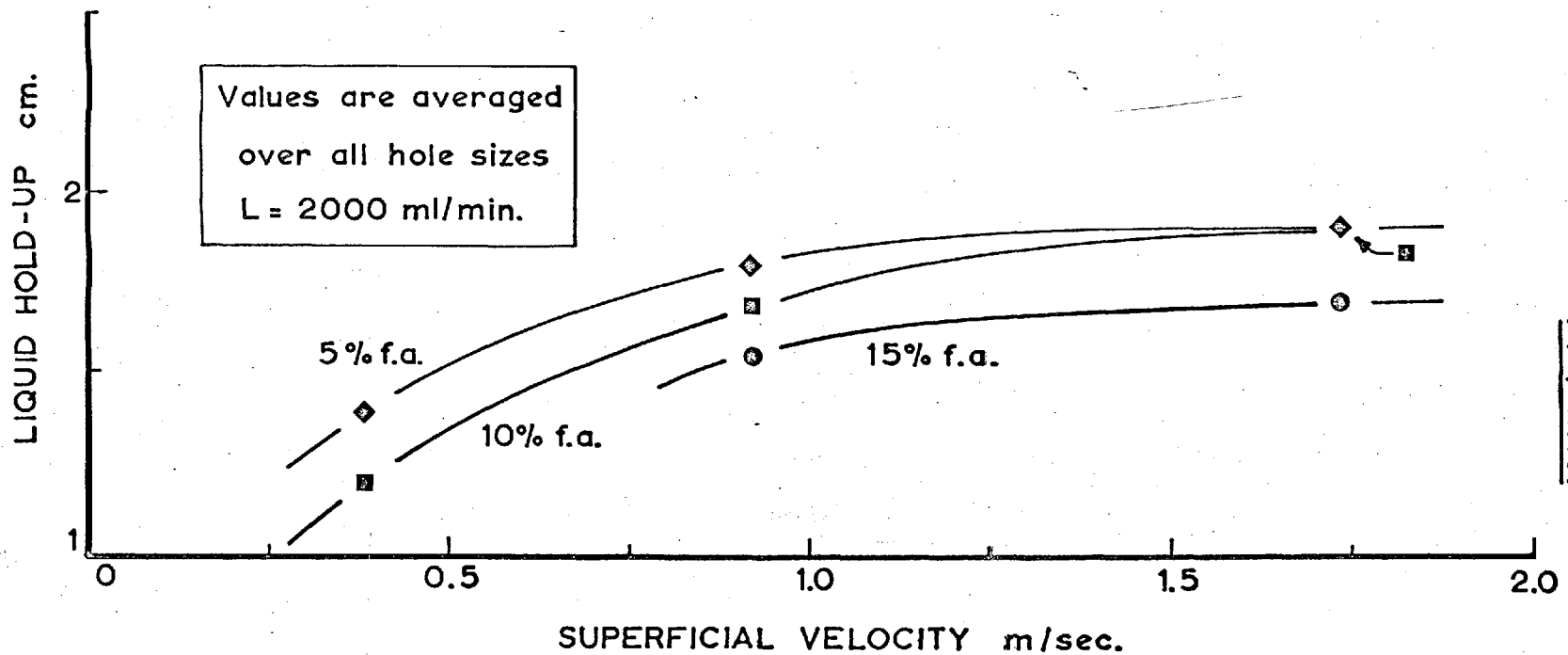

FIG. 2.10.

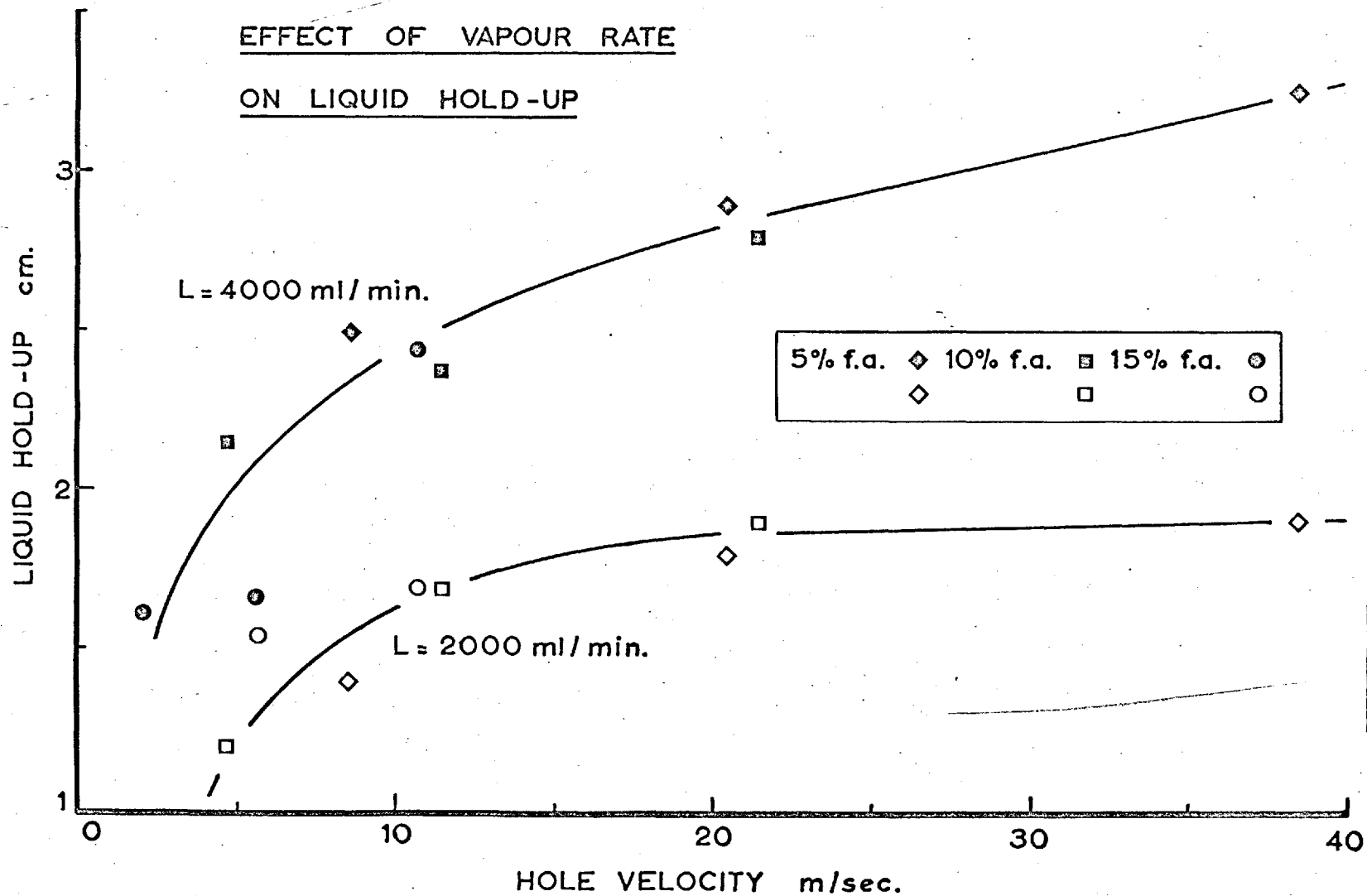
EFFECT OF VAPOUR RATE
ON LIQUID HOLD-UP
LIQUID HOLD-UP cm.
3
2
1
L = 4000 ml/min.
L = 2000 ml/min.
5% f.a.
10% f.a.
15% f.a.
0
10
20
30
40
HOLE VELOCITY m/sec.

FIG. 2.11.

their work. Figures 2.5., 2.6. and 2.7. show that hole size had no appreciable effect, except at the lowest vapour rate, on the profiles. Hole size had no effect on hold-up at any vapour rate. Figure 2.5. shows that at low vapour rates 1/16in. holes produced a rather more regular foam and a somewhat greater foam height. This behaviour was also observed in chapter 1.3.2ii.

The effects of hole size and plate free area on the total liquid hold-up can be studied more clearly in figures 2.8. to 2.11. inclusive. Figure 2.8. shows the combined effect of hole size and free area on hold-up; however, averaging over all hole sizes as in figures 2.9. and 2.10. clearly indicates the effect of free area on the total hold-up at different liquid flow rates. Hole size is clearly of very secondary importance in determining the liquid hold-up on the plate. That the lower free areas produce a greater liquid hold-up at any vapour rate is also clearly apparent. Hole velocity may be used to correlate liquid hold-up as shown in figure 2.11. The fit is not good however for the high free area plates at low vapour rates.

As shown, the dispersion density profiles yield very little information about the dispersion structure as observed visually and, indeed, a description or explanation of either is impossible. It can only be said that there is no distinct change in the character of the density profile or in the liquid hold-up as the dispersion structure changes.

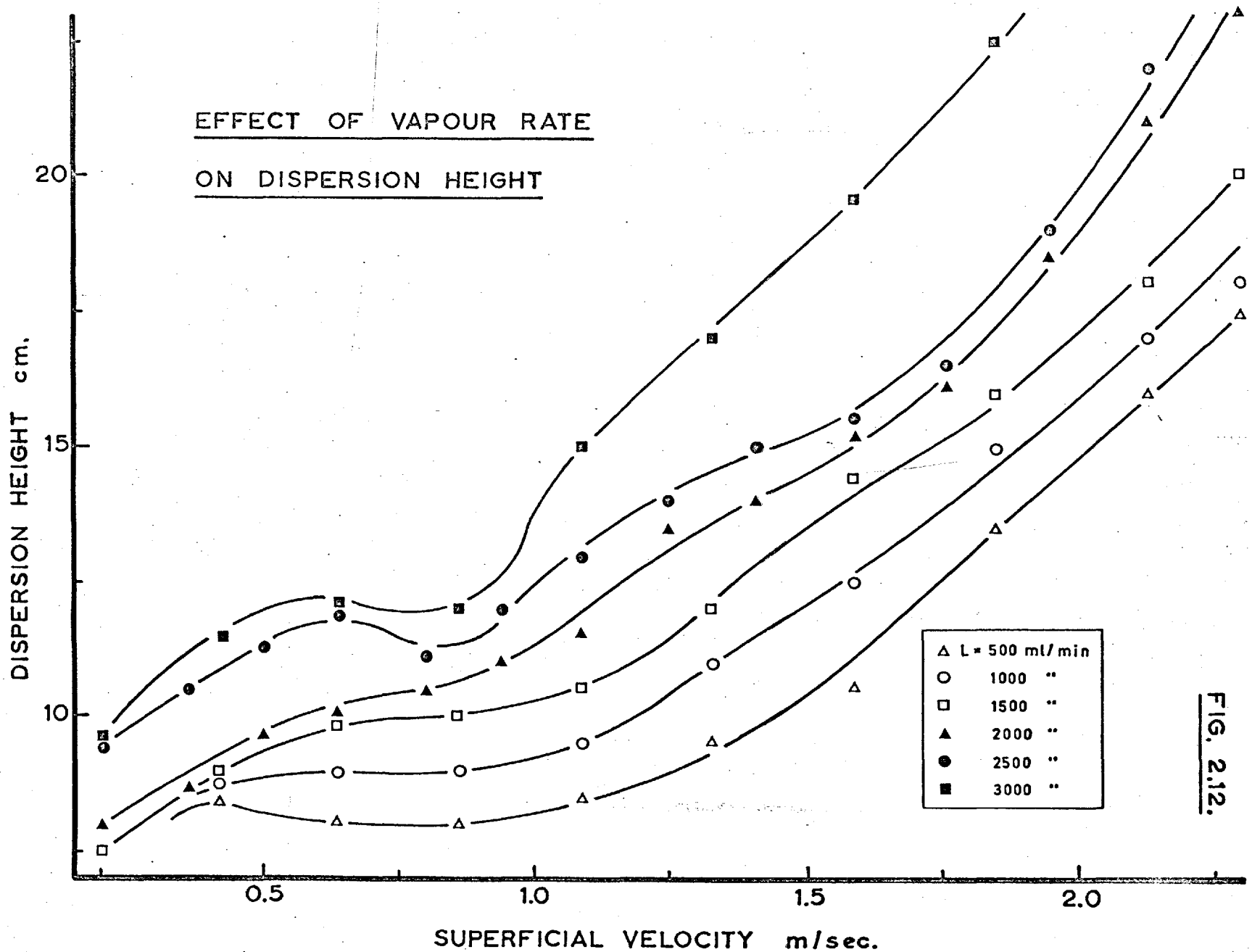
EFFECT OF VAPOUR RATE
ON DISPERSION HEIGHT
DISPERSION HEIGHT cm.
20
15
10
0.5
1.0
1.5
2.0
SUPERFICIAL VELOCITY m/sec.
L = 500 ml/min
1000 "
1500 "
2000 "
2500 "
3000 "

FIG. 2.12.

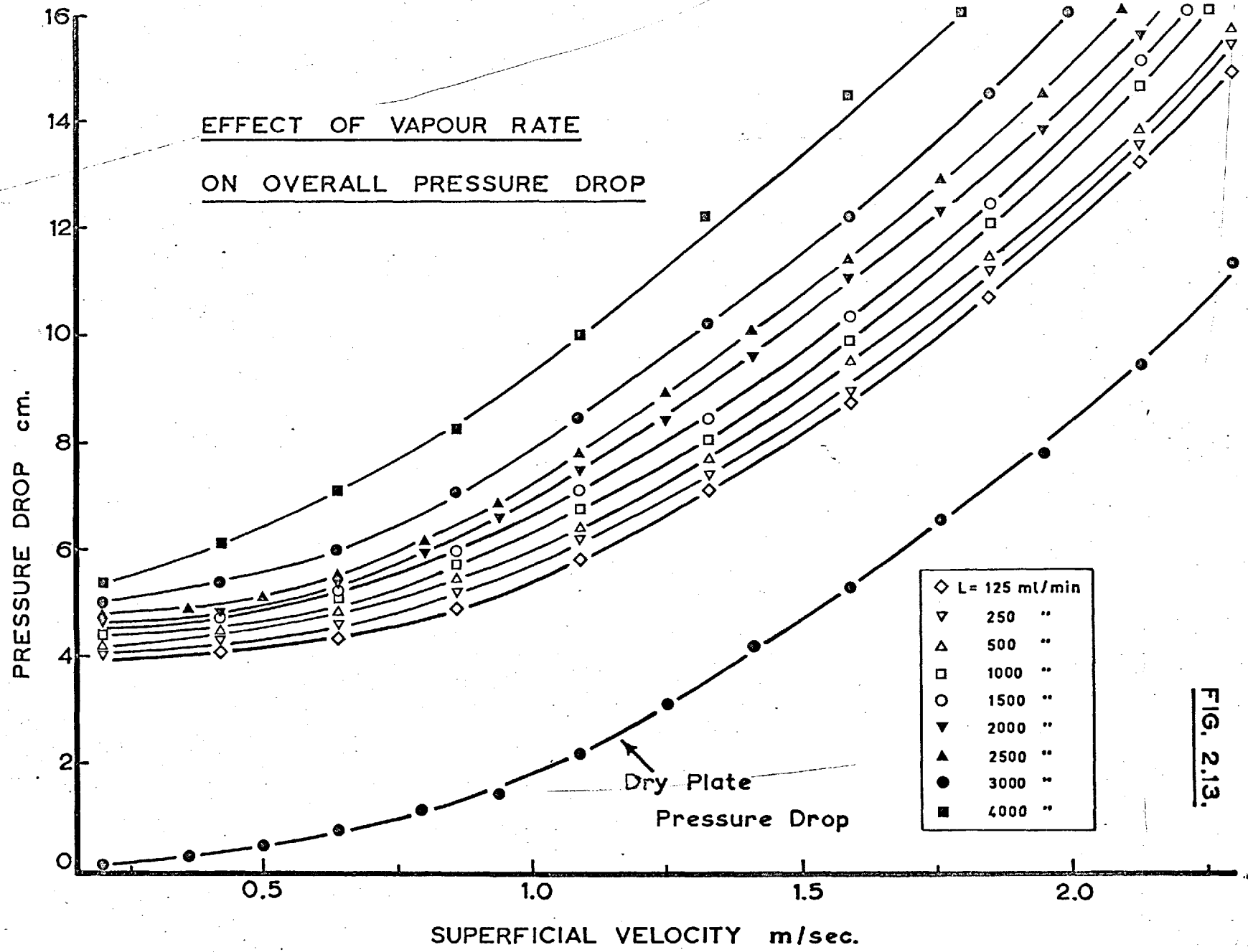
EFFECT OF VAPOUR RATE
ON OVERALL PRESSURE DROP
PRESSURE DROP cm.
SUPERFICIAL VELOCITY m/sec.
0
2
4
6
8
10
12
14
16
0.5
1.0
1.5
2.0
L= 125 ml/min
250 "
500 "
1000 "
1500 "
2000 "
2500 "
3000 "
4000 "
Dry Plate
Pressure Drop

FIG. 2.13.

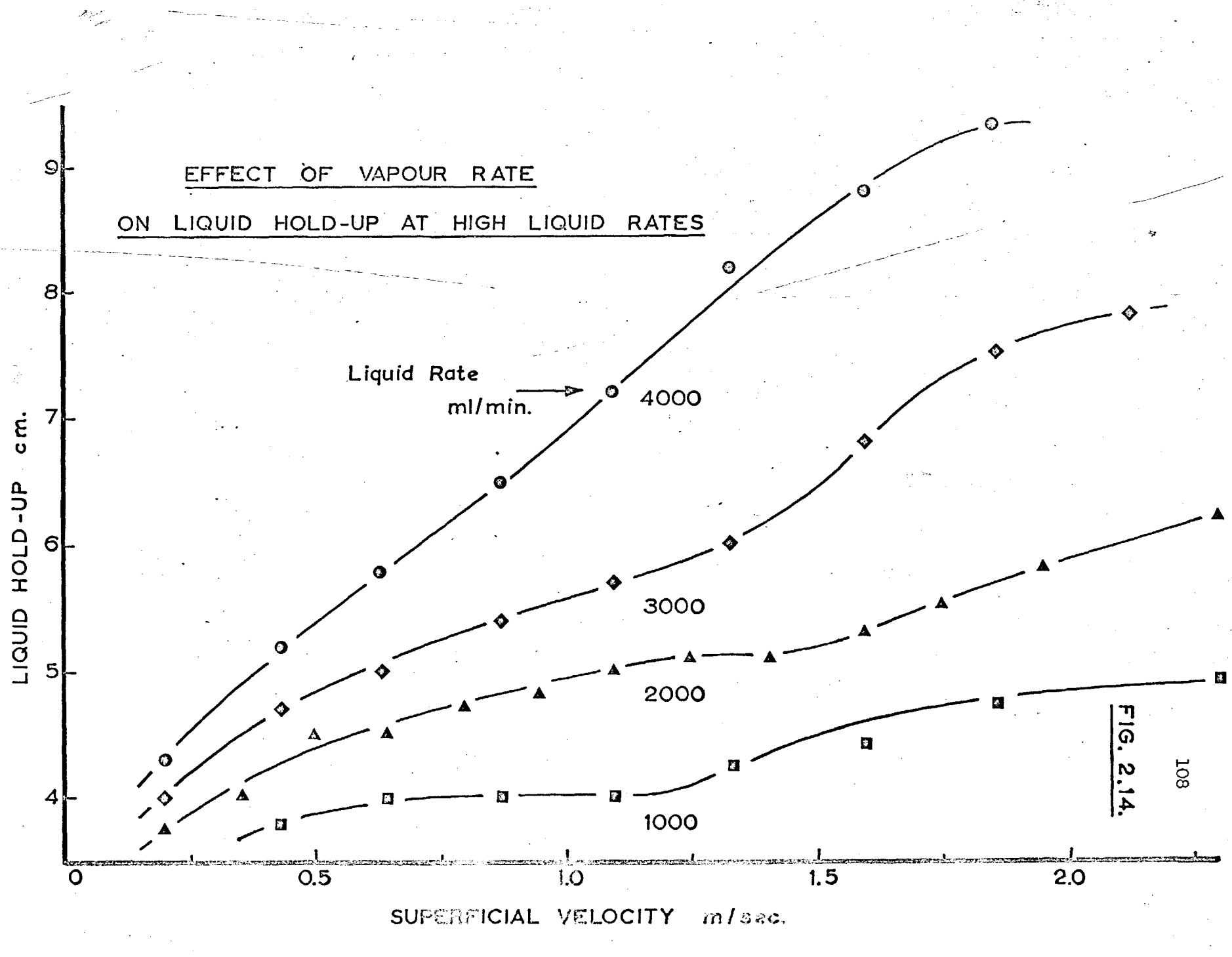
EFFECT OF VAPOUR RATE
ON LIQUID HOLD-UP AT HIGH LIQUID RATES
Liquid Rate
ml/min.
4000
3000
2000
1000
LIQUID HOLD-UP cm.
SUPERFICIAL VELOCITY m/sec.
0
0.5
1.0
1.5
2.0
4
5
6
7
8
9

FIG. 2.14.

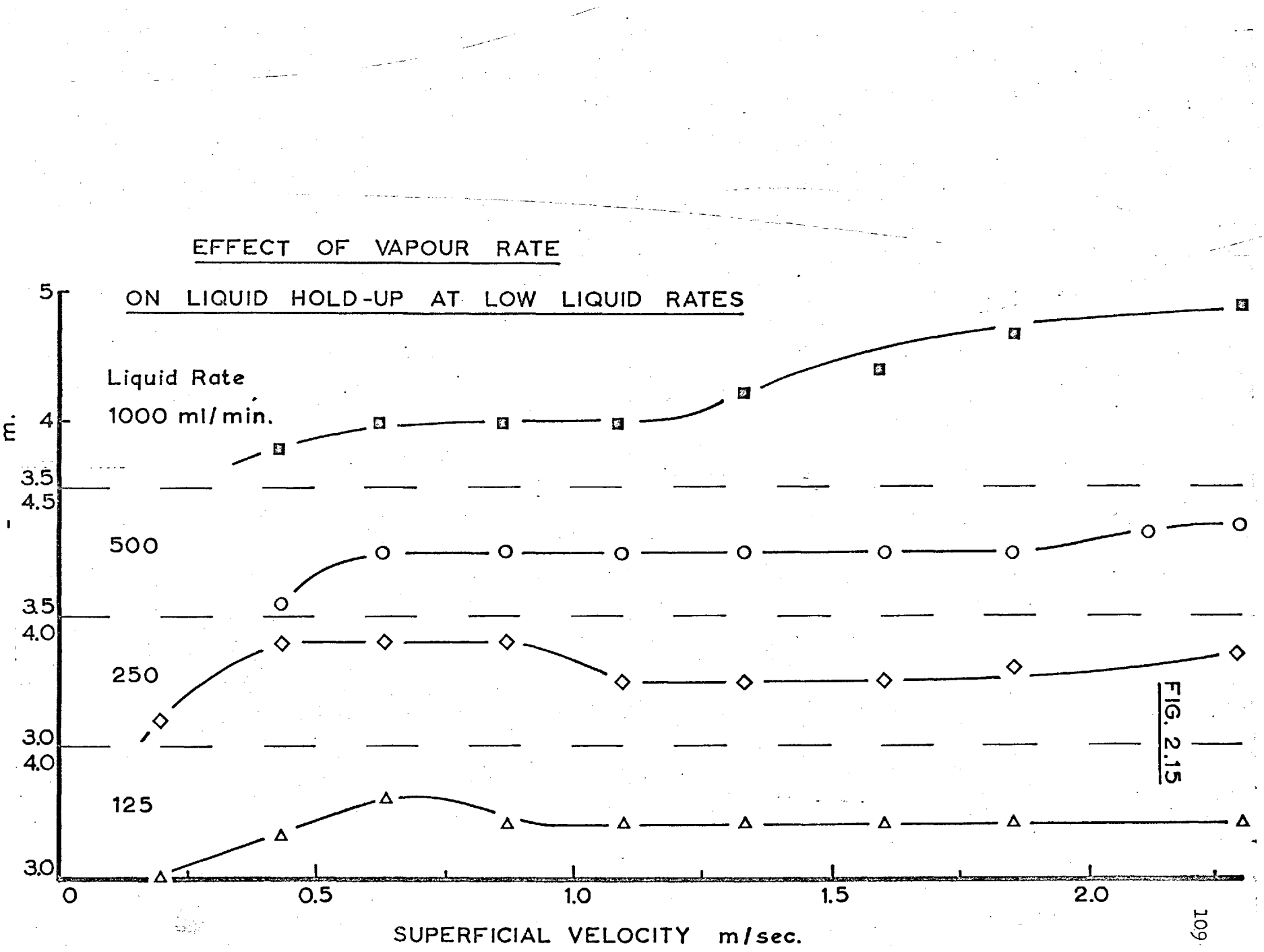
EFFECT OF VAPOUR RATE
ON LIQUID HOLD-UP AT LOW LIQUID RATES
Liquid Rate
1000 ml/min.
500
250
125
5
4
3.5
4.5
3.5
4.0
3.0
4.0
3.0
0
0.5
1.0
1.5
2.0
SUPERFICIAL VELOCITY m/sec.
FIG. 2.15

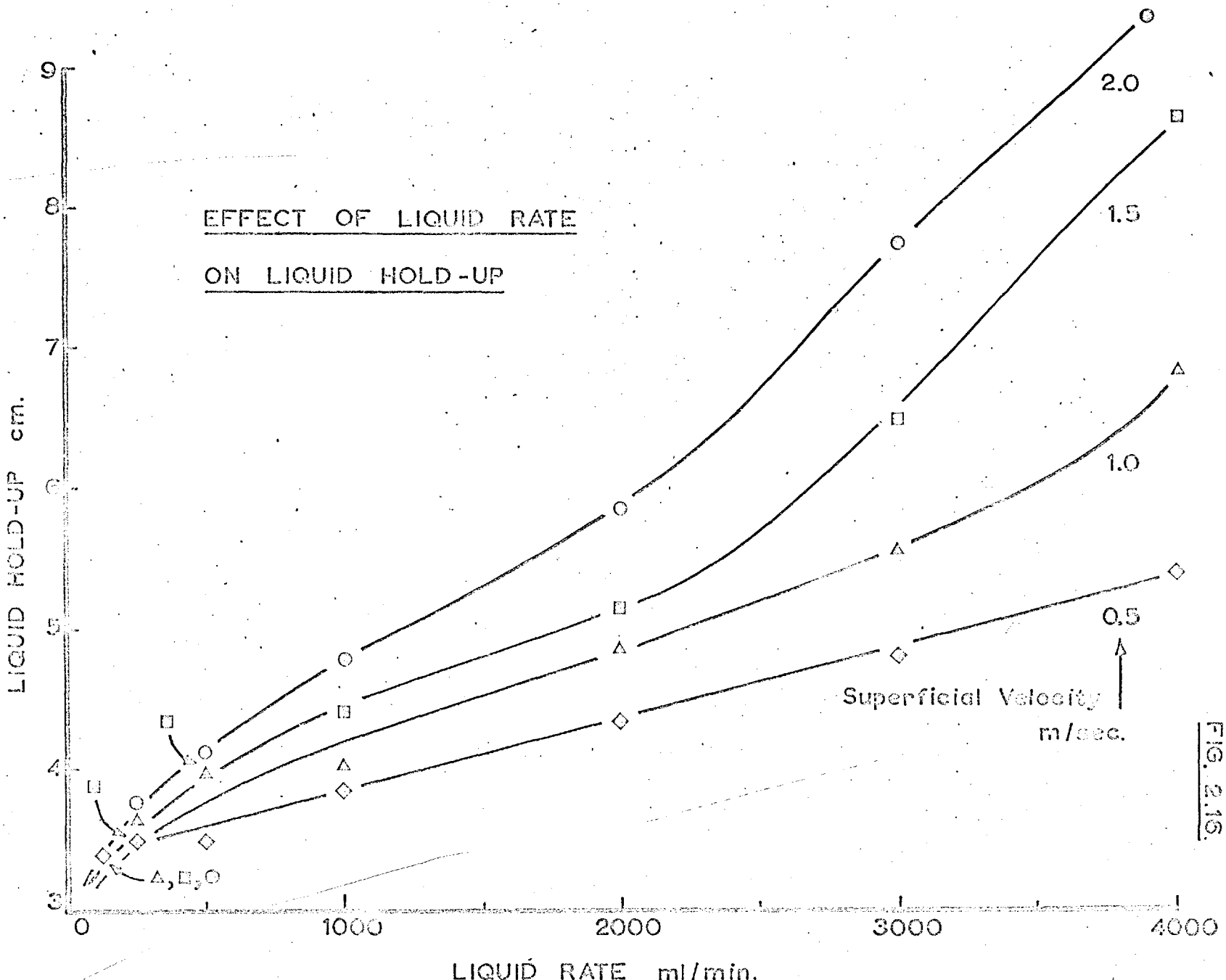
EFFECT OF LIQUID RATE
ON LIQUID HOLD-UP
LIQUID HOLD-UP cm.
LIQUID RATE ml/min.
2.0
1.5
1.0
0.5
Superficial Velocity
m/sec.
0
1000
2000
3000
4000
3
4
5
6
7
8
9

FIG. 2.19.

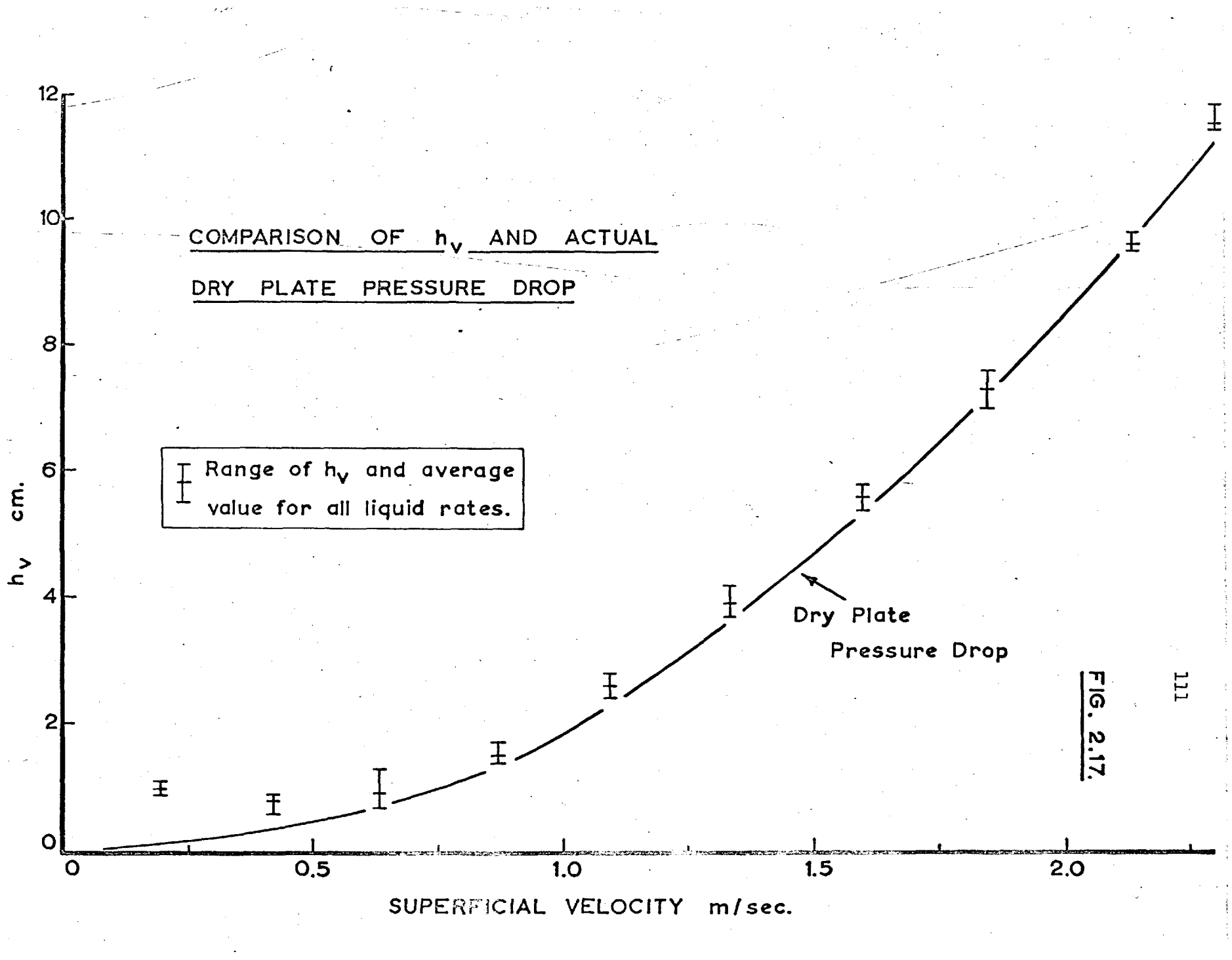
COMPARISON OF h_v AND ACTUAL
DRY PLATE PRESSURE DROP
Range of h_v and average value for all liquid rates.
Dry Plate
Pressure Drop
h_v cm.
SUPERFICIAL VELOCITY m/sec.
0
2
4
6
8
10
12
0
0.5
1.0
1.5
2.0

FIG. 2.17.

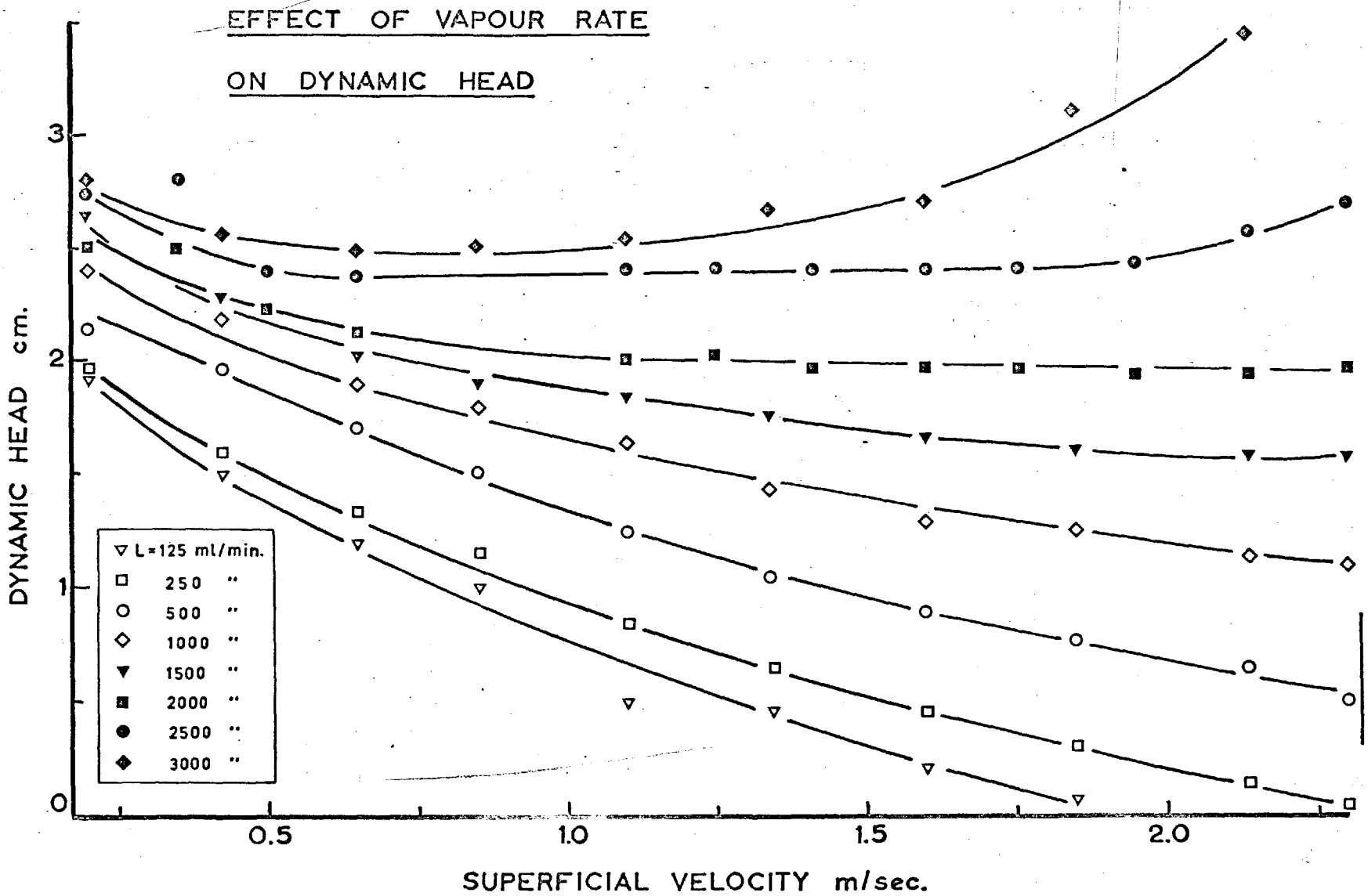
EFFECT OF VAPOUR RATE
ON DYNAMIC HEAD
DYNAMIC HEAD cm.
SUPERFICIAL VELOCITY m/sec.
0
1
2
3
0.5
1.0
1.5
2.0
L=125 ml/min.
250 "
500 "
1000 "
1500 "
2000 "
2500 "
3000 "

FIG. 2.18.

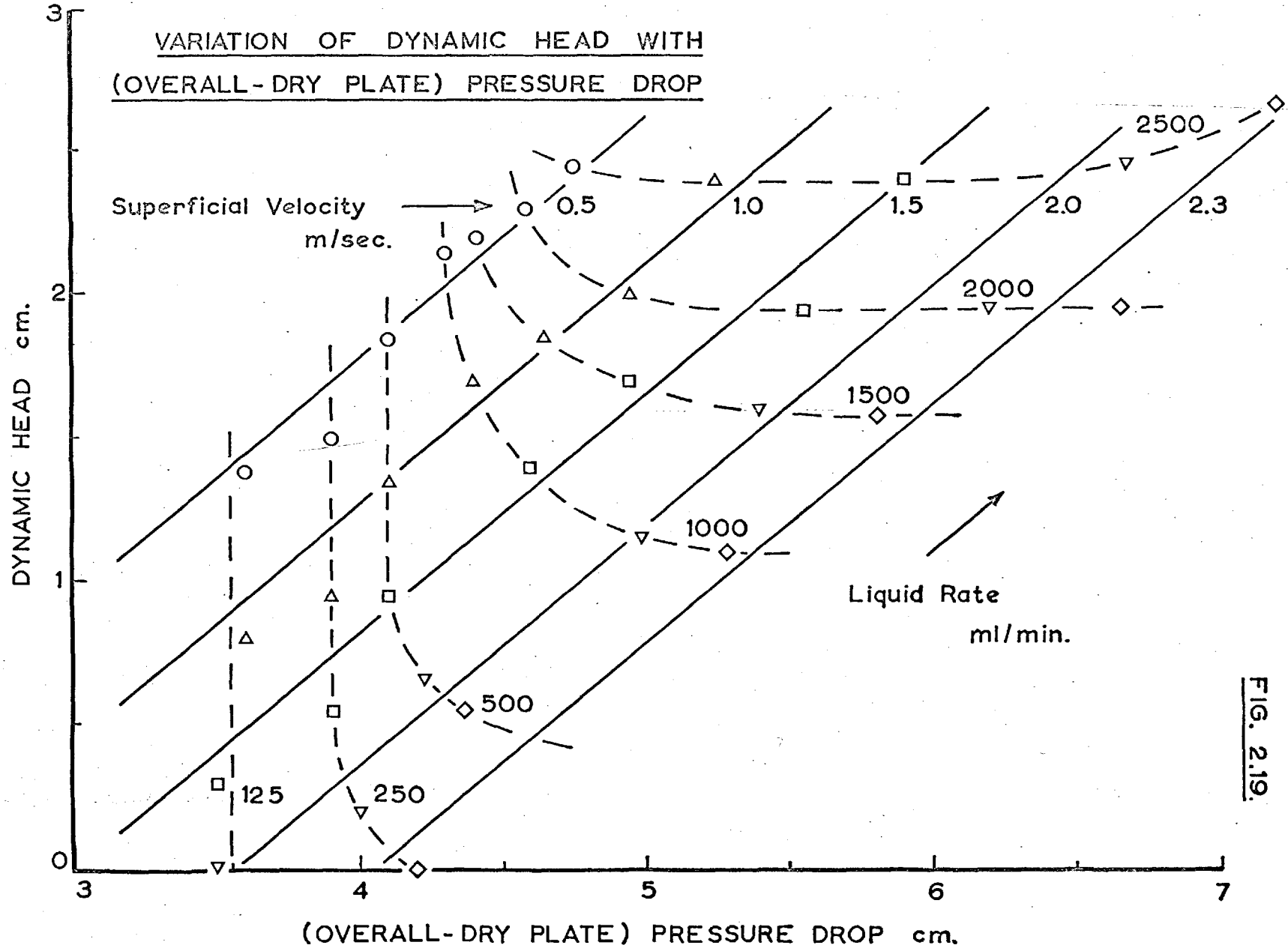
VARIATION OF DYNAMIC HEAD WITH
(OVERALL-DRY PLATE) PRESSURE DROP
Superficial Velocity
m/sec.
0.5
1.0
1.5
2.0
2.3
2500
2000
1500
1000
500
250
125
Liquid Rate
ml/min.
DYNAMIC HEAD cm.
(OVERALL-DRY PLATE) PRESSURE DROP cm.
0
1
2
3
4
5
6
7

FIG. 2.19.

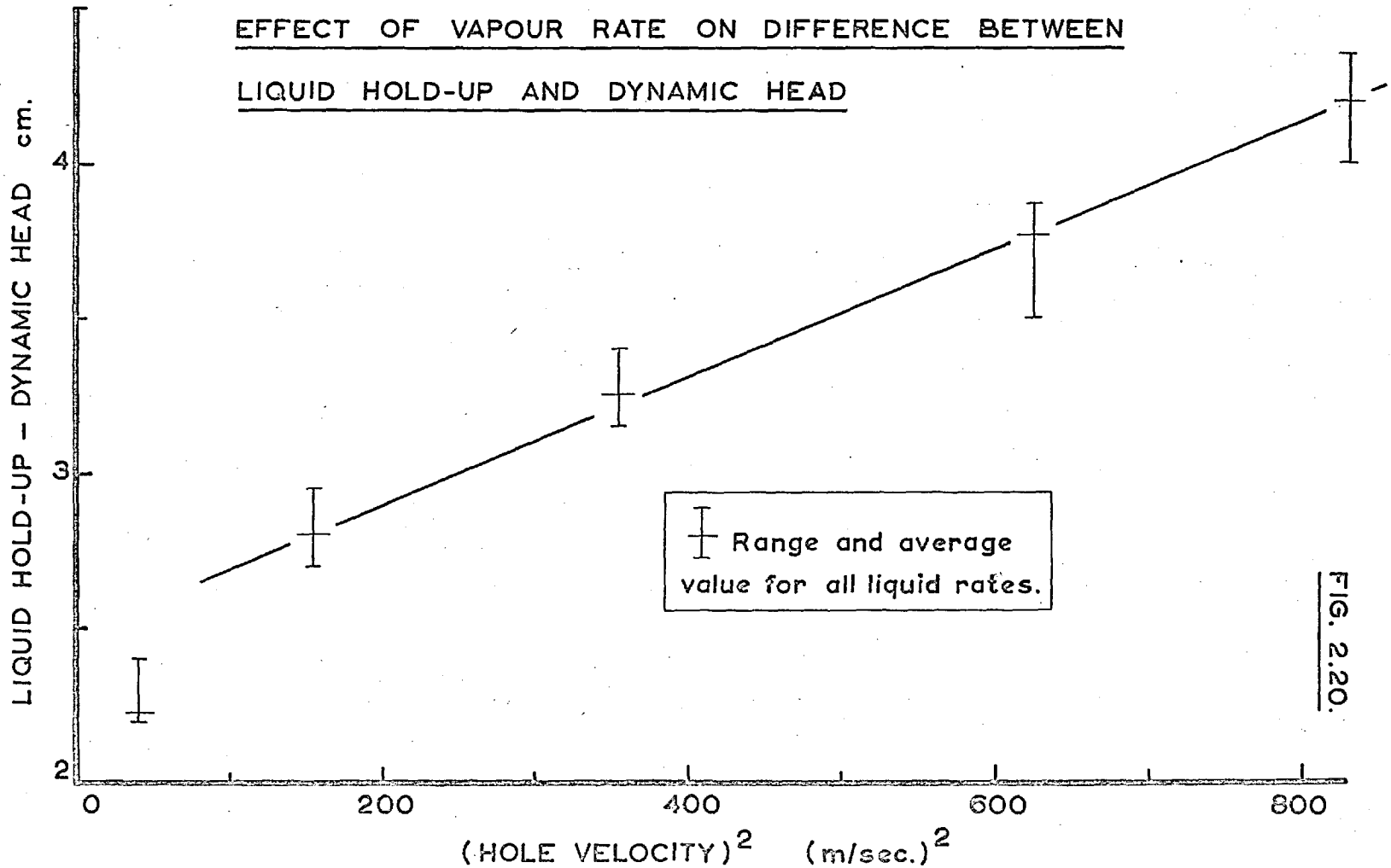
EFFECT OF VAPOUR RATE ON DIFFERENCE BETWEEN
LIQUID HOLD-UP AND DYNAMIC HEAD
LIQUID HOLD-UP - DYNAMIC HEAD cm.
2
3
4
0
200
400
600
800
(HOLE VELOCITY)^2 (m/sec.)^2
Range and average value for all liquid rates.

FIG. 2.20.

2.3.2. Pressure Drop Studies

The results obtained from the series of detailed observations of one plate geometry - 1/16in. holes, 10% free area - are presented in figures 2.12 to 2.20 inclusive.

As expected, the foam height varied with velocity as shown in figure 2.12. The effect of liquid rate can also be observed. The dispersion heights were in fact measured by eye and hence are not very accurate; however, a definite inflection can be seen in many of the curves in the region of 1 M/sec.

The overall pressure drop curves presented in figure 2.13. increase steadily with vapour rate and show no inflection points in contrast with the curves for dispersion height. Plotted also is the experimental dry plate pressure drop curve. With increasing vapour rate, the divergence between the dry plate and overall pressure drop also increases with liquid rate. The height of the outlet weir was 1 cm. but, at very low vapour rates, it would appear that the overall pressure drop was tending to 4 cm. of water.

During this series of experiments, the total liquid hold-ups were measured as the head of liquid in the inlet downcomer rather than by use of the δ-radiation technique. It had been shown earlier that, since the inlet downcomer resistance was small, the two methods gave comparable results with a maximum error of $2\frac{1}{2}\%$. Curves of the total liquid hold-up at different liquid rates as a function of vapour rate are given in figures

2.14. and 2.15. At the lower liquid rates, the hold-up increases initially, but at about 1 M/sec it steadies out to a fairly constant value. The liquid hold-up however increases continuously at the higher liquid rates, there being a slight inflection of the curve at around 1 M/sec. The effect of liquid rate at any given vapour rate may be seen more clearly from figure 2.16.

It is logical to split the total plate pressure drop into that due to the liquid on the plate (h_l) and that due to the passage of the vapour through the plate and dispersion (h_v), then:-

$$h_t = h_l + h_v \qquad \text{EQ. 2.1.}$$

Now from the above measurements, values for h_t and h_l are directly available. Thus values of h_v may be obtained by use of equn 2.1. In fact many previous workers have assumed that h_v is simply the pressure drop due to the same vapour flow through the dry plate (h_{dp}). However, as mentioned in chapter 1.8. other workers (14, 27, 47) have found that the term h_v was always greater than the dry plate pressure drop by a small amount termed the residual head (h_r); thus:-

$$h_v = h_{dp} + h_r \qquad \text{EQ. 2.2.}$$

Arnold et al.(47) found that h_r was of the order of 10% of the total plate pressure drop and ranged from 0.1 to 0.5in. water. Hunt et al.(14) concluded that the residual head could be considered constant at approximately 0.5in. water. They further noted that physical properties of the system such as viscosity, surface tension and density had no effect on h_r.

Low free area plates were found to produce slightly higher residual heads. Mayfield et al. (27) in their experiments found that h_r was very small ranging from 0 to 0.2in. water and it was considered to be negligible in comparison with the total plate pressure drop.

The manner in which h_v varied with the dry plate pressure drop can be seen from figure 2.17. At superficial velocities above about 0.5 M/sec, h_r is only slightly greater than the dry plate pressure drop. The separation between the curves is only 0.1 to 0.3 cm. water (0.05 to 0.15in.) which is much lower than the residuals found by Arnold et al. (47) and Hunt et al. (14). At superficial velocities below 0.5 M/sec. the residual head is much greater and may even be larger than the actual dry plate pressure drop at the lowest velocities. This is clearly due to inactivity of large sections of the plate.

There is clearly no effect of liquid rate or liquid hold-up on the values of h_v or h_r; this is in agreement with a tentative suggestion in the Delaware Report of the A.I.Ch.E. Research Programme (1) based on observations on bubble cap plates.

That the residual heads obtained in these studies are significantly smaller than those obtained by Hunt and Arnold and their co-workers is probably due to inaccurate measurement by them of the true liquid hold-up on the plate (h_l) - all presumed that dynamic head measurements gave an accurate assessment of the total liquid hold-up. Assuming the vapour momentum correlation proposed by Bernard et al. (40), the total liquid

hold-ups for the systems studied should have been about 0.5 to 1.0 cm. water greater than the dynamic head measurements. Allowing for this correction, the revised values of h_v would have been much closer to the dry plate pressure and in agreement with the results reported in this thesis. It is difficult to see why Mayfield's observations agree so closely with the present results for his hold-up measurement technique was the same as that of Hunt and Arnold.

Macmillan (5) who directly measured the liquid hold-up still obtained a residual head of the order of 1 cm. water at the highest vapour rates. However, Macmillan found that the dry plate pressure drop was proportional to the vapour rate to the 1.8 power. In the present work, the very carefully measured dry plate pressure drop varied as the vapour rate to the power 2.0.

Various hypotheses have been proposed to explain the existence of the residual pressure drop. It has been suggested that the surface tension forces required to produce a bubble are responsible for the increase in the pressure drop. However, Davidson and Schüler (48) have clearly shown that such forces are in fact negligible. The photographic observations reported in this thesis show that even at high vapour rates, the vapour still flows through the hole in an intermittent manner. Inevitably, this will increase the pressure drop across an operating plate above that for continuous flow through the dry plate. Furthermore, the liquid collar observed in the hole, whilst streamlining the orifice, will decrease the diameter

and increase the actual velocity and may affect the pressure drop. The residual pressure drop is therefore rather a complex function of the bubbling mechanism and for all practical design purposes it is perfectly reasonable either to ignore it or ascribe it a constant value of 0. lin. water.

As explained above, and reported elsewhere (40, 52) in detail, it was found that only dynamic head manometers placed in the central region of the plate gave reproducible results. The effects of vapour and liquid rates on the measured dynamic head can be seen in figure 2. 18. At the lower liquid rates, the dynamic head steadily decreases as the vapour rate is increased. At the highest liquid rates, the initial depression as the vapour rate increases is countered by a later rise in pressure.

Comparison of the dynamic head with the corresponding difference between overall and dry plate pressure drop ($h_t - h_{dp}$), which is a direct measure of the actual liquid hold-up (h_l), is shown in figure 2. 19. As can be seen, there is a marked effect of both liquid and vapour rates. However, Macmillan (5) found that for any given plate free area, the term ($h_l - l_d$) was a linear function of the hole velocity squared. Later Bernard et al. (40) managed to correlate ($h_l - l_d$) for various free areas as a function of change of vapour momentum. For the present work for one plate free area, it was possible to produce a very good correlation in terms of hole velocity squared as shown in figure 2. 20.which shows the range and average values of the function for all liquid rates at each vapour rate. The fit at the lowest vapour rate is not good but as expected the difference tends to zero

as the vapour rate tends to zero.

If the simple momentum correlation proposed by Bernard et al. (40) was in fact correct, then at a hole velocity of 18.5 M/sec. the momentum correction should be approximately 0.4 cm. water. However the observed divergence was 3.3 cm. water. Allowing for the bubbling correction h_r this may be reduced to 3.1 cm. water but even so, the observed divergence is still far greater than would be expected on the basis of the momentum correlation.

Campbell and Thomas (57) in their studies on a large (1 ft.) air/water simulator have also found that the dynamic head varied with position on the plate. For experimental runs with a 10% free area plate ($\frac{1}{8}$in. hole size) at a hole velocity of approximately 15 M/sec. the authors present curves showing that the dynamic head measured in the middle of the plate floor is consistently 2.5 cm. water lower than measurements in the calming sections at the inlet and outlet weirs. In the calming sections, there are unlikely to be very large kinetic effects due to the vapour and in these regions the measured dynamic head probably approximates closely to the actual liquid hold-up. Thus Campbell and Thomas have also observed differences between h_l and h_d of the same magnitude as reported in this thesis.

Clearly the relationship between dynamic head and liquid hold-up is much more complex than was suggested by Bernard et al. (40). The difference between h_l and h_d is insensitive to liquid flow rate or hold-up,

but simple reasoning based on overall momentum or kinetic energy changes do not explain the difference.

To resolve this problem a much clearer understanding of the processes controlling the two phase dispersion is essential. Until then dynamic head measurements made in the bubbling region of a plate must be treated with extreme caution. However, measurements made in calming sections probably give good estimates of the true liquid hold-up on the plate.

Chapter 2.4. GENERAL CONCLUSIONS

The photographic studies have shown that, at around 1 M/sec. superficial velocity, a change in structure of the dispersion occurs. The hydrodynamic studies reflect this change in the curves of dispersion height which shows a dip in the region of the transition. At superficial velocities above 1 M/sec. the liquid hold-up at high liquid rates increases more rapidly than before, but at low liquid rates the hold-up becomes constant above the transition velocity.

However, the pressure drop curves give no indication whatsoever of a change in régime. Thus hydrodynamically there does not appear to be an optimum region of operation; mass transfer and plate efficiency studies may however shed light on the relative usefulness of the two structural régimes.

For the purpose of design, it is reasonable to split the total plate pressure drop into the vapour pressure drop (h_v) and the liquid pressure drop (h_l) as in equation 2.1. Furthermore, the vapour pressure drop can be expressed as the sum of the dry plate pressure drop and the residual head as given in equation 2.2., and in fact this latter term (h_r) may be ignored.

At the moment, there are no adequate design correlations predicting liquid hold-up on a plate. This is because workers in the past have relied upon the use of dynamic head measurements to give liquid heads.

In fact, as has been shown, there is no straightforward relationship between them.

In agreement with previous workers (5, 6), hole size has been shown to be unimportant in determining liquid hold-up. The important geometric factors affecting the hold-up are weir height and free area. Using hole velocity as a basis, it is possible to correlate liquid hold-up as a function of free area for a given weir height and vapour and liquid loadings.

Fractionation Research Incorporated recommend the use of very large holes of the order of $\frac{1}{2}$in. to 1in. diameter in their design procedures for large distillation columns. Studies on hole sizes of this magnitude are not reported in the literature; but if hole size can be considered unimportant at even this level, it would be sensible to use very large holes. Blockage problems with resinous and tarry mixtures would be eliminated and corrosion troubles can be reduced. It may be, however, that the weeping mechanism in large diameter holes is very different from that in conventionally sized holes, in which case the flexibility of the tray might be reduced.

Naturally the above remarks can only apply strictly to the hydrodynamic design of columns and, as such, may contradict the mass transfer design requirements. However, the photographic and dispersion density studies show very clearly that hole size has little or no effect on the character of the dispersion at all but the very lowest vapour rates. Very similar dispersions are also generated by 5% and 10% free area plates. It would thus appear that these hydrodynamic factors may have similar effects on

the mass transfer performance of a column.

The aim of the studies reported in this thesis has not been to develop yet more empirical design correlations of an all too shaky character, but rather to investigate the processes producing the two phase mixture obtained on a sieve plate. The findings are of a rather qualitative nature and show up very strongly the complete lack of any quantitative understanding of the physical processes occurring in gas-liquid dispersions. Until these physical mechanisms are more clearly appreciated it is very unlikely that any significant advance will be made in the accurate design of distillation columns. With the advent of the large and powerful computers and the great advances in numerical methods in mathematics, it is now becoming feasible to investigate such complex physical problems.

PART 3

DEVELOPMENT OF A MATHEMATICAL MODEL TO DESCRIBE THE HYDRAULIC CHARACTERISTICS OF A SIEVE PLATE

PART 3

DEVELOPMENT OF A MATHEMATICAL MODEL TO DESCRIBE THE HYDRAULIC CHARACTERISTICS OF A SIEVE PLATE

Chapter 3.1. INTRODUCTION

The ultimate aim in research into a process such as distillation is naturally to obtain a full quantitative knowledge of the processes involved. To define the phenomenon of distillation adequately, knowledge of not only the mass transfer but also the hydrodynamic processes is essential.

Up to the present time, many experimental investigations of various aspects of the process have been performed. However the underlying physical mechanisms are not at all well understood and interpretation of the experimental information has been very limited. If, however, sensible correlations for mixing, hold-up etc. are to be developed in terms of operating parameters such as flow rates, plate geometry and weir height, it is essential to have a better understanding of the processes controlling the dispersion.

Attempts to produce mass transfer models have been made by various workers. Many are reproduced in the Michigan University A.I.Ch.E. Research Program report (2). In all cases, the authors have been forced to assume that the fluid hold-ups and mixing characteristics of the plate are known. Very recently Bernard (6) has attempted to extend

the eddy-diffusion model to take account of entrainment. However, considerable computational difficulties have so far prevented satisfactory predictions of efficiency.

There have been no successful attempts to develop mathematical models describing the hydrodynamic situation on a sieve plate. The possible unreliability of any mathematical description of the physics of the interaction of the gas and liquid phases and the inevitable complexity of any solution procedure may well be the reason for so little attention to this fundamental problem.

Because of the urgent need for a better understanding of the two-phase hydrodynamics, the model reported in this thesis has been developed.

Chapter 3.2. DEVELOPMENT OF EQUATIONS OF MOTION FOR THE TWO-PHASE MIXTURE

3.2.1. Development of Equations in the General Case

3.2.1i. Equations of Continuity

Consider an element of surface $d\underline{S}$ in a three dimensional space, then the extent and orientation is defined by the projections on the Cartesian axes as dS_k, $k = 1, 2, 3$. Also, for any arbitrary volume V of fluid, enclosed in a surface S, the outward pointing directions through the surface are by convention defined as positive.

If the volume fraction of any fluid in this small volume be f, then the fraction of the boundary surface occupied by the fluid is also f. Thus the outward flow through any elemental surface dS_i normal to axis x_i is given by:

$$\text{Flow} = \rho f V_i dS_i$$

Then the total flow across the element $d\underline{S}$ is obtained by summing over all i (using the summation convention for repeated suffices):

$$\text{Total flow} = \rho f V_k dS_k \qquad \text{- EQ. 3.2.1.}$$

Now the rate of accumulation in the arbitrary volume is the nett inflow through the total surface, hence:

$$\frac{\partial}{\partial t}\left[\int_V (\rho f) dV\right] = \int_S \rho f V_k (-dS_k) \qquad \text{- EQ. 3.2.2.}$$

By Green's Theorem, in general:

$$\int_S y_k dS_k = \int_V y_{k,k} dV$$

Thus applying Green's Theorem to equn 3.2.2.

$$\frac{\partial}{\partial t}\left[\int_V (\rho f)dV\right] = -\int_V (\rho f V_k)_{,k} dV$$

or:

$$\int_V \left(\frac{\partial}{\partial t}(\rho f)\right)dV = -\int_V ((\rho f V_k)_{,k})\, dV$$

Hence, since volume V was arbitrarily chosen:

$$\frac{\partial}{\partial t}(\rho f) = -(\rho f V_k)_{,k}$$

Or, writing the material balance for each phase, assuming incompressibility of the fluids:

$$\frac{\partial}{\partial t}(f_l) = -(f_l u_k)_{,k} \qquad \text{- EQ. 3.2.3A}$$

$$\frac{\partial}{\partial t}(f_v) = -(f_v v_k)_{,k} \qquad \text{- EQ. 3.2.3B.}$$

3.2.1ii Equations of Momentum

Applying Newton's Second Law of Motion to the arbitrary volume V in direction i:

Nett force in direction i on volume = Rate of momentum change in direction i

The external forces acting on the volume are as follows:-

(i) The gravitational field acts on the volume in the vertical direction and is of magnitude $f\rho\phi_i$ (where $\phi_i = -g\delta_{ik}$ if k is the vertical coordinate and by convention is positive upwards and δ_{ik} is the Kronecker Delta Function).

(ii) The interphase stress is the force exerted by the other phase per unit volume. By convention σ_i is taken as positive for the liquid phase.

Thus the total external force acting on the volume is:

$$\int_V (f\rho\phi_i + \sigma_i)\, dV$$

The forces acting on the phase through the bounding surface are:

(i) The force inwards due to pressure acting on the fluid in direction i $= (-fp).dS_i$ or $= -fp\,\delta_{ik}.dS_k$ on summation.

(ii) The force in direction i resulting from viscous stress on the surface $dS_k = fP_{ik}\,dS_k$ where P_{ik} is the viscous stress tensor.

Thus the total force acting over the surface is:

$$\int_S (-fp\,\delta_{ik} + fP_{ik})\, dS_k$$

The rate of change of momentum in direction i of material in the volume is given by:

$$\frac{\partial}{\partial t}\int_V (f\rho V_i)\, dV$$

The rate of flow of momentum in direction i out through the whole surface is given by:

$$\int_S (f\rho V_i).V_k dS_k$$

Thus applying Newton's Second Law:

$$\int_V (f\rho\phi_i + \sigma_i)\, dV + \int_S (-fp\,\delta_{ik} + fP_{ik})\, dS_k$$

$$= \int_V \left(\frac{\partial}{\partial t}(f\rho V_i)\right) dV + \int_S (f\rho V_i V_k)\, dS_k \qquad \text{- EQ. 3.2.4.}$$

Again, applying Green's Theorem to equn 3.2.4.:

$$\int_V (f\rho\,\phi_i + \sigma_i)\,dV + \int_V (-fp\,\delta_{ik} + fP_{ik})_{,k}\,dV$$

$$= \int_V \left(\frac{\partial}{\partial t}(f\rho V_i)\right) dV + \int_V (f\rho V_i V_k)_{,k}\,dV \qquad \text{- EQ. 3.2.5.}$$

The volume considered is arbitrary, thus equating the integrands of equn 3.2.5.:

$$f\rho\phi_i + \sigma_i + (-fp\,\delta_{ik} + fP_{ik})_{,k} = \frac{\partial}{\partial t}(f\rho V_i) + (f\rho V_i V_k)_{,k} \qquad \text{- EQ. 3.2.6.}$$

Rearranging equn 3.2.6.:

$$(fp\delta_{ik})_{,k} = (fp)_{,i}$$

one may obtain the equation of motion for any phase:

$$\frac{\partial}{\partial t}(f\rho V_i) = f\rho\phi_i + \sigma_i + (fP_{ik})_{,k} - (fp)_{,i} + (f\rho V_i V_k)_{,k} \qquad \text{- EQ. 3.2.7.}$$

Then, applying equn 3.2.7. to the liquid and vapour phases, one obtains the separate equations of motion:

$$\frac{\partial}{\partial t}(f_l\rho_l u_i) = F_i^{\,l} - (f_l p)_{,i} - (f_l\rho_l u_i u_k)_{,k} \qquad \text{- EQ. 3.2.8A.}$$

$$\frac{\partial}{\partial t}(f_v\rho_v v_i) = F_i^{\,v} - (f_v p)_{,i} - (f_v\rho_v v_i v_k)_{,k} \qquad \text{- EQ. 3.2.8B.}$$

where: $$F_i^{\,l} = f_l\rho_l\phi_i + \sigma_i + (f_l P^l_{ik})_{,k} \qquad \text{- EQ. 3.2.9A.}$$

$$F_i^{\,v} = f_v\rho_v\phi_i - \sigma_i + (f_v P^v_{ik})_{,k} \qquad \text{- EQ. 3.2.9B.}$$

By use of the phase material balances (equns 3.2.3A and 3.2.3B), these can be reduced to:

$$f_l \rho_l \frac{\partial u_i}{\partial t} = F_i^{\,l} - (f_l p)_{,i} - f_l \rho_l u_k u_{i,k} \qquad \text{- EQ. 3.2.10A.}$$

$$f_v \rho_v \frac{\partial v_i}{\partial t} = F_i^{\,v} - (f_v p)_{,i} - f_v \rho_v v_k v_{i,k} \qquad \text{- EQ. 3.2.10B.}$$

For the detailed form of the interphase stress tensor see section E below.

3.2.liii Equation of Pressure

The fluids are assumed to be incompressible, so that one may divide each of equns 3.2.3A. and 3.2.3B. by the appropriate density; addition then gives:

$$(f_v v_k + f_l u_k)_{,k} = -\frac{\partial}{\partial t}(f_v + f_l) = 0 \qquad \text{- EQ. 3.2.11.}$$

since $f_v + f_l = 1$, by definition.

Differentiating equations 3.2.8A. and 3.2.8B. with respect to direction i, summing over all directions and simplifying by use of equn 3.2.11., one obtains:

$$\frac{F_{k,k}^{\,v}}{\rho_v} + \frac{F_{k,k}^{\,l}}{\rho_l} - \left[p\left(\frac{f_v}{\rho_v} + \frac{f_l}{\rho_l}\right)\right]_{,kk} - (f_v v_i v_k + f_l u_i u_k)_{,ik} = 0$$

This may be written in a more convenient form as:

$$q_{,kk} = Q \qquad \text{- EQ. 3.2.12.}$$

where $q = p(f_v/\rho_v + f_l/\rho_l)$

and $$Q = \left(\frac{F_{k,k}^{\,v}}{\rho_v} + \frac{F_{k,k}^{\,l}}{\rho_l}\right) - (f_v v_i v_k + f_l u_i u_k)_{,ik}$$

or substituting equns. 3.2.9A. and 3.2.9B.:

$$Q = \left(\frac{1}{\rho_l} - \frac{1}{\rho_v}\right)\sigma_{k,k} + \left(\frac{f_v P^v_{ik}}{\rho_v} - f_v v_i v_k + \frac{f_l P^l_{ik}}{\rho_l} - f_l u_i u_k\right)_{,ik} \qquad \text{- EQ. 3.2.13.}$$

3.2.liv. The Interphase Stress

The frictional force between the two phases will clearly depend upon the relative motion of the phases, and upon the interfacial area which in turn depends on f_l. Furthermore, there should be no stress when either phase is absent or when the relative velocity of the phases is zero.

The simplest function to satisfy these conditions is:

$$\sigma_i = k f_v f_l (v_i - u_i) \qquad \text{- EQ. 3.2.14.}$$

3.2.lv. The Viscous Stress Tensor

In its most general form, the viscous stress tensor for a Stokesian fluid may be written as (see, for example, Aris (39)):

$$P_{ik} = \alpha\delta_{ij} + \beta e_{ik} + \gamma e_{ij} e_{jk} \qquad \text{- EQ. 3.2.15.}$$

where α, β and γ are functions of the invariants Θ, Φ, Ψ of the rate of strain tensor e_{ij}.

Since the fluids are considered incompressible, $\alpha = 0$. Also, if the fluids are Newtonian in behaviour, that is stress and strain are linearly related, $\gamma = 0$.

In the simplest form β is constant, then if $\beta = 2\varepsilon$, where ε is the eddy viscosity.

$$P_{ik} = 2\varepsilon e_{ik} \qquad \text{- EQ. 3.2.16.}$$

Differentiating equn 3.2.15. with respect to k:

$$P_{ik,\,k} = 2\varepsilon\, e_{ik,\,k}$$

But:

$$e_{ik} = \tfrac{1}{2}\left(V_{i,\,k} + V_{k,\,i}\right)$$

Then, for either phase:

$$\left(fP_{ik}\right)_{,\,k} = \varepsilon\left(f\left(V_{i,\,k} + V_{k,\,i}\right)\right)_{,k} \qquad \text{- EQ. 3.2.17.}$$

3.2.2. Boundary Conditions for the Variables

3.2.2i. Liquid Velocities

(A) At a solid boundary, $u_i = 0$ (all i) since there is no slip at the boundary nor flow through it.

(B) Along the inlet and outlet weirs, the liquid flow rate will be defined and it is assumed that the flow is in the direction normal to the plane of the weir - see foam density boundary conditions.

(C) At a hole, the liquid velocities are indeterminate since there is no liquid present.

3.2.2ii. Vapour Velocities

(A) At a solid boundary, $v_i = 0$ (all i) since there is no slip at the boundary, nor flow through it.

(B) Along the inlet and outlet weirs, the vapour velocities are indeterminate - see foam density boundary conditions.

(C) At a hole, the flow is assumed unidirectional, normal to the plate, and the hole velocity is defined.

3.2.2iii Foam Density

(A) At a solid boundary, applying the liquid phase material balance - equn 3.2.3A.:

$$\frac{\partial}{\partial t}(f_l) = -(f_l u_k)_{,k} = -\left[f_l (u_k)_{,k} + u_k (f_l)_{,k}\right]$$

But at a solid boundary, using condition (A) above:

$u_k = 0$ and $u_{k,i} = 0$ for all k and $i \neq n$

$$\therefore \frac{\partial}{\partial t}(f_1) = -f_1 u_{n,n} \qquad \text{- EQ. 3.2.18.}$$

where n is the direction normal to the boundary.

(B) Along inlet and outlet weirs it is assumed that there is no vapour carryover through the weirs, and that consequently only liquid is present. Thus $f_1 = 1$.

(C) At a hole, again flow is assumed steady, and weeping and entrainment are considered absent. Thus $f_1 = 0$.

3.2.2iv Pressure

Determination of the pressure boundary conditions for any fluid mechanical problem is most difficult. It is impossible to find in the literature satisfactory ways of defining the boundary conditions for any but the simplest of situations.

Solution of the Poisson Equation for the pressure requires that either the actual pressure or its normal gradient be everywhere defined on the boundary of the system. In fact, as shown below, it has been found possible to define the normal gradient of pressure everywhere on the boundary thus providing Von Neuman boundary conditions on the solid boundaries and mixed conditions in the holes and at weirs.

Whilst it is possible to produce boundary conditions for the pressure explicitly in p, solution of the pressure equation is more straight-

forward in terms of the variable q and the boundary conditions in terms of this variable have been deduced.

To solve the pressure equation for the full map of pressures, the solution must be obtained on the boundary as well as in the interior and for this, the value of the parameter Q must also be determined everywhere on the boundary.

In general at any boundary:

$$\frac{\partial v_k}{\partial t} = \frac{\partial u_k}{\partial t} = 0 \quad \text{(all k)}$$

since at a solid boundary all velocities are zero, and at other boundaries, steady state conditions are assumed. Hence from equn. 3.2.10A and 3.2.10B for any direction i:

$$F_i^l = (f_l p)_{,i} + f_l \rho_l u_k u_{i,k} \qquad \text{- EQ. 3.2.19A.}$$

$$F_i^v = (f_v p)_{,i} + f_v \rho_v v_k v_{i,k} \qquad \text{- EQ. 3.2.19B.}$$

Division of these equations by the appropriate density and then adding gives:

$$\frac{F_i^l}{\rho_l} + \frac{F_i^v}{\rho_v} = q_{,i} + (f_l u_k u_{i,k} + f_v v_k v_{i,k}) \qquad \text{- EQ. 3.2.20.}$$

(A) At a solid boundary, since all velocities are zero, equn. 3.2.20. reduces to:

$$q_{,i} = \frac{F_i^v}{\rho_v} + \frac{F_i^l}{\rho_l}$$

Now $\sigma_i = 0$ for all i. Hence substituting equns 3.2.9A. and 3.2.9B. in the above yields, for the normal direction:

$$q_{,n} = \phi_n + \left(\frac{f_l P^l_{nk}}{\rho_l}\right)_{,k} + \left(\frac{f_v P^v_{nk}}{\rho_v}\right)_{,k} \qquad \text{- EQ. 3.2.21.}$$

Applying equn 3.2.17. for the direction normal to the boundary:

$$(fP_{nk})_{,k} = \varepsilon \left(f\left(V_{n,k} + V_{k,n}\right)\right)_{,k}$$

expanding and eliminating:

$$(f P_{nk})_{,k} = \varepsilon \left(f_{,n} V_{n,n} + f_{,k} V_{k,n} + f V_{n,nn} + f V_{k,kn}\right)$$

- EQ. 3.2.22.

(B) <u>At a hole</u>, since flow is steady, applying equn 3.2.10B. directly we obtain:

$$(f_v p)_{,i} = F_i^v - f_v \rho_v v_k v_{i,k}$$

Now:

$$q_{,i} = \left(\frac{f_v p}{\rho_v}\right)_{,i} + \left(\frac{f_l p}{\rho_l}\right)_{,i}$$

But:

$$(f_l p)_{,i} = f_l p_{,i} + p f_{l,i}$$

$$= - p f_{v,i}$$

$$= - q \rho_v f_{v,i}$$

Thus for the direction normal to the plate:

$$q_{,n} = \frac{(f_v P)_{,n}}{\rho_v} - q\frac{\rho_v}{\rho_l} f_{v,n}$$

or:

$$q_{,n} + q\frac{\rho_v}{\rho_l} f_{v,n} = \frac{F^v_n}{\rho_v} - v_n v_{n,n}$$

Substituting for F^v_n:

$$q_{,n} + q\frac{\rho_v}{\rho_l} f_{v,n} = \phi_n + \frac{(f_v P^v_{nk})_{,k}}{\rho_v} - v_n v_{n,n} \qquad \text{- EQ. 3.2.23.}$$

But: $$(f_v P^v_{nk})_{,k} = (f_v)_{,k} P^v_{nk} + P^v_{nk,k}$$

$$= \varepsilon_v (v_{n,nn} + v_{k,kn} + 2 f_{v,n} v_{n,n}) \qquad \text{- EQ. 3.2.24.}$$

(C) At a weir, exactly the same arguments apply as for a hole. It can be shown that:

$$q_{,n} + q\frac{\rho_l}{\rho_v} f_{l,n} = \phi_n + \frac{(f_l P^l_{nk})_{,k}}{\rho_l} - u_n u_{n,n} \qquad \text{- EQ. 3.2.25.}$$

where:

$$(f_l P^l_{nk})_{,k} = \varepsilon_l (u_{n,nn} + u_{k,kn} + 2 f_{l,n} u_{n,n}) \qquad \text{- EQ. 3.2.26.}$$

(D) Value of Q at a solid boundary. In general, Q is given by equn 3.2.13. This form may be simplified at the boundaries. Since all velocities are zero on a solid boundary:

$$\sigma_{i,i} = 0 \qquad i \neq n$$

Hence: $$\sigma_{k,k} = \sigma_{n,n}$$

Now: $(fP_{ik})_{,ik} = f_{,ik} P_{ik} + 2f_{,i} P_{ik,k} + f P_{ik,ik}$

But $P_{ik} = \varepsilon (V_{i,k} + V_{k,i})$

Thus for either phase in general:

$$(fP_{ik})_{,ik} = \varepsilon \Big[f_{,ik} (V_{i,k} + V_{k,i}) + 2 f_{,i} (V_{i,kk} + V_{k,ik}) + f V_{i,ikk} \Big] \quad \text{- EQ. 3.2.27.}$$

Since at a solid boundary:

$$V_i = 0 \quad \text{all } i$$

and $V_{i,k} = 0 \qquad k \neq n$

equn 3.2.27. reduces to:

$$(fP_{ik})_{,ik} = 2\varepsilon \Big[f_{,kn} V_{k,n} + f_{,k} (V_{k,nn} + V_{i,ik}) + f V_{i,ikk} \Big] \quad \text{- EQ. 3.2.28.}$$

Also:

$$(f V_i V_k)_{,ik} = f_{,ik} (V_i V_k) + 2 f_{,i} (V_i V_k)_{,k} + f (V_i V_k)_{,ik} \quad \text{- EQ. 3.2.29.}$$

and, at a solid boundary this reduces to:

$$(f V_i V_k)_{,ik} = 2f (V_{n,n})^2 \quad \text{- EQ. 3.2.30.}$$

Hence at a solid boundary:

$$Q = \left(\frac{1}{\rho_l} - \frac{1}{\rho_v}\right) \sigma_{n,n} - 2 \left(f_l (u_{n,n})^2 + f_v (v_{n,n})^2 \right) + 2 \frac{\varepsilon_l}{\rho_l} \Big[f_{l,kn} u_{k,n} + f_{l,k} (u_{k,nn} + u_{i,ik}) + f_l u_{i,ikk} \Big] + 2 \frac{\varepsilon_v}{\rho_v} \Big[f_{v,kn} v_{k,n} + f_{v,k} (v_{k,nn} + v_{i,ik}) + f_v v_{i,ikk} \Big] \quad \text{- EQ. 3.2.31.}$$

(E) Value of Q at a hole. As in all cases above, consider a point in the plane of the hole remote from the influence of the solid plate. Then equns 3.2.13., 3.2.27. and 3.2.29. are applicable.

Since no liquid is present we know that:

$$\sigma_i = 0 \qquad \text{all } i$$

and $$\sigma_{i,k} = 0 \qquad k \neq n$$

Furthermore, equn 3.2.27. for the vapour phase reduces to:

$$(f_v P^v_{ik})_{,ik} = \varepsilon_v \left[2 f_{v,nk} v_{k,n} + 2 f_{v,n} (v_{n,nn} + v_{k,nk}) + v_{i,ikk} \right] \qquad \text{- EQ. 3.2.32.}$$

and for the liquid phase it reduces to:

$$(f_l P^l_{ik})_{,ik} = \varepsilon_l \left[2 f_{l,nk} u_{k,n} + 2 f_{l,n} (u_{n,nn} + u_{k,nk}) \right] \qquad \text{- EQ. 3.2.33.}$$

By similar argument for each phase, equn 3.2.29. reduces to:

$$(f_v v_i v_k)_{,ik} = f_{v,nn} v_n^2 + 2 f_{v,n} v_n v_{n,n} + 2 v_{n,n}^2 + 2 v_n v_{k,kn} \qquad \text{- EQ. 3.2.34.}$$

and:

$$(f_l u_i u_k)_{,ik} = f_{l,nn} u_n^2 + 2 f_{l,n} u_n u_{n,n} \qquad \text{- EQ. 3.2.35.}$$

Now applying equn 3.2.3B. in the hole:

$$(f_v v_k)_{,k} = 0$$

$$\therefore \quad f_{v,n} v_n + v_{n,n} = 0 \qquad \text{- EQ. 3.2.36.}$$

and again applying the liquid phase continuity equn 3.2.3A.:

$$(f_l u_k)_{,k} = 0$$

$$\therefore \quad f_{l,n} u_n = 0 \qquad \text{- EQ. 3.2.37.}$$

Substituting equns 3.2.36. and 3.2.37. in equns 3.2.34. and 3.2.35. respectively:

$$(f_v v_i v_k)_{,ik} = f_{v,nn} v_n^2 + 2 v_{k,kn} v_n \qquad \text{- EQ. 3.2.38.}$$

$$(f_l u_i u_k)_{,ik} = f_{l,nn} u_n^2 \qquad \text{- EQ. 3.2.39.}$$

Hence at a hole:

$$Q = \left(\frac{1}{\rho_l} - \frac{1}{\rho_v}\right) \sigma_{n,n} - \left(f_{l,nn} u_n^2 + f_{v,nn} v_n^2 + 2 v_n v_{k,kn}\right)$$

$$+ \frac{\varepsilon_v}{\rho_v}\left[2 f_{v,nk} v_{k,n} + 2 f_{v,n}\left(v_{n,nn} + v_{k,nk}\right) + v_{i,ikk}\right]$$

$$+ \frac{\varepsilon_l}{\rho_l}\left[2 f_{l,nk} u_{k,n} + 2 f_{l,n}\left(u_{n,nn} + u_{k,nk}\right)\right] \qquad \text{- EQ. 3.2.40.}$$

(F) Value of Q at a weir. Conditions at a weir are directly comparable with those at a hole, and it immediately follows that:

$$Q = \left(\frac{1}{\rho_l} - \frac{1}{\rho_v}\right) \sigma_{n,n} - \left(f_{v,nn} v_n^2 + f_{l,nn} u_n^2 + 2 u_n u_{k,kn}\right)$$

$$+ \frac{\varepsilon_l}{\rho_l}\left[2 f_{l,nk} u_{k,n} + 2 f_{l,n}\left(u_{n,nn} + u_{k,nk}\right) + u_{i,ikk}\right]$$

$$+ \frac{\varepsilon_v}{\rho_v}\left[2 f_{v,nk} v_{k,n} + 2 f_{v,n}\left(v_{n,nn} + v_{k,nk}\right)\right] \qquad \text{- EQ. 3.2.41.}$$

Chapter 3.3. METHOD OF SOLUTION OF THE EQUATIONS

3.3.1. Introduction

The equations describing the system are a set of extremely complex simultaneous partial differential equations. As yet, no analytical solution procedure has been devised to solve such a group of equations and existing numerical solution techniques have to be relied upon.

As can be seen from chapter 3.2.1., the variation with time of the variables $\underline{u}$, $\underline{v}$ and f_1 are derived explicitly in the Euler and continuity equations (3.2.10A., 3.2.10B., 3.2.3A.). The pressure however is determined by the Poisson Equation (3.2.12.) in terms of the other seven defining parameters at any time.

Clearly, therefore, if the variables $\underline{u}$, $\underline{v}$ and f_1 be updated through any small time change by solution of relevent Euler equations, the new pressure field associated with the new values may be found by solution of the Poisson equation. The new values of pressure and the new values for all the other variables may then be used to resolve the Euler equations and obtain refined estimates of $\underline{u}$, $\underline{v}$ and f_1. By repeatedly using this iterative technique all the variables should settle down to steady values satisfying the overall mass balance obtained from equations 3.2.3A. and 3.2.3B.:

At all times:

$$\frac{\partial}{\partial t}(f_v) + \frac{\partial}{\partial t}(f_1) = 0$$

$$\therefore \quad (f_1 u_k + f_v v_k)_{,k} = 0 \qquad \text{- EQ. 3.3.1.}$$

FIG. 3.1.

FLOW DIAGRAM FOR

GENERAL SOLUTION PROCEDURE

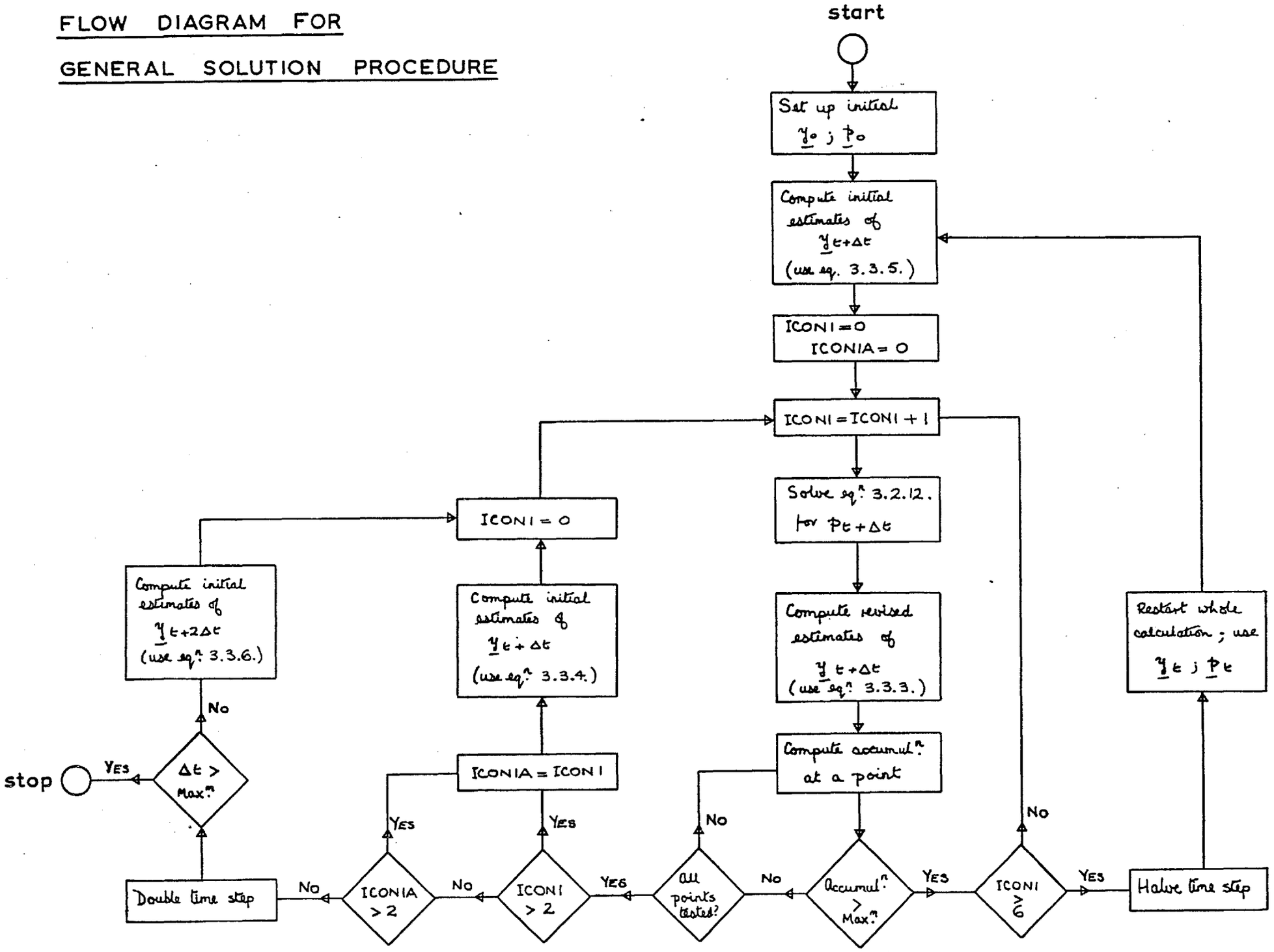

Thus the solution procedure may be separated into two parts:

(1) Time development solution

(2) Pressure equation solution

Iteration round the two parts will be continued until satisfactorily convergence is achieved.

The detailed flow diagram of the solution procedure is given in figure 3.1. As can be seen, the flow scheme takes account of the rate with which convergence is being achieved with any given time step length during the calculation. If at any time convergence consistently occurs after only a few iterations, the present step length may be increased somewhat to improve the overall speed of solution. If, on the other hand, convergence is slow or even not achieved during some phase of the calculation the time step used is too large and should be reduced to improve the convergence rate.

3.3.2. Form of the Numerical Approximations to the Equations

Of the various numerical solution techniques available for the solution of differential equations, the most powerful and clearly the most suitable for the present problem is the finite-difference method. The behaviour of finite-difference approximated parabolic equations is well studied and known to be stable under a wide range of conditions. Furthermore, a standard solution technique for the Poisson equation is available using finite-difference methods.

Appropriate finite-difference equations for the various function derivatives are derived in detail in chapter 3.4.2. As shown in that chapter, it is possible to derive both symmetric and asymmetric finite-difference formulae. If the differential equations are applied at the boundaries and represented in symmetric finite-difference form, then the same number of boundary conditions as equations are required to evaluate the values of the variables at the hypothetical points. If asymmetric formulae are used to represent the equations at the boundaries, then there is no need to apply the boundary conditions at all - this is clearly unreasonable. Thus the differential equations should only be applied in the interior of the region and represented in symmetric finite-difference form. The boundary conditions for the velocities of the phases cannot be disputed and thus arbitrary conditions must be chosen for foam density and pressure.

In the initial development of the defining equations, an arbitrary simplification was made of the form of the dispersion and foam density wa

made a point continuous function. It is therefore difficult to choose any physically probable condition. However, a convenient and possibly not unreasonable boundary condition is:

$$f_{1,n} = 0 \qquad \text{- EQ. 3.3.2.}$$

thus implying that the wall effect is not very great.

Definition of pressure at a boundary is extremely difficult; almost universally pressure has been eliminated from situations being studied by the use of the concept of vorticity. Such a transformation is of definite advantage in 2-dimensional flow but does not simplify computation in complex 3-dimensional flow problems of the kind under investigation. Whenever possible, authors (e.g. Aris (39)) have considered flow problems without discussing pressure at boundaries. Recently, Fromm (58) has investigated the flow patterns of the wake downstream of an obstacle in a bounded medium. Fromm considered, apparently quite arbitrarily, that the normal gradient of pressure at any boundary was zero. Although it can be argued that such an assumption is physically untenable, the results he obtained were remarkably similar to the experimental patterns. Gravitational forces were not considered by Fromm.

For the present two-phase flow case where hydrostatic forces are of importance, the analogous boundary condition would be:

$$q_{,n} = \phi_n \qquad \text{- EQ. 3.3.3.}$$

This in fact is the boundary condition that equations 3.2.21., 3.2.23. and

3.2.25. reduce to under static conditions.

To allow for the effects of the holes and weirs, it may be better to use the modified conditions at a hole:

$$q_{,n} = \phi_n - v_n v_{n,n} \qquad \text{- EQ. 3.3.4.}$$

and at a weir:

$$q_{,n} = -u_n u_{n,n} \qquad \text{- EQ. 3.3.5.}$$

$$(\text{since } \phi_n = 0)$$

The only justification for the use of such boundary conditions is the reported success of others who have used them. The fact that such assumptions have had to be made highlights the really fundamental failure of physicists and fluid mechanicists to understand and define the effects of pressure on boundaries.

3.3.3. Time Development Solution

If the equations for the velocities and foam density be written in the appropriate space finite-difference form (see chapter 3.4.), then for each grid point, there is a set of seven ordinary differential equations in time. This set may be written as:

$$\frac{d\underline{y}_i}{dt} = f^i(\underline{y}, \underline{p}) \qquad \text{- EQ. 3.3.6}$$

where y^i is a typical dependent variable and underlining denotes the set. In fact the variable f_v is required in these equations but is readily eliminated since $f_v + f_l = 1$. The set of pressures ($\underline{p}$) must be obtained independently at each time by solving the pressure equation for the present $\underline{y}$.

The set of differential equations 3.3.6. may in general be solved by using the Trapezoidal Rule, thus:

$$\frac{y^i_{t+\Delta t} - y^i_t}{\Delta t} = \tfrac{1}{2}\left[f^i(\underline{y}_t, \underline{p}_t) + f^i(\underline{y}_{t+\Delta t}, \underline{p}_{t+\Delta t})\right] \qquad \text{- EQ. 3.3.7.}$$

with the initial estimates of $\underline{y}_{t+\Delta t}$ given by using the modified Euler equation:

$$\frac{y^i_{t+\Delta t} - y^i_{t-\Delta t}}{2\Delta t} = f^i(\underline{y}_t, \underline{p}_t) \qquad \text{- EQ. 3.3.8.}$$

For the initial time step, estimates of $\underline{y}_{t+\Delta t}$ may be obtained using the Euler equation:

$$\frac{y^i_{t+\Delta t} - y^i_t}{\Delta t} = f^i(\underline{y}_t, \underline{p}_t) \qquad \text{- EQ. 3.3.9.}$$

If, during the computation, the existing time step interval becomes too short, initial estimates of the variables for a new time step length double the previous one may be obtained by use of:

$$\frac{y^{i}_{t+2\Delta t} + 3y^{i}_{t} - 4y^{i}_{t-\Delta t}}{6\Delta t} = f^{i}(\underline{y}_t, \underline{p}_t) \qquad \text{- EQ. 3.3.10.}$$

These are simple examples of "predictor-corrector" methods which are discussed fully by Hamming (37).

The details of the computational scheme for the time development solution can be found in figure 3.1. As can be seen, a variable time step length has been used. If after six iterations at any time t with a given time step Δt the accumulation function (equn 3.3.1.):

$$(f_v v_k + f_l u_k)_{,k}$$

at every point is not satisfactorily small, the time step length is halved, and the whole computation procedure restarted from time t_o, the set $\underline{y}_t$ being used as the initial field $\underline{y}_o$.

On the other hand, if at time t, the field converges in less than 3 iterations, the time is advanced to $t + \Delta t$. If, again, the accumulation is small in less than 3 iterations, the time step length is doubled and the time advanced to $t + 2\Delta t$; however, if the convergence rate is slower at time $t + \Delta t$, the old step length is retained.

The detailed procedure recommended for updating the velocity and foam density maps is:

(1) Assume full map of q including values at hypothetical points as well as $\underline{u}$, $\underline{v}$, $\underline{f_1}$.

(2) Use momentum equations (equns. 3.2.10A., 3.2.10B.) to update interior velocities. Add boundary values.

(3) Apply momentum equations at the boundaries to generate velocities at hypothetical points.

(4) Compute velocity gradients at boundaries using symmetric formulae.

(5) Compute f_1 on boundaries using equn. 3.2.18.

(6) Compute hypothetical point value of f_1 using $f_{1,n} = 0$.

(7) Compute full map of Q.

(8) Solve pressure equn. 3.2.12. to give q everywhere and compute value at hypothetical point using boundary condition.

3.3.4. Pressure Equation Solution

As mentioned earlier, the pressure equation (equn 3.2.12) belongs to the well-known class of Poisson equations with Von Neuman boundary conditions. Numerical solution procedures for such equations have been widely studied and a number of methods have been developed. Such methods are reviewed by Greenspan (35), Smith (36), Varga (38) and Russell (42).

The most powerful method for large arrays, and the one actually used is the method of "successive over-relaxation" (S.O.R.).

If the pressure equation be written in finite-difference form at any point 'o' then:

$$q_o = Q_o - \sum_{i=1}^{8} \alpha_i q_i = \gamma_o \qquad \text{- EQ. 3.3.7.}$$

Clearly, if a given $\underline{q}$ are the true values for the entire field, then they will satisfy equation 3.3.7. Otherwise substitution of $\underline{q}$ in the right hand side of equation 3.3.7. will generate a set of q_o that are in error. However, by suitably weighting the various values of q in the vicinity of the point considered, it is possible to produce successive values of q_o that converge to the true value. This then leads to the S.O.R. solution procedure, for if at any position 'o', the 'm'th estimate of q_o is q_o^m:

$$q_o^{m+1} = (1 - w)\, q_o^m + w\, \gamma_o^m \qquad \text{- EQ. 3.3.8.}$$

The quantity w is termed the "relaxation parameter" and for over-relaxation

$$w > 1.$$

There are in fact two basic methods of S. O. R. applying equn 3. 3. 8 they are point S. O. R. and line S. O. R. In the former method, one iteration is made at each successive point in the matrix using, either the most recent information about all the points $\underline{q}_i$, or the values at step m - in fact for point S. O. R. it is faster to use the most recent information. Line S. O. R. applies the technique to a whole line of points simultaneously. The points in the line are then solved by Gauss Elimination. This method uses $\underline{q}_i^m$.

In general, line S. O. R. is much faster than point S. O. R. but for large matrices working space requirements may be excessive, as indeed they are for the present problem.

Varga (38) shows clearly that consistent ordering of the points in the matrix is imperative - a detail only lightly mentioned by Greenspan (35). If the points are incorrectly ordered the iteration matrix will be unsymmetric and convergence will be slow or, even more likely, divergence will occur. This means that the differential equation must be applied at the boundary and then the hypothetical points beyond the boundary must be obtained in terms of the normal gradient on the boundary. Furthermore, the repeated sweeps of the matrix must be made in the same sense about a single origin. This origin must be ascribed a fixed arbitrary value.

Early attempts to solve the pressure equation using asymmetric boundary formulae based on Greenspan (35) failed for the basic reasons discussed by Varga (38) and apparently not fully appreciated by Greenspan.

FIG. 3.2

EFFECT OF THE RELAXATION FACTOR ON CONVERGENCE RATE

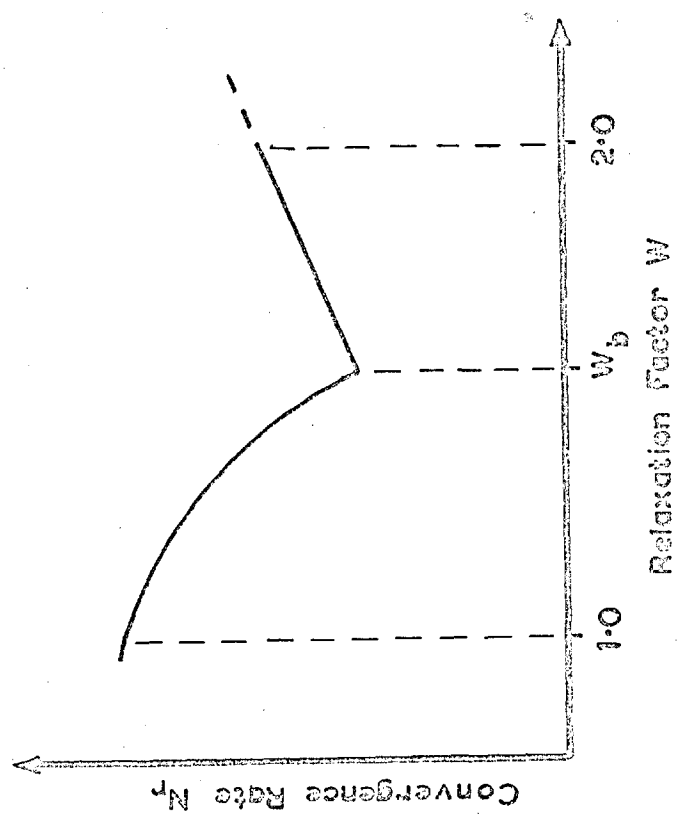

The rate at which convergence is achieved for the properly posed problem depends very strongly upon the choice of the relaxation factor w. The optimum value w_b lies between 1 and 2; for $w>2$ instability always results. In general w_b depends upon the size and shape of the matrix, and in fact is a very complex function of the iteration matrix. It is thus usually impossible to determine w_b theoretically. Methods have been developed for determining w_b numerically. These study the behaviour of the solution over approximately 100 iterations using a factor $w = 1$, (Wachspress (43)). However, in the present case, it is easier to find w_b by trial and error for the general behaviour of the convergence rate N_r as w is varied between 1 and 2 as shown in figure 3.2. By plotting the number of iterations required for convergence against w, the value of w_b can be assessed fairly accurately. In fact, it is preferable to use a value slightly larger than w_b as the effect on the overall convergence rate of over-estimating w is far less critical than under-estimating w by a comparable amount.

As the solution of the pressure equation at any time is part of a much larger loop, the degree of convergence necessary need not be very high. Indeed the pressure field will not change greatly between successive time steps. In consequence the number of iterations may be drastically limited to about 10, thus saving considerable computing time.

3.3.5. The Effect of Flow Discontinuities on the Boundaries

The holes on the plates and the weirs represent sources and sinks for both the vapour and liquid phases and in consequence, it may be thought that they have to be considered as discontinuities and treated specially.

Methods of dealing with discontinuities are most complicated and rarely very successful, c.f. Russell (42). Indeed, to devise a suitable scheme capable of overcoming any troubles associated with the present problem would be most difficult.

However, Rosenbrock and Storey (45) have shown that discontinuities apparent in the analytical solution are often smoothed out by the finite difference grid used in the numerical solution. As discussed in Chapter 3.4., the holes and weirs are represented by single points and rows respectively, whereas the analytical conditions in these regions are specified in terms of typical conditions in the interior of a hole or weir. The same is true for the analytical boundary conditions for a solid boundary. Thus in finite-difference form, conditions at a hole or weir are partly defined in terms of the local conditions on the solid boundary. The reverse is true for a solid boundary grid point in the proximity of a hole or weir. Rosenbrock and Storey point out that such discontinuities do not in fact exist physically, and since singularity problems introduced in the analytical representation are blurred by the finite difference formulae a reasonable physical picture may still be obtained.

Chapter 3.4. CHOICE OF GRID SYSTEM AND DEVELOPMENT OF FINITE DIFFERENCE APPROXIMATIONS

3.4.1. Choice of a Suitable Grid System to Represent a Column

To describe a plate a three dimensional grid system is required. However, if a plate of infinite width is considered (i.e. no wall effect), there will be some symmetry in the direction normal to the line of bulk liquid flow across the plate. In such a case, a line of holes would represent a line of symmetry. A "strip solution" between adjacent lines of holes was therefore assumed and a suitable three dimensional grid system was established.

Rectangular grid systems are the most convenient for many reasons; but because holes are punched in a triangular pattern a rectangular grid system proved unsatisfactory in the horizontal plane. An equilateral triangular grid pattern matching the plate geometry fitted perfectly. In the vertical plane, a rectangular grid fitted the geometry.

Because a rather simplified description of the region was being investigated, it was further decided that boundaries should coincide with standard grid points, rather than require special attention with non-standard finite difference formulae.

The mesh sizes and total grid lengths were chosen after considering the possible coarseness of the mesh to describe the processes adequately and the storage limitations of the computer available (IBM 7090). It was

FIG. 3.3

GRID REPRESENTATION OF PLATE GEOMETRY

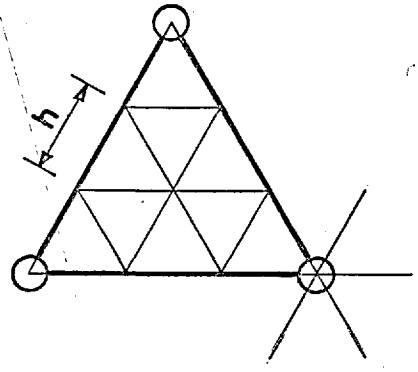

The contribution of each grid point at any hole to a major triangle is 1/6

Thus the total number of grid points associated with each major triangle

$$= \underset{\text{(holes)}}{3 \times 1/6} + \underset{\text{(interior)}}{1} + \underset{\text{(edges)}}{6 \times 1/2} = 9/2$$

Thus the effective free area = $(3 \times 1/6)/(9/2) = 1/9$

Now the true free area of the plate = $0.91\ (d/p)^2$

Thus, since $d/p = 1/3$,

the error of the grid representation = 9%

FIG. 3.4

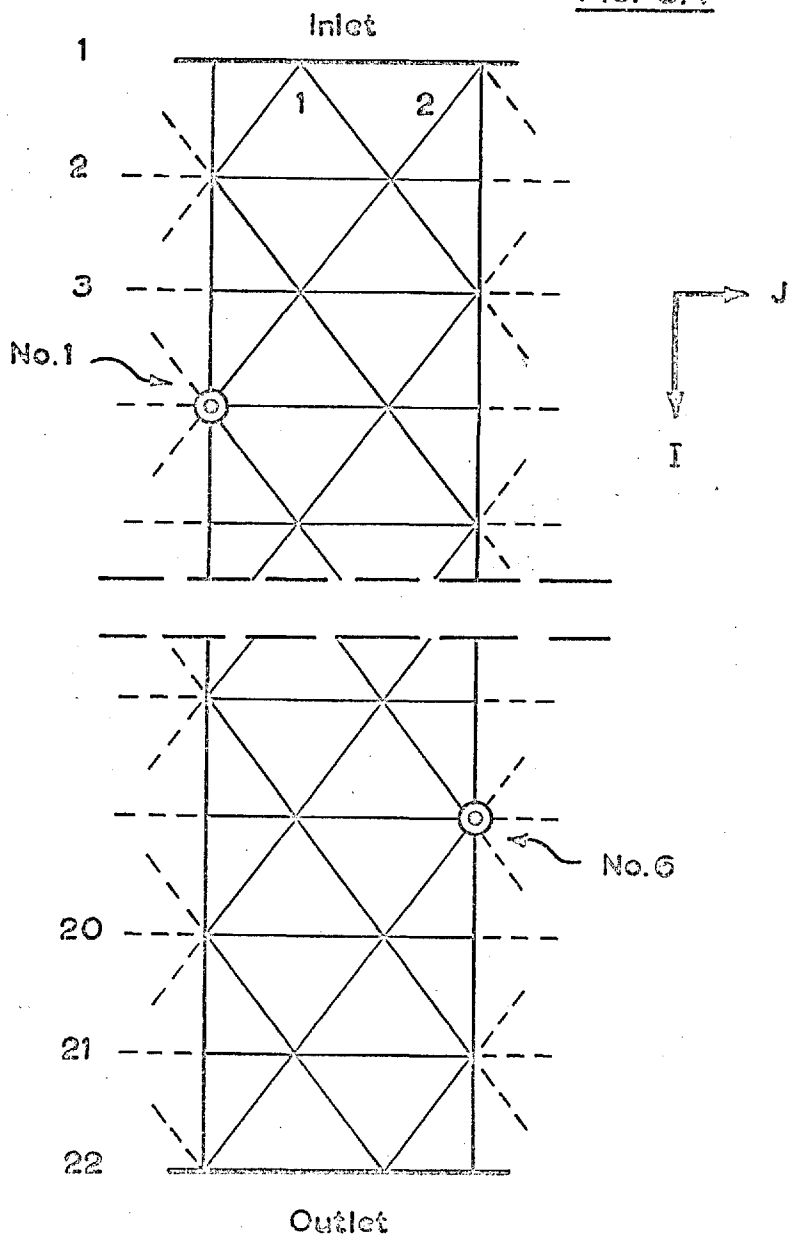

HORIZONTAL GRID PATTERN SHOWING

POSITION OF HOLES

clearly convenient to make the mesh size (h) some multiple or sub-multiple of the hole pitch (p). If the mesh size were equal to or greater than the pitch, the grid would be too coarse to describe the non-uniformity of flow through the plate holes. Also, if the mesh size were made smaller than the hole diameter (d), then there may be more than one grid point associated with a hole, and the analysis of the flow through the holes would be rather complex. Hence we have the situation:

$$d \lesssim h \lesssim p$$

If in fact the mesh size equals the hole diameter, the resulting grid possesses properties very similar to those of the actual plate, (see figure 3.3.) and the grid hole velocity is very close to the plate hole velocity for a given superficial velocity.

The vertical mesh size could be fixed much more arbitrarily. In fact storage limitations required that as coarse a grid as possible be used. A length 0.5in. was chosen. The inlet and outlet weirs are treated as slits in the wall and were centred along a plane of grid points.

The minimum reasonable plate separation is about 10ins. and this was taken as the vertical grid height, giving 21 vertical grid planes. The total length of flow path was therefore severely reduced to 6 holes as shown in figure 3.4. Even so, this very small system is of similar dimensions to the small perspex column use for the photographic and pressure drop studies reported in parts 1 and 2 of this thesis. It would therefore be hoped that the predictions produced by the mathematical model would agree with the observations in the small column.

3.4.2. Development of Finite Difference Approximations for Function Derivatives

In the solution of the equations all possible derivatives of the first and second order for the three co-ordinate directions i, j and k are required.

For any function w varying along an arc S in direction n, we have:

$$\frac{\partial w}{\partial S_n} = a_{ni} \frac{\partial w}{\partial x_i} + a_{nj} \frac{\partial w}{\partial x_j} + a_{nk} \frac{\partial w}{\partial x_k} \qquad \text{- EQ. 3.4.1.}$$

where the a_{ni} are the direction cosines of the direction n. For a sufficiently small change in S_n, assuming a Taylor Series expansion:

$$w_n - w_o = \delta_n \frac{\partial w}{\partial S_n} + \frac{1}{2!} \delta_n^2 \frac{\partial^2 w}{\partial S_n^2} + \frac{1}{3!} \delta_n^3 \frac{\partial^3 w}{\partial S_n^3} + 0(\delta_n^4) \ldots\ldots$$

- EQ. 3.4.2.

where δ_n = actual distance between points o and n.

Expanding equn 3.4.1., one obtains:

$$\frac{\partial^2 w}{\partial S_n^2} = a_{ni}^2 w_{,ii} + a_{nj}^2 w_{,jj} + a_{nk}^2 w_{,kk} + 2(a_{ni}a_{nj}w_{,ij} + a_{ni}a_{nk}w_{,ik} + a_{nj}a_{nk}w_{,jk}) \qquad \text{- EQ. 3.4.3.}$$

$$\frac{\partial^3 w}{\partial S_n^3} = a_{ni}^3 w_{,iii} + a_{nj}^3 w_{,jjj} + a_{nk}^3 w_{,kkk} + 3\Big(a_{ni}^2 a_{nj} w_{,iij} + a_{ni}^2 a_{nk} w_{,iik} + a_{ni} a_{nj}^2 w_{,ijj} + a_{nk} a_{nj}^2 w_{,jjk} + a_{ni} a_{nk}^2 w_{,ikk} + a_{nj} a_{nk}^2 w_{,jkk}\Big) + 6 a_{ni} a_{nj} a_{nk} w_{,ijk}$$

- EQ. 3.4.4.

FIG. 3.5

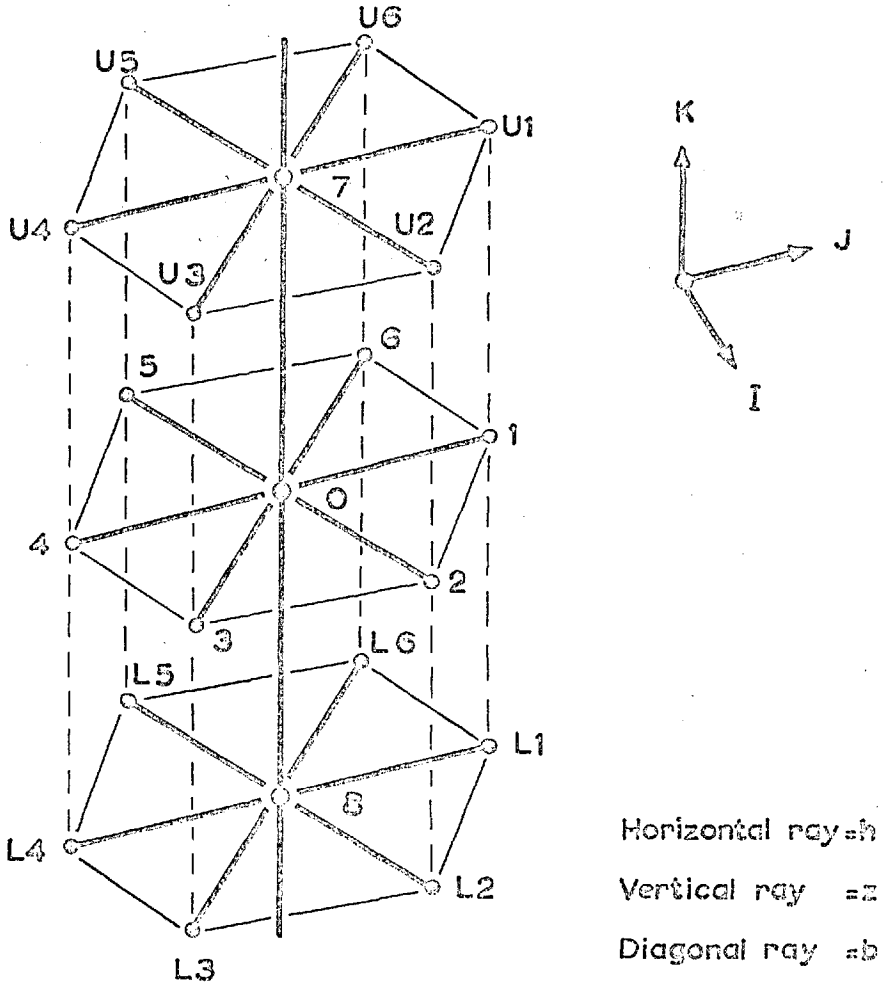

REFERENCE SYSTEM FOR GRID POINTS

TABLE 3.1.

LOWER GRID				MIDDLE GRID				UPPER GRID			
a_n	a_{ni}	a_{nj}	a_{nk}	a_n	a_{ni}	a_{nj}	a_{nk}	a_n	a_{ni}	a_{nj}	a_{nk}
a_8	0	0	-1	a_0	0	0	0	a_7	0	0	1
a_{L1}	0	1	-1	a_1	0	1	0	a_{U1}	0	1	1
a_{L2}	$\frac{\sqrt{3}}{2}$	$\frac{1}{2}$	-1	a_2	$\frac{\sqrt{3}}{2}$	$\frac{1}{2}$	0	a_{U2}	$\frac{\sqrt{3}}{2}$	$\frac{1}{2}$	1
a_{L3}	$\frac{\sqrt{3}}{2}$	$\frac{-1}{2}$	-1	a_3	$\frac{\sqrt{3}}{2}$	$\frac{-1}{2}$	0	a_{U3}	$\frac{\sqrt{3}}{2}$	$\frac{-1}{2}$	1
a_{L4}	0	-1	-1	a_4	0	-1	0	a_{U4}	0	-1	1
a_{L5}	$\frac{-\sqrt{3}}{2}$	$\frac{-1}{2}$	-1	a_5	$\frac{-\sqrt{3}}{2}$	$\frac{-1}{2}$	0	a_{U5}	$\frac{-\sqrt{3}}{2}$	$\frac{-1}{2}$	1
a_{L6}	$\frac{-\sqrt{3}}{2}$	$\frac{1}{2}$	-1	a_6	$\frac{-\sqrt{3}}{2}$	$\frac{1}{2}$	0	a_{U6}	$\frac{-\sqrt{3}}{2}$	$\frac{1}{2}$	1

TABLE 3.2.

	ω_{ij}	ω_{ji}	ω_{jk}	ω_{ijj}	ω_{iij}	ω_{ijk}	ω_{iii}	ω_{iik}	ω_{jkk}	ω_{ijjj}	ω_{iijj}	ω_{ijjk}	ω_{iiii}	ω_{iiij}	ω_{iikk}	ω_{jkkk}	ω_{ijkk}	ω_{iikk}	ω_{iijk}
	h			h^2						h^3									
$\omega_1 - \omega_0$	1	0	0	1/2	0	0	0	0	0	1/6	0	0	0	0	0	0	0	0	0
$\omega_2 - \omega_0$	1/2	$\sqrt{3}/2$	0	1/8	$\sqrt{3}/4$	0	3/8	0	0	1/48	$\sqrt{3}/16$	0	$\sqrt{3}/16$	3/16	0	0	0	0	0
$\omega_3 - \omega_0$	$-1/2$	$\sqrt{3}/2$	0	1/8	$-\sqrt{3}/4$	0	3/8	0	0	$-1/48$	$\sqrt{3}/16$	0	$\sqrt{3}/16$	$-3/16$	0	0	0	0	0
$\omega_4 - \omega_0$	-1	0	0	1/2	0	0	0	0	0	$-1/6$	0	0	0	0	0	0	0	0	0
$\omega_5 - \omega_0$	$-1/2$	$-\sqrt{3}/2$	0	1/8	$\sqrt{3}/4$	0	3/8	0	0	$-1/48$	$-\sqrt{3}/16$	0	$-\sqrt{3}/16$	$-3/16$	0	0	0	0	0
$\omega_6 - \omega_0$	1/2	$-\sqrt{3}/2$	0	1/8	$-\sqrt{3}/4$	0	3/8	0	0	1/48	$-\sqrt{3}/16$	0	$-\sqrt{3}/16$	3/16	0	0	0	0	0
	b			b^2						b^3									
$\omega_{U1} - \omega_0$	1	0	1	1/2	0	1	0	0	1/2	1/6	0	1/2	0	0	0	1/6	1/2	0	0
$\omega_{U2} - \omega_0$	1/2	$\sqrt{3}/2$	1	1/8	$\sqrt{3}/4$	1/2	3/8	$\sqrt{3}/2$	1/2	1/48	$\sqrt{3}/16$	1/8	$\sqrt{3}/16$	3/16	3/8	1/6	1/4	$\sqrt{3}/4$	$\sqrt{3}/4$
$\omega_{U3} - \omega_0$	$-1/2$	$\sqrt{3}/2$	1	1/8	$-\sqrt{3}/4$	$-1/2$	3/8	$\sqrt{3}/2$	1/2	$-1/48$	$\sqrt{3}/16$	1/8	$\sqrt{3}/16$	$-3/16$	3/8	1/6	$-1/4$	$\sqrt{3}/4$	$-\sqrt{3}/4$
$\omega_{U4} - \omega_0$	-1	0	1	1/2	0	-1	0	0	1/2	$-1/6$	0	1/2	0	0	0	1/6	$-1/2$	0	0
$\omega_{U5} - \omega_0$	$-1/2$	$-\sqrt{3}/2$	1	1/8	$\sqrt{3}/4$	$-1/2$	3/8	$-\sqrt{3}/2$	1/2	$-1/48$	$-\sqrt{3}/16$	1/8	$-\sqrt{3}/16$	$-3/16$	3/8	1/6	$-1/4$	$-\sqrt{3}/4$	$\sqrt{3}/4$
$\omega_{U6} - \omega_0$	1/2	$-\sqrt{3}/2$	1	1/8	$-\sqrt{3}/4$	1/2	3/8	$-\sqrt{3}/2$	1/2	1/48	$-\sqrt{3}/16$	1/8	$-\sqrt{3}/16$	3/16	3/8	1/6	1/4	$-\sqrt{3}/4$	$-\sqrt{3}/4$
$\omega_{L1} - \omega_0$	1	0	-1	1/2	0	-1	0	0	1/2	1/6	0	$-1/2$	0	0	0	$-1/6$	1/2	0	0
$\omega_{L2} - \omega_0$	1/2	$\sqrt{3}/2$	-1	1/8	$\sqrt{3}/4$	$-1/2$	3/8	$-\sqrt{3}/2$	1/2	1/48	$\sqrt{3}/16$	$-1/8$	$\sqrt{3}/16$	3/16	$-3/8$	$-1/6$	1/4	$\sqrt{3}/4$	$-\sqrt{3}/4$
$\omega_{L3} - \omega_0$	$-1/2$	$\sqrt{3}/2$	-1	1/8	$-\sqrt{3}/4$	1/2	3/8	$-\sqrt{3}/2$	1/2	$-1/48$	$\sqrt{3}/16$	$-1/8$	$\sqrt{3}/16$	$-3/16$	$-3/8$	$-1/6$	$-1/4$	$\sqrt{3}/4$	$\sqrt{3}/4$
$\omega_{L4} - \omega_0$	-1	0	-1	1/2	0	1	0	0	1/2	$-1/6$	0	$-1/2$	0	0	0	$-1/6$	$-1/2$	0	0
$\omega_{L5} - \omega_0$	$-1/2$	$-\sqrt{3}/2$	-1	1/8	$\sqrt{3}/4$	1/2	3/8	$\sqrt{3}/2$	1/2	$-1/48$	$-\sqrt{3}/16$	$-1/8$	$-\sqrt{3}/16$	$-3/16$	$-3/8$	$-1/6$	$-1/4$	$-\sqrt{3}/4$	$-\sqrt{3}/4$
$\omega_{L6} - \omega_0$	1/2	$-\sqrt{3}/2$	-1	1/8	$-\sqrt{3}/4$	$-1/2$	3/8	$\sqrt{3}/2$	1/2	1/48	$-\sqrt{3}/16$	$-1/8$	$-\sqrt{3}/16$	3/16	$-3/8$	$-1/6$	1/4	$-\sqrt{3}/4$	$\sqrt{3}/4$
	z			z^2						z^3									
$\omega_7 - \omega_0$	0	0	1	0	0	0	0	0	1/2	0	0	0	0	0	0	1/6	0	0	0
$\omega_8 - \omega_0$	0	0	-1	0	0	0	0	0	1/2	0	0	0	0	0	0	$-1/6$	0	0	0

Substitution of equns 3.4.3. and 3.4.4. into the Taylor Series eq. 3.4.2. yields the change in w in terms of the approximated derivatives. The set of coefficients $\underline{a_{ni}}$ are obtained by considering the geometry of the grid system as shown in figure 3.5, and have been tabulated in Table 3.1.

The set of equations giving the change in w in terms of the function derivatives may be summarised as:

$$\underline{w_o - w_a} = \underline{\sum \alpha . \delta_n . \text{derv.}(w)}$$

The coefficients $\underline{\alpha}$ and the appropriate set of derivatives are given in Table 3.2.

By choosing suitable combinations of elements of the set $\underline{w - w_a}$, it is possible to obtain finite difference approximations of all the first and second order derivatives of w with the minimum third order error. The approximations so obtained are:

$$w_{,i} = \frac{(w_2 + w_3) - (w_5 + w_6)}{2\sqrt{3}.h}$$

$$\varepsilon \doteq \frac{\sqrt{3}}{4} w_{,ijj} + \frac{\sqrt{3}}{4} w_{,iii}$$

$$w_{,j} = \frac{(w_i - w_4)}{2h}$$

$$\varepsilon \doteq \frac{1}{3} w_{,jjj}$$

$$w_{,k} = \frac{(w_7 - w_8)}{2z}$$

$$\varepsilon \doteq \frac{1}{3} w_{,kkk}$$

$$w_{,ii} = \left[(w_2 + w_3 + w_5 + w_6) - (w_1 + w_4)/2 - 3w_o \right] / \left(\frac{3}{2} h^2\right)$$

$$\varepsilon \doteq 0\,|h^4|$$

$$w_{,jj} = \frac{(w_1 + w_4 - 2w_o)}{h^2} \qquad \varepsilon \doteq 0\left|h^4\right|$$

$$w_{,kk} = \frac{(w_7 + w_8 - 2w_o)}{z^2} \qquad \varepsilon \doteq 0\left|z^4\right|$$

$$w_{,ij} = \frac{(w_2 - w_3) - (w_6 - w_5)}{\sqrt{3}h^2} \qquad \varepsilon \doteq 0\left|h^4\right|$$

$$w_{,ik} = \left[\left((w_{u2} + w_{u3}) - (w_{u5} + w_{u6})\right) - \left((w_{12} + w_{13}) - (w_{15} + w_{16})\right)\right] / 4\sqrt{3}b^2 \qquad \varepsilon \doteq 0\left|b^4\right|$$

$$w_{,jk} = \frac{(w_{u1} - w_{u4}) - (w_{11} - w_{14})}{4b^2} \qquad \varepsilon \doteq 0\left|b^4\right|$$

Also:

$$w_{,ii} + w_{,jj} + w_{,kk} = \frac{2}{3h^2}\left(\sum_{a=1}^{6} w_a - 6w_o\right) \qquad \varepsilon \doteq 0\left|h^4\right|$$

- EQs. 3.4.5.

Computation of the parameter Q involves second order derivatives of the viscous stress tensor (P_{ik}) and the necessary derivatives are in terms of third order derivatives of velocity. In the interior of the region these may be determined straightforwardly; however, in the region of

the boundaries, these derivatives must be determined by means of unbalanced formulae.

Greenspan (35) shows that for a line of grid points equally spaced (distance h) numbered 0, 1, 2 inwards from the boundary as shown below:

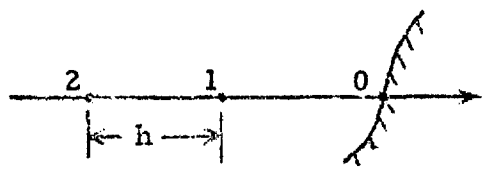

the outward pointing gradient of any function w at the boundary is given by:

$$\left(\frac{\partial w}{\partial n}\right)_o = \left(\frac{3}{2h}\right) w_o - \left(\frac{2}{h}\right) w_1 + \left(\frac{1}{2h}\right) w_2 \qquad \text{- EQ. 3.4.6.}$$

To obtain third order derivatives at the boundary in the normal direction, equation 3.4.6 must be applied successively for first, second and then third order values in terms of the appropriate interior derivatives. The equation may be applied unmodified in the principal directions J or K; if, however, in direction I there is no actual grid point at position 1, then the average value of the two nearest points in the J direction may be used.

Chapter 3.5. REVIEW OF PRESENT POSITION

As developed above, the proposed mathematical representation of the physical situation has been fully posed. Furthermore as explained, there are no analytical solution techniques available to solve these rather complex equations. Numerical procedures have been proposed which, from knowledge of application in other fields of numerical analysis, should permit the solution of the equations.

Because the computer available, the IBM 7090, is rather slow and does not have a very large fast store, the general problem has had to be reduced drastically to provide a system requiring a realistic solution time. Even so, with the greatly simplified situation described in Chapter 3.4., a computing time of the order of 7 to 10 hours will probably be required. This figure is very large partly because of the considerable use of tape decks holding intermediate computational data, and partly because the fast store is inadequate even to carry the whole of the object program. This necessitates the use of the cumbersome facility called "Overlay" which calls in sections of the program from magnetic tape when required. These factors make the compilation of a very long and involved program extremely difficult.

At present the intermediate tape manipulations of data and the use of Overlay have been fully "debugged". The programs for both the "Time Development" and pressure equation solutions have been written but are

still being "debugged". This stage is proving to be extremely time consuming partially because of the nature of the problem, but mainly because of the lack of time available for the necessary tests on the machine.

When the programme is working satisfactorily it should produce maps of both foam density and pressure distribution over the plate and these can be compared with experimentally determined values. In fact the mathematical analysis should also be applicable to fluidized bed and other similar two-phase systems.

APPENDIX A.1.1

APPENDIX A1. 1.

DETAILS OF 4in. PERSPEX SIMULATION COLUMN

For photographic reasons, as explained, the simulation column was required to have flat viewing walls, and it was also desirable that as much as possible of the column be transparent to assist observation from all angles. For these reasons, a column was designed and built almost entirely out of perspex. To further assist the photographic studies, the test plates with weirs attached were also manufactured out of perspex. This was considered reasonable as the wetting properties of perspex and brass or steel are similar. The constructional details of the column can be seen in figure A1. 1. and a line flow diagram for the equipment is given in figure A1. 2.

The overall dimensions of the interior of the column were 4. 25in. x 4. 6in. The distance between the weirs was 3. 5in. and this gave a plate bubbling area of 3. 5in. x 4. 25in. Since the distance between the inlet and outlet perspex foam baffles was also 3. 5in., the effective column cross sectional area was the same as the plate bubbling area.

The plate insert was sealed into the column by pressure against the neoprene gasket placed round the edge of the wall. The inserts, downcomer and splash baffle, could be readily changed by unbolting one wall of the column, thus releasing the pressure on the gasket.

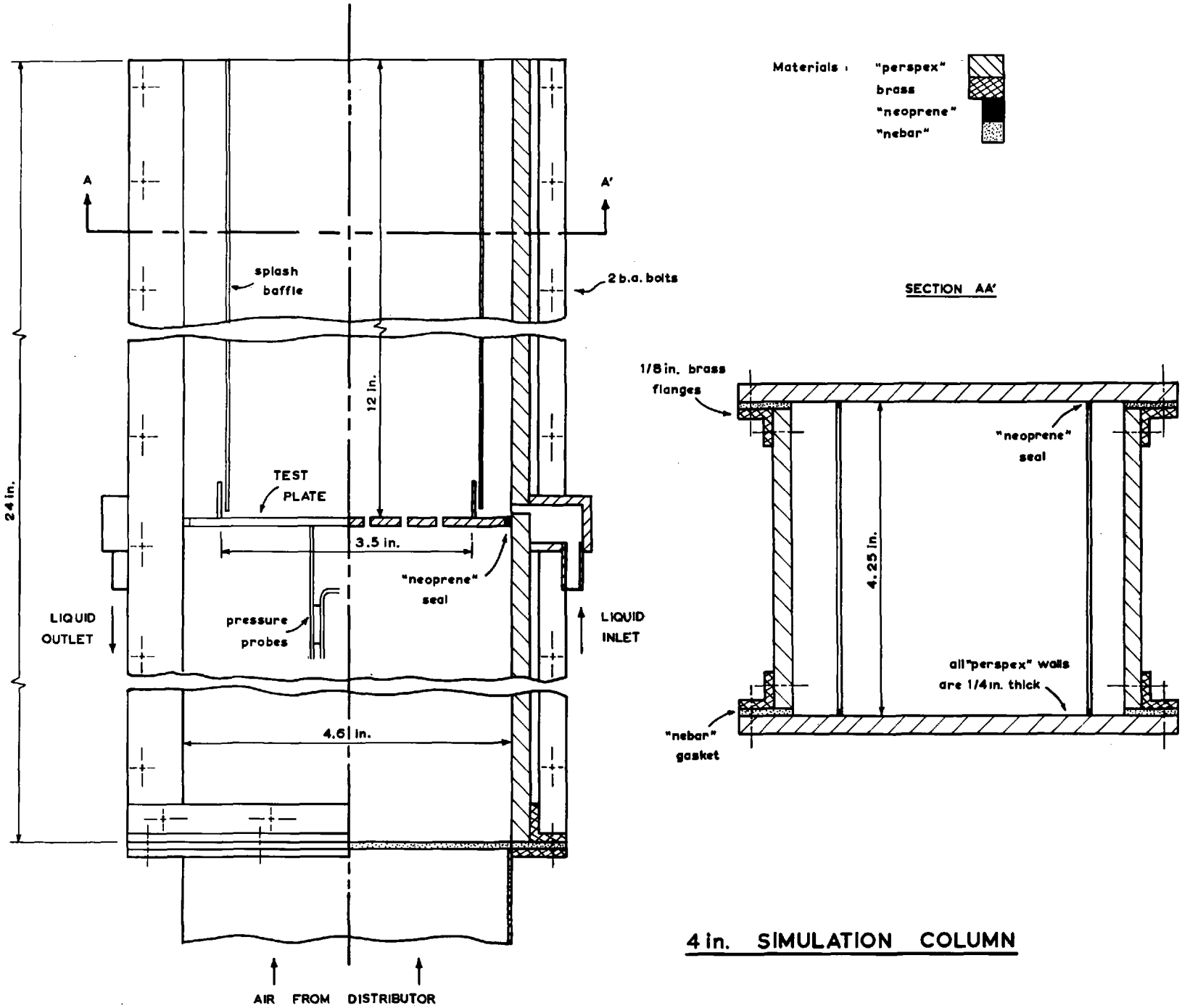

4 in. SIMULATION COLUMN

FIG. A1.1

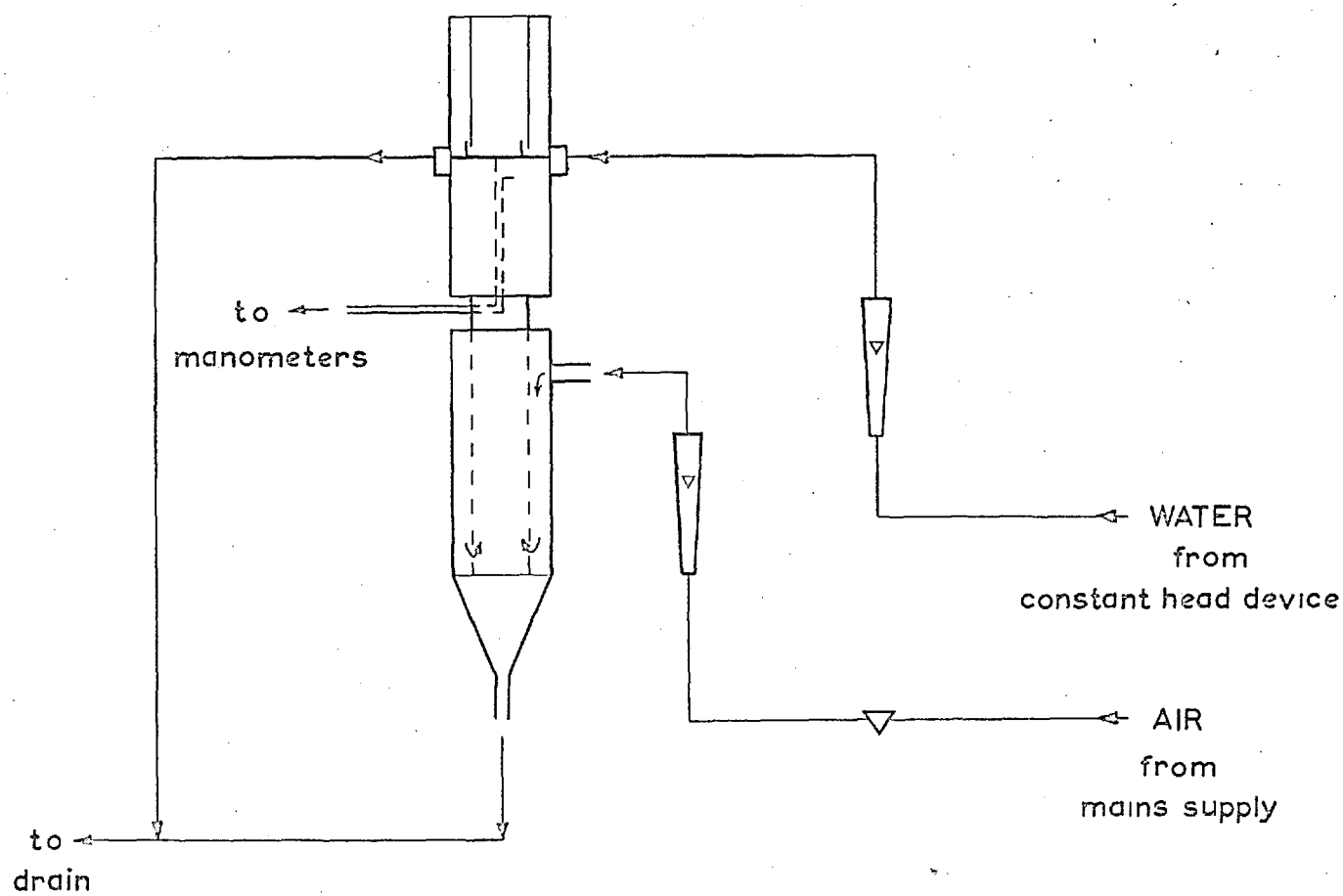

FLOW DIAGRAM FOR SIMULATION COLUMN

FIG. A1.2

The water flow to the test plate was from the mains supply via a 'constant head' device and rotameter. It entered the column through a weir box at plate level and flowed onto the test plate under the inlet foam baffle and over the inlet weir. After flowing over the outlet weir, the water was led to a drain. Inlet and outlet foam baffles were incorporated in the design to aid simulation of large column conditions.

The air entered the rectangular column from a distributor placed directly beneath it; this distributor had been designed to provide very smooth air flow to the test plate. The air was supplied from the mains and its flow rate measured with a rotameter.

The overall and dynamic head probes were made from 1/16in. O.D. stainless steel hyperdermic tube. The plastic leads from these two probes were led out through the bottom of the column to their respective manometers. The overall pressure drop was measured on a standard water filled U-tube manometer, while the dynamic head was measured on an inclined single limb manometer.

For the studies of the effect of viscosity on the dispersion properties, the water/glycerol mixtures were pumped from a large reservoir directly to the rotameter by means of a Stewart Turner pump. The liquid leaving the test plate then returned to the reservoir. The amount of water evaporated during a run was very slight and it was thus not necessary to continually add make-up water.

BIBLIOGRAPHY

BIBLIOGRAPHY

1	A.I.Ch. E. Research Committee	Final Report University of Deleware, 1958
2	A.I.Ch. E. Research Committee	Final Report University of Michigan, 1960
3	A.I.Ch. E. Research Committee	Final Report North Carolina State College, 1959
4	Gerster, J.A.	Communication to Distillation Panel ABCM/BCPMA, May 1958
5	Macmillan, W.P.	Ph.D. Thesis, University of London, 1962
6	Bernard, J.D.T.	Ph.D. Thesis, University of London, 1967
7	Pozin, M.	J. Appl. Chem. (U.S.S.R.), 27, No. 1, 9, 1954
8	Crozier R.D.	Ph.D. Thesis, University of Michigan, 1956
9	Calderbank, P.H. and Moo-Young, M.B.	International Symposium on Distillation, Brighton, England, 1960
10	Zuiderweg, F.J. and Harmens A.	Chem. Eng. Sci., 9, 89, 1958
11	Planck, C.A.	Ph.D. Thesis, North Carolina State College, 1957
12	Calderbank, P.H., Evans, F. and Rennie, J.	International Symposium on Distillation, Brighton, England, 1960
13	Prince, R.G.H. and Chan, B.K.C.	Trans. Inst. Chem. Eng. 43, No. 2., 1965
14	Hunt, C.A., Hanson, D.N. and Wilke, C.R.	A.I.Ch.E. Journal, 1, 441, 1955

15	Ashraf, F.A., Cubbage, T.L. and Huntington, R.L.	Ind. Eng. Chem., 26, 1038, 1934
16	Holbrook, G.E. and Baker, E.M.	Trans. Am. Inst. Chem. Engrs., 30, 520, 1934
17	Strang, L.C.	Trans. Inst. Chem. Engrs., 12, 169, 1934
18	Sherwood, T.K. and Jenny, F.J.	Ind. Eng. Chem., 27, 265, 1935
19	Souders, M. and Brown, G.G.	Ind. Eng. Chem., 26, 98, 1934
20	Kirschbaum, E.	Distillation and Rectification, Chemical Publishing Co.Inc. 1948
21	Prince, R.G.H.	International Symposium on Distillation, Brighton, England, 1960
22	Rennie, J. and Smith, W.	A.I.Ch.E. - I.Chem.E. Joint Meeting, London, 1965
23	Jones, J.B. and Pyle, C.	Chem. Eng. Prog., 51, 424, 1955
24	Bostian, H.	Meeting Am. Inst. Petroleum Refining Division, 1964
25	Lockhart, F.J. and Legget, C.W.	Advances in Petroleum Refining, Interscience, 1958
26	Leibson, I., Holcomb, E.G., Cacoso, A.G., and Jacmic, J.J.	A.I.Ch.E. Journal, 2, 296, 1956
27	Mayfield, F.D., Church, W.L. and Green, A.C.	Ind. Eng. Chem., 44, 2238, 1952
28	Helsby, F.W.	Ph.D. Thesis, University of London, 1958
29	Cheng, S.I. and Teller, A.J.	A.I.Ch.E. Journal, 7, 282, 1961
30	Teller, A.J. and Rood, R.E.	A.I.Ch.E. Journal, 8, 369, 1962
31	Standart, G. and Kastanek F.	Separation Sci., 1, 27, 1966
32	De Geoderen, C.W.J.	Chem. Eng. Sci., 20, 1115, 1965

33	Pozin, M.E., Mukhlenov, I.P., and Ya. Tarat, E.	J. Appl. Chem. (U.S.S.R.), 30, 43, 1957
34	Landau, L.D., and Lifshitz, E.M.	Fluid Mechanics, Pergamon, 1959
35	Greenspan, D.	Numerical Analysis of Elliptic Boundary Value Problems, Harper, 1965
36	Smith, G.D.	Numerical Solution of Partial Differential Equations, OUP, 1965
37	Hamming, R.W.	Numerical Methods for Scientists and Engineers, McGraw Hill, 1962
38	Varga, R.S.	Matrix Iterative Analysis, Prentice-Hall, 1962
39	Aris, R.	Vectors, Tensors and Basic Equations of Fluid Mechanics, Prentice-Hall, 1962
40	Bernard, J.D.T., Macmillan, W.P., Sargent, R.W.H., and Schroter, R.C.	Proceedings of the Symposium on Distillation, A.B.C.M/B.C.P.M.A. London, 1964
41	Bernard, J.D.T. and Sargent, R.W.H.	Trans. Inst. Chem. Eng. 44, No. 8, 1966
42	Russell, D.B.	Ph.D. Thesis, University of Oxford, 1961
43	Wachspress, E.L.	S.I.A.M. Journal, 11, 994, 1963
44	Bainbridge, G.	Ph.D. Thesis, University of London, 1965
45	Rosenbrock, H.H. and Storey, G.	Computational Techniques for Chemical Engineers, Pergamon, 1966
46	Foss, A.S. & Gerster, J.A.	Chem. Eng. Prog., 52, 28, 1956
47	Arnold, D.S., Planck, C.A. and Schoenborn, E.M.	Chem. Eng. Prog., 48, 633, 1952

48	Davidson, J. F. and Schuler, B. O. G.	Trans. Inst. Chem. Eng., 38, 335, 1960
49	Jameson, G. J. and Kupferberg, A.	Chem. Eng. Sci. in press
50	Porter, K. E., King, M. B. and Varshney, K. C.	Trans. Inst. Chem. Eng., 44, No. 7, 1966
51	Kolodzie, P. A. and Van Winkle, M.	A. I. Ch. E. Journal 3, 305, 1957
52	Barnes, R. L. and Lewis, A. J.	Research Report, Imperial College, 1965
53	Porter, K. E. and Davies, B. T.	Symposium on Two Phase Flow, Exeter, England, 1965
54	Gardner, J. B.	Personal communication, February 1967
55	Davidson, J. F. and Walters, J. K.	J. Fluid Mech., 17, No. 3, 1963
56	Brown, B.	Ph. D. Thesis, University of London, 1960
57	Campbell, M. and Thomas, W. J.	Trans. Inst. Chem. Eng., 45, No. 2., 1967
58	Fromm, J.	Methods in Computational Physics, Vol 3., Academic Press, 1964